FINAL TECHNICAL REPORT

Technetium Reduction and Permanent Sequestration by Abiotic and Biotic Formation of Low-Solubility Sulfide Mineral Phases

ID: ER64806-1033401-0015142
SC Division SC-23.1
Program Manager: Roland F. Hirsch

Paul G. Tratnyek (lead principal investigator),*
Bradley Tebo, Dimin Fan, Roberto Anitori
Department of Environmental and Biomolecular Systems
Oregon Health & Science University
20000 NW Walker Rd., Beaverton, OR 97006-8921

Jim Szecsody and Danielle Jansik
Environmental Systems Group, Energy and Environment Division
Pacific Northwest National Laboratory
P.O. Box 999, MS K7-59, Richland, WA 99354

*Email: tratnyek@ohsu.edu
Phone: 503-346-3431

14 November 2015

1. Table of Contents

2. List of Figures

3. List of Tables

4. Keywords

Pertechnetate, Technetium Sulfide, Sequestration, Reduction, Oxidation, Zerovalent Iron, nZVI, Sulfidation, TEM, XAS, XPS, μXRD, Mössbauer

5. Acknowledgements

Calculations performed at PNNL were performed using the Molecular Science Computing Capability in the William R. Wiley Environmental Molecular Science Laboratory (EMSL), a national scientific user facility sponsored by the U.S. Department of Energy's Office of Biological and Environmental Research and located at the Pacific Northwest National Laboratory, operated for the Department of Energy by Battelle. In addition, this work makes use of the open source quantum chemistry package NWChem maintained by the EMSL user facility. We would also like to thank the PNNL Institutional Computing (PIC) program at Pacific Northwest National Laboratory (PNNL) for a small block of computing time.

6. Abstract

One way to minimize the mobility of the Tc^{VII} oxyanion pertechnetate (TcO_4^-) is to effect reduction under sulfidogenic conditions (generated abiotically by Fe^0 or biotically) to form TcS_x, which is significantly slower to oxidize than $Tc^{IV}O_2$. In sediment systems, TcS_x and other precipitates may oxidize more slowly due to oxygen diffusion limitations to these low permeability precipitate zones. In addition, the TcO_4^- reduction rate may be more rapid in the presence of sediment because of additional reductive surface phases. This project aims to provide a fundamental understanding of the feasibility of immobilization of TcO_4^- as TcS_x in the vadose zone or groundwater by application nano zero-valent iron (nZVI), and sulfide or sulfate.

Biotic batch experiments have used the sulfate-reducing bacterium (SRB) *Desulfotomaculum reducens*. The iron sulfide mineral mackinawite was generated under these conditions, while vivianite was formed in nZVI only controls. The sulfide/bacteria-containing system consistently reduced aqueous pertechnetate rapidly (> 95% in the first hour), a rate similar to that for the sulfide-free, nZVI only system. Reduced Tc (aged for 3 months) generated in both SRB/nZVI systems was highly resistant to reoxidation. In reduced samples, Tc was found associated with solid phases containing Fe and S (*D. reducens*/nZVI) or Fe (nZVI only). Experiments using *D. reducens* without nZVI provided some additional insights. Firstly, stationary phase cultures were able to slowly reduce pertechnetate. Secondly, addition of pertechnetate at the beginning of cell growth (lag phase) resulted in a faster rate of Tc reduction, possibly indicating a direct (e.g. enzymatic) role for *D. reducens* in Tc reduction.

Abiotic batch experiments were conducted with Na_2S as the sulfide source. Pertechnetate reduction was rapid in the presence of sulfide and nZVI, although the rate was suppressed at the higher S/Fe ratios tested. This suppression appeared to be due to the formation of Tc-containing colloids. As with the biotic experiments, pertechnetate reduced under sulfidic conditions was highly resistant to reoxidation. The microscopic morphology of abiotically-transformed nZVI particles varied significantly with those in the biotic experiment, although mackinawite was formed in both systems (as indicated by μXRD and Mössbauer spectroscopy). Preliminary XAS analysis pointed to a mixture of

Tc-O and Tc-S binding in the abiotic sulfide/nZVI system, while the major reduced solids under non-sulfidic conditions were $TcO_2 \bullet nH_2O$.

The presence of sediment and advective flow to the TcO_4^-/nZVI/sulfide system results in additional processes occurring. Although the natural Hanford sediment used has sufficient available ferrous iron to slowly reduce TcO_4^-, under anaerobic conditions, that rate is orders of magnitude slower than reduction by nZVI/sulfide. Batch and 1-D column experiments showed that the TcO_4^- reduction rate increased with the sediment surface area (with the same nZVI mass). As in batch systems, column studies showed that the presence of sulfide with TcO_4^- at low (2-5 mM) concentrations increased the TcO_4^- reduction rate and high (10-30 mM) sulfide decreased the rate. This change is attributed to the formation of sulfide precipitates on the nZVI and sediment surfaces. Injection of low and high sulfide (i.e. pretreatment) prior to TcO_4^-/sulfide injection also greatly decreased the TcO_4^- reduction rate, likely decreasing the generation of ferrous iron from the nZVI. Although the high sulfide systems have slower Tc reduction rates, 190 times more Tc mass precipitated than in the low sulfide systems and the highest fraction of Tc mass remained immobilized.

7. Background

Technetium-99 is a highly mobile subsurface contaminant at U.S. Department of Energy (DOE) sites, and its mobility gives it one of the highest risks of exposure. Contamination by Tc above the drinking water standard is found in groundwater monitoring wells at the Hanford and Savannah River Sites and at the Paducah Gas Diffusion Plant. Lower, but significant, levels of Tc contamination are found in groundwater at the Oak Ridge Site and the Idaho National Engineering Laboratory.

The predominant and mobile form of technetium in the subsurface is the Tc^{VII} oxyanion pertechnetate (TcO_4^-). Under reducing conditions TcO_4^- is readily reduced to Tc^{IV}, which forms highly insoluble oxides such at $TcO_2 \cdot nH_2O$. Many studies have investigated the reduction of TcO_4^-, by abiotic and biotic means, on the premise that this could be used for long-term immobilization of the contaminant for remediation activities

at DOE sites. However, a difficulty with this strategy is that (re)oxidation of Tc^{IV} oxides is relatively facile and therefore remobilization is possible.

One way to minimize the prospect of remobilization is to effect reduction under sulfidogenic conditions, so that most Tc^{IV} will be immobilized as Tc_2S_7, which should remain relatively insoluble even under oxic conditions. For this purpose, a feasible and practical way to create well-poised sulfidogenic conditions is the injection of fine-grained zero-valent iron (Fe^0)—or related materials composed of various combinations of Fe^0, S^0, Fe^{II}, and S^{II}. These materials will react directly with Tc^{VII} yielding a degree of immobilization by reduction and precipitation, but the Fe^0 also will scavenge dissolved oxygen and nitrate and generate significant concentrations of dissolved H_2, thereby stimulating sulfate- and sulfur- reducing bacteria (collectively referred to as SRB), which will favor sequestration of Tc in less reoxidizable forms (esp., Tc_2S_7).

Fine-grained Fe^0 and related chemical reductants—ranging in size from 10's of microns to 10's of nanometers—are available and suitable for introduction into the deep subsurface (vadose and saturated zones) by a variety of injection technologies. This makes the approach proposed here applicable for in situ chemical reduction at sites like Hanford, where the vadose zone and groundwater contamination by Tc is 80-120 m deep. The outcome of such scenarios, however, will depend on complex mixture of multi-scale processes, where the spatial distribution of the injected material will have heterogeneous effects on the in situ biogeochemistry, which—in turn—will determine what mixture of fundamental processes control the overall (im)mobilization of Tc.

The overall objective of this work was to provide the fundamental understanding necessary to evaluate the feasibility of reductive immobilization of TcO_4^- in the vadose zone or groundwater by controlled application of Fe^0, Fe^0/S^0 (and sulfate or organic carbon, if necessary) to stimulate microbial sulfate reduction. This proposed work was focused on these biogeochemical mechanisms of interaction between Fe^0, S^0, and Tc (not the technology to emplace Fe^0 and Fe^0/S^0 in the vadose or saturated zones). The specific objectives were to demonstrate that (1) Fe^0 or Fe^0/S^0 injection into relevant porous media produces stable sulfidogenic conditions, (2) sulfidogenic aquifer conditions reduce TcO_4^- to stabile Tc^{IV} sulfides, and (3) Tc^{IV} sulfides are resistant to remobilization upon

reoxidation and remobilization of Tc is further inhibited by small scale (mm-μm) reduced areas caused by the injected reductant and subsequent microbial response.

8. Objectives

Our three major objectives were pursued in parallel, but in closely integrated efforts:

1. ***Stimulation of sulfidogenesis with injectable Fe0 or Fe^0/S^0***: There is nearly universal consensus that abiotic reduction of sulfate by Fe^0 is a negligible process, but field data from Fe^0 reactive barriers indicated large amounts of sulfate reduction despite low populations of sulfate reducing bacteria (SRB). We determined the precise relationship between Fe^0, SRB, and sulfate reduction using electrochemical and batch experiments with nano- to micron-sized Fe^0, Fe^0/S^0, pure culture and natural inocula, and a variety of mineral matrix materials. Mineralogical analysis included high-resolution electron microprobe characterization of the mineral surface coatings that form under these conditions.

2. ***Sequestration of Tc under sulfate reducing conditions***: Prior studies have shown that Tc^{IV} is sequestered by biogenic iron sulfides, and by Fe^0, and that sulfides form on Fe^0 when sulfate is present, but the combination of these processes has never been studied. Mesocosms containing natural consortia from FRC, Hanford, or other DOD sites were characterized using cultivation approaches and molecular analyses of the major microbial populations (especially SRB) and measurements of sulfate reduction rates/activities. Then, we will determined the fate of Tc in the presence of Fe^0-stimulated sulfate reduction—with emphasis on the type and distribution of reduced Tc-S phases (esp. Tc_2S_7)—using chemical and microbiological methods similar to those noted above for Objective 1.

3. ***Controls on remobilization of Tc precipitates***: Tc2S7 is highly insoluble based on geochemical equilibrium in homogeneous systems. However, in a heterogeneous sediment system at a high sediment-to-water ratio, we expected that mass transfer limitations would further limit its remobilization. This is because the highly reduced zones in the immediate vicinity of injected Fe^0, Fe^0/S^0 will have decreased permeability due to precipitation of sulfides (and oxides) in the pore space. This was

investigated with batch and columns experiments, using electron microprobe analysis of reduced, and reduced/oxidized sediments to identify Tc-Fe-S phases.

9. Technical Approach

9.1. Objective 1: Characterize stimulation of sulfidogenesis with injectable Fe^0 and Fe^0/S^0

There is nearly universal consensus that abiotic reduction of sulfate by Fe^0 is a negligible process (even though it is thermodynamically quite favorable). However, the available data regarding the fate of sulfate during in situ applications of Fe^0 for remediation suggest there are aspects of this issue that are not fully understood. For example, field data from Fe^0 reactive barriers tend to indicate large amounts of sulfate reduction, but very low populations of SRB (Johnson et al. 2005; Da Silva et al. 2007; Johnson et al. 2008). At the same time, while it is well known that SRB play a large role in microbially influenced corrosion (MIC) (Little et al. 2003; Beech and Sunner 2004; Videla and Herrera 2005), there is little known about how MIC influences contaminant reduction/precipitation in Fe^0-containing systems. We investigated the precise relationship between Fe^0, sulfate reduction, and sulfate reducing bacteria using electrochemical model systems and batch microcosms containing nano- to micron-sized Fe^0, Fe^0/S^0, and pure culture and natural inocula.

Task 1A. We hypothesized that *there will be no abiotic sulfate reduction by Fe^0or Fe^0/S^0, and that sulfate will act as a passivating anion, inhibiting breakdown of the (oxide) passive film on the Fe^0, thereby slowing hydrogen production* (by anaerobic corrosion, eq. 2).

Task 1B. *Sulfide from solution reacts (abiotically) with Fe^0 (or Fe^0/S^0) surfaces creating an iron sulfide coating that is mildly but not fully passivating with respect to hydrogen production.*

Task 1C. The previous two tasks concern only abiotic processes, but we hypothesized that *after colonization of the Fe^0 by SRB, sulfate reduction and precipitation of iron sulfides will become faster, and overall rates of hydrogen production will be*

increased because of pitting associated with microbially influenced corrosion (MIC).

Task 1D. In systems containing Fe^0 and reduced sulfur (with and without SRB activity), we *hypothesized that reduction/precipitation of oxyanion contaminants (here pertechnetate, but more generally also chromate, uranyl, arsenate, etc.) will create new passivating phases that slow down corrosion (and therefore TcO_4^- sequestration) rates in the short-term, but that conserve the reducing capacity of the Fe^0 in the medium-long term, thereby helping to poise the system against reoxidation.*

9.2. Objective 2: Characterize sequestration of Tc under sulfate reducing conditions

SRB are widely distributed in soil, sediment, and groundwater, and SRB, despite being obligate anaerobes, are able to tolerate a wide range of environmental conditions, including O_2. It is also likely that anaerobic microenvironments in predominantly aerobic aquifers or vadose zones support the growth of these microorganisms. SRB are therefore able to survive, or even thrive, in many subsurface environments provided that their basic requirements are met for anoxia, sulfate or sulfur as electron acceptors, and a supply of electron donor (e.g., H_2). Since introduction of Fe^0 (or Fe^0/S^0) creates anoxic conditions and generates H_2, this offers a potentially very robust way to create and sustain SRB activity.

Task 2A. We hypothesized that *sulfate- and sulfur-reduction stimulated by Fe^0 addition will lead to conditions that favor the formation of Tc^{IV} sulfides.*

Task 2B. We hypothesized that *active biogenic iron sulfide formation and biogenic FeS are more effective in immobilizing Tc than addition of synthetic or mineral forms of FeS or FeS_2 alone.*

9.3. Objective 3: Characterize controls on remobilization of Tc^{IV} precipitates

TcO_4^- that is reduced by the combination of Fe^0 and SRB will form one or more Tc^{IV} species including TcO_2 and Tc_2S_7 (or TcS_x) as precipitates. If the reduced zone becomes oxidized, some of the TcO_2 will reoxidize to TcO_4^- and be remobilized (assuming no other coatings on the TcO_2). Tc_2S_7 (or TcS_x) may also be oxidized, but the rate will be much slower ((Lukens et al. 2005); oxidation half-life 629 days for system with no diffusion limitations). In the vadose or saturated zones, the FeS_2 and other oxide coatings (generated from the Fe^0 at high pH) will coat oxides (TcO_2 and TcS_x) and fill some of the pore space (lowering permeability). Some aspects of these physical effects can be represented in batch reactors, but the mechanisms involved in potential remobilization of Tc under field conditions will be better evaluated in 1-D/2-D porous media model systems. Laboratory 1-D columns or 2-D flow systems will have the high sediment/water ratio of the field, as well as developed low permeability zones of sulfide/oxide precipitation.

Task 3A. We hypothesized that *reduced Tc (TcO_2 and TcS_x) in packed bed porous media will resist oxidation/remobilization due to a combination of chemical and physical processes, including: (i) presence of TcS_x species, (ii) oxide/sulfide coatings on Tc precipitates, and (iii) development of lower permeability zones at precipitation locations.*

Task 3B. In packed bed porous media, we hypothesized that *the portion of reduced Tc (TcO_2 and TcS_x) that is not mobilized upon oxidization of the system will be influenced by variations in pore structure.*

Task 3C. Although the presence of TcS_x species and development of lower permeability zones will contribute resistance to Tc oxidation, we hypothesized that *oxide/sulfide coatings on Tc precipitates also contribute to maintaining Tc immobilized as Tc^{IV} precipitates.*

10. Results and Discussion

10.1. Characterization of the effects of sulfidation on abiotic processes involved in the sequestration of Tc by zerovalent iron

All of the results from this portion of the project are reported, in full, in two peer-reviewed journal articles (Fan et al. 2013; Fan et al. 2014). The abstracts from these articles are given below, and the full text of each article is included in the appendices.

1. Fan, D., R. P. Anitori, B. M. Tebo, P. G. Tratnyek, J. S. Lezama Pacheco, R. K. Kukkadapu, M. H. Engelhard, M. E. Bowden, L. Kovarik, and B. W. Arey. 2013. Reductive sequestration of pertechnetate ($^{99}TcO_4^-$) by nano zero-valent iron (nZVI) transformed by abiotic sulfide. Environ. Sci. Technol. 47(10): 5302-5310. [10.1021/es304829z]

Abstract: Despite increasing recognition that natural attenuation (NA) of chlorinated solvents involves abiotic as well as biotic degradation processes, current approaches to assessing the potential for abiotic NA are inadequate. Recognizing that reducing iron minerals play a major role in contaminant reduction by abiotic NA, this study set out to explore the use of chemical reactive probes (CRPs) to characterize the thermodynamic and kinetic aspects of contaminant reduction by these phases. A set of thermodynamic CRPs were selected and used to determine the reduction potentials (E_{CRP}) by spectrophotometric determination of CRP speciation at equilibrium, and calculations using the Nernst equation. The measured E_{CRP} were found to vary upon mineral type, Fe(II) concentration, and mineral loading. Reduction potentials were also measured electrochemically with a Pt rotating disc electrode (RDE) (E_{Pt}). Despite showing consistent trend as E_{CRP}, E_{Pt} were 150—200 mV more positive than E_{CRP}, likely due to the poor electrode responses to reducing iron minerals. Contaminant reduction experiments with three different kinetic CRPs with four iron oxides at 1mM Fe(II) concentration showed that the observed reduction rate constants in general followed the order of mineral reduction potential, although kinetic effects were also observed, likely resulting from intrinsic differences between different minerals. Combination of experimentally measured reduction rate constants with published rate constants, including chlorinated

ethenes, showed qualitatively consistent reactivity pattern between the kinetic CRPs and chlorinated ethenes, indicating the potential utility of CRPs in assessment of abiotic NA.

2. Fan, D., R. P. Anitori, B. M. Tebo, P. G. Tratnyek, J. S. Lezama Pacheco, R. K. Kukkadapu, L. Kovarik, M. H. Engelhard, and M. E. Bowden. 2014. Oxidative remobilization of technetium sequestered by sulfide-transformed nano zerovalent iron. Environ. Sci. Technol. 48(13): 7409–7417. [10.1021/es501607s]

Abstract: Our previous study showed that formation of TcS_2-like phases is favored over TcO_2 under sulfidic conditions stimulated by nano zerovalent iron. This study further investigates the stability of Tc(IV) sulfide upon reoxidation by solution chemistry, solid phase characterization, and X-ray absorption spectroscopy. Tc dissolution data showed that Tc(VII) reduced by sulfide-transformed nZVI has substantially slower reoxidation kinetics than Tc(VII) reduced by nZVI only. The initial inhibition of Tc(IV) dissolution at S/Fe = 0.112 is due to the redox buffer capacity of FeS, which is evidenced by the parallel trends in oxidation-reduction potentials (ORP) and Tc dissolution kinetics. The role of FeS in inhibiting Tc oxidation is further supported by the Mössbauer spectroscopy and micro X-ray diffraction data at S/Fe = 0.112, showing persistence of FeS after 24-h oxidation but complete oxidation after 120-h oxidation. X-ray absorption spectroscopy data for S/Fe = 0.011 showed significantly increasing percentages of TcS_2 in the solid phase after 24-h oxidation, indicating stronger resistance of TcS_2 to oxidation. At S/Fe = 0.112, the XAS results revealed significant transformation of Tc speciation from TcS_2 to TcO_2 after 120-h oxidation. Given that no apparent Tc dissolution occurred during this period, the speciation transformation might play a secondary role in hindering Tc oxidation. Collectively, the results indicate that sequestrating Tc as TcS_2 under stimulated sulfate reduction is a promising strategy to improve the long-term stability of reduced Tc in subsurface remediation.

10.2. Characterization of the effects of sulfidation on biotic processes involved in the sequestration of Tc by zerovalent iron

10.2.1. Sulfate reducing bacterial cultures

The majority of the nZVI experiments utilized a pure culture of the anaerobic sulfate-reducing bacterium (SRB) *Desulfotomaculum reducens*. Initial growth experiments were conducted at 37°C in a commonly used SRB culture medium (Widdel-Pfennig, WP). Subsequently, we conducted a number of optimization experiments to develop a growth medium that more closely mimicked the *in situ* Hanford subsurface at the 300A area - Hanford synthetic groundwater medium, HS300 (a modified version of PNNL growth medium SGW1). The aforementioned optimization experiments included: (i) culturing at different temperatures (24, 27, 30, 37°C) - 27°C was the lowest temperature that provided growth over a reasonable period of time; (ii) differing carbonate concentrations - 3 mM was chosen. 30 mM HEPES buffering was used to maintain the culture pH at 7.8 in the presence of nZVI, which results in the development of alkaline conditions without buffering; and (iii) use of 100% N_2 as the culturing headspace gas. In summary, the majority of the *D. reducens* nZVI and ^{99}Tc experiments were conducted using the following "Hanford" conditions: 27°C with gentle shaking (150 rpm) in HS300 growth medium composed of basal salts, vitamins, trace elements, 30 mM HEPES, 3 mM carbonate, 20 mM Na lactate and 10 mM sulfate, pH 7.8, 100% N_2 headspace, 1 atm. A small number of experiments were also conducted using SRB culture enrichment consortium FC1, derived from a sediment sample from an iron permeable reactive barrier used to bioremediate uranium (Fry Canyon, Utah; sediment courtesy of Chris Fuller).

10.2.2. Biotic ^{99}Tc reduction by SRB and subsequent resistance to reoxidation

The results and conclusions below are, unless otherwise specified, from batch experiments (60, 120, or 200 mL) that included all or some of the following treatment groups:

- *D. reducens* cells + nZVI (500 mg/L)
- *D. reducens* cells only
- nZVI only (500 mg/L)

- Culture medium only

For experiments in which ^{99}Tc was used, 10 μM or 30 μM pertechnetate (TcO_4^-) was included. The major findings and conclusions are summarized below.

- *D. reducens* grew in the presence of nZVI, and its growth was often stimulated, indicating that the nZVI produced sulfidogenic conditions (see project Objective 1—*Characterize stimulation of sulfidogenesis with injectable Fe^0 and Fe^0/S^0*). The successful growth of cells was also an important observation, as a number of publications have indicated that nZVI acts as a bactericidal agent.
- Biotic sulfate (SO_4^{2-}) reduction and the concomitant production of hydrogen sulfide (H_2S) occurred with or without nZVI. Lower sulfide levels were seen in the nZVI treatments, and were due to the formation of FeS.
- Control treatments without cells showed no sulfate reduction or adsorption of sulfate/sulfide by nZVI.
- Removal of TcO_4^- was rapid (on the order of minutes) and essentially complete in both *D. reducens*/nZVI [pertechnetate added at stationary phase] and nZVI only treatments. In contrast, pertechnetate removal was slower and incomplete with *D. reducens* cells only (7% removal in 5 hr). These findings indicated that:
    - nZVI and/or FeS was responsible for rapid and efficient ^{99}Tc reduction at circumneutral pH.
    - *D. reducens* cells may be able to reduce pertechnetate via a direct, cell-mediated mechanism. This hypothesis of active cellular removal of TcO_4^- was partly supported by batch experiments in which *D. reducens* cells were able to almost completely remove pertechnetate from solution when it was added at lag phase (removal was not complete when it was added at the log or stationary phases of cell growth).
- The presence of Tc-containing colloids (< 200 nm) in the *D. reducens* only treatments was inferred via the use of 0.2 μM and 0.02 μM filtration. This effect was also seen in

the medium only control, but only at about 50% of the level observed in the *D. reducens* treatments.

- We were able to replicate our *D. reducens* pertechnetate reduction results using the SRB-containing enrichment consortium FC1.
- *Re-oxidation experiments.*
    - Experiments in which air was bubbled through suspensions containing reduced ^{99}Tc-containing solids (generated with 10 uM pertechnetate and then aged for three months) from both the *D. reducens* and the FC1 systems indicated a strong resistance to reoxidation. For example, in the FC1 system the sulfide-containing system (FC1 + nZVI) displayed less than 10% reoxidation over approximately 200 hr. By comparison, about 30% reoxidation occurred in the sulfide-free nZVI only system. A similar pattern was seen when reoxidation was conducted without aging of reduced Tc-containing solids (from 10 uM pertechnetate) formed in the presence of cells, sulfide and nZVI.
    - A different pattern of reoxidation was seen when 30 uM pertechnetate was used in the *D. reducens* reduction stage and the generated reduced Tc-containing solids subsequently immediately reoxidized, or after 1 or 4 months of aging. The sulfide-containing solids were initially more resistant to reoxidation, but after a few days of aeration a greater total amount of pertechnetate had been resolubilized than in the sulfide-free nZVI only treatment.

In summary, sulfide/SRB-containing systems consistently reduced aqueous pertechnetate rapidly (> 95% in the first hour), a rate similar to that for the sulfide-free, nZVI only system. However, the sulfide system was superior with respect to reoxidation of ^{99}Tc when the system contained 10 uM pertechnetate.

10.2.3. Analysis of 99Tc-containing solid phases produced in the D. reducens/nZVI system

Individual *D. reducens* cells in the nZVI system were associated with two morphologically different solid phases (determined using SEM): aggregates of circular

nanoscale material typical of nZVI, and plate-like structures that appeared as highly crystalline needles when examined by TEM (Figure 1, Figure 2).

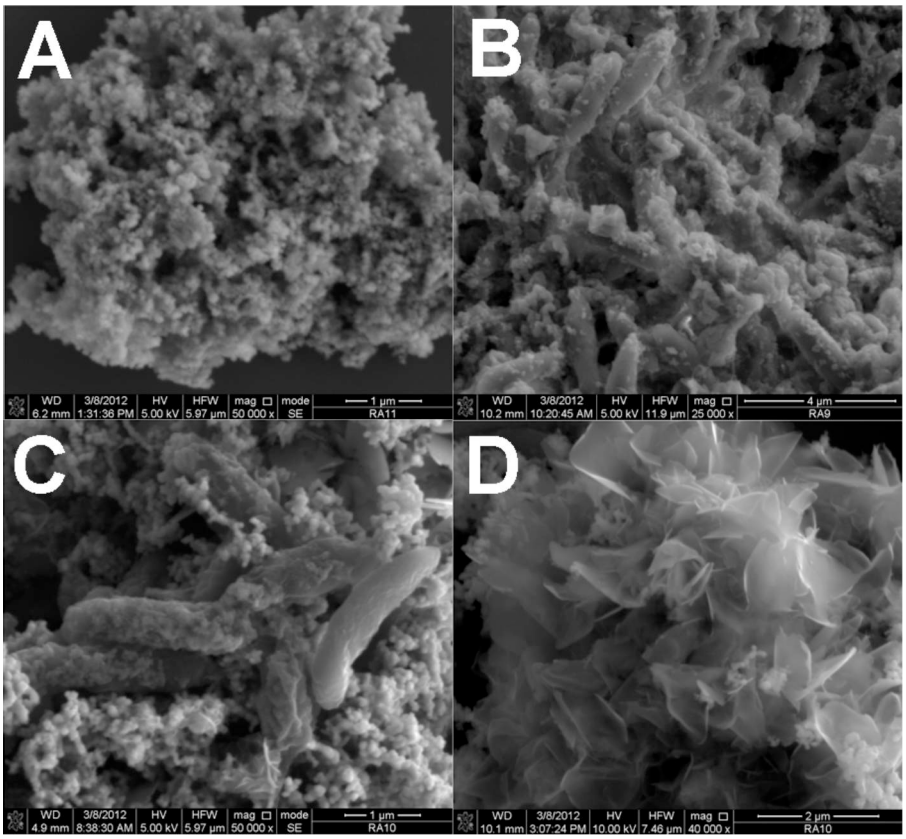

Figure 1. SEM appearance of material from nZVI only (A), *D. reducens* only (B) and *D. reducens* + nZVI (C, D).

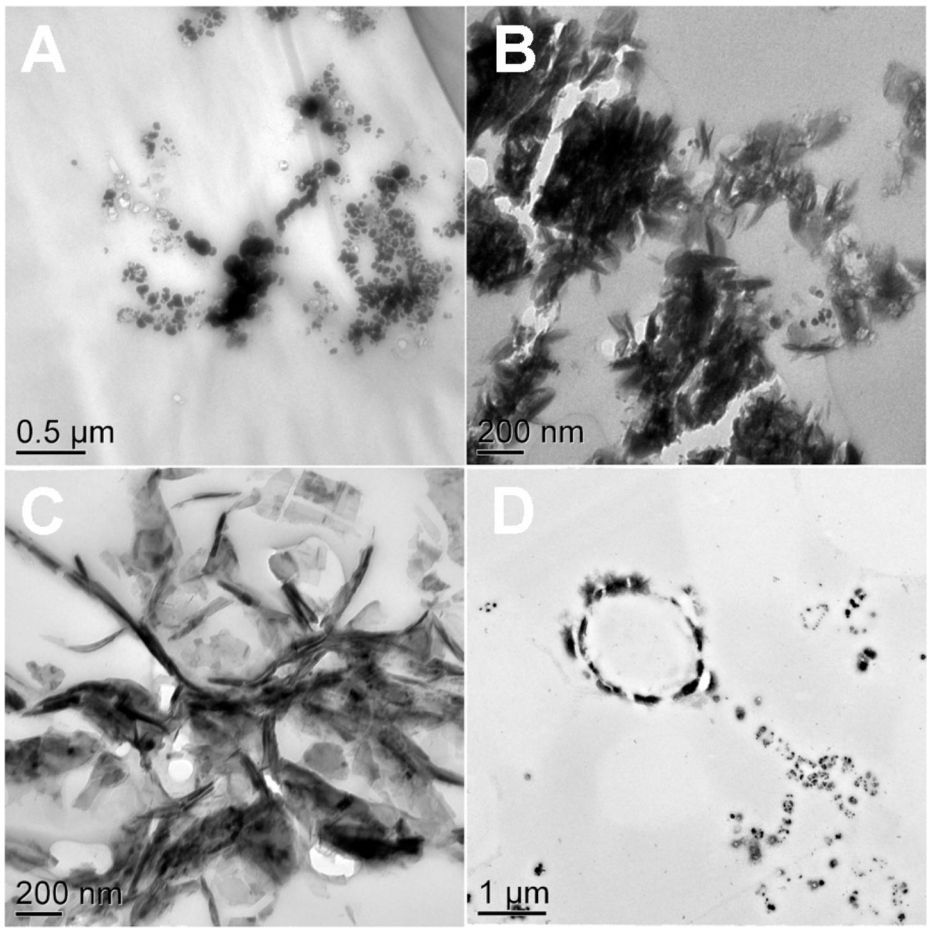

Figure 2. Solid phase morphologies seen by TEM in the nZVI only (A, B) and *D. reducens* + nZVI (C, D) treatments. (A) nZVI particles, including some arranged in a chain structure; (B) short, bar-like precipitates suggestive of vivianite; (C) Needle-like mackinawite; (D) cross-section of a *D. reducens* cell coated in precipitates.

- The circular aggregates were identified as nZVI by SEM, TEM and EDS.
- The needles were identified as mackinawite by TEM, measurement of crystal plane d-spacings from HRTEM images (Figure 3), and analysis of Selected Area Electron Diffraction (SAED) patterns.
- ^{99}Tc was found associated with both the circular aggregates and the crystalline needles. Iron and sulfur were also present in the aggregates (mostly Fe) and the needles (at approximately equal amounts).
- The nZVI only (sulfide-free) experimental system also contained ^{99}Tc in Fe-containing solid phases, presumably as Tc oxides.

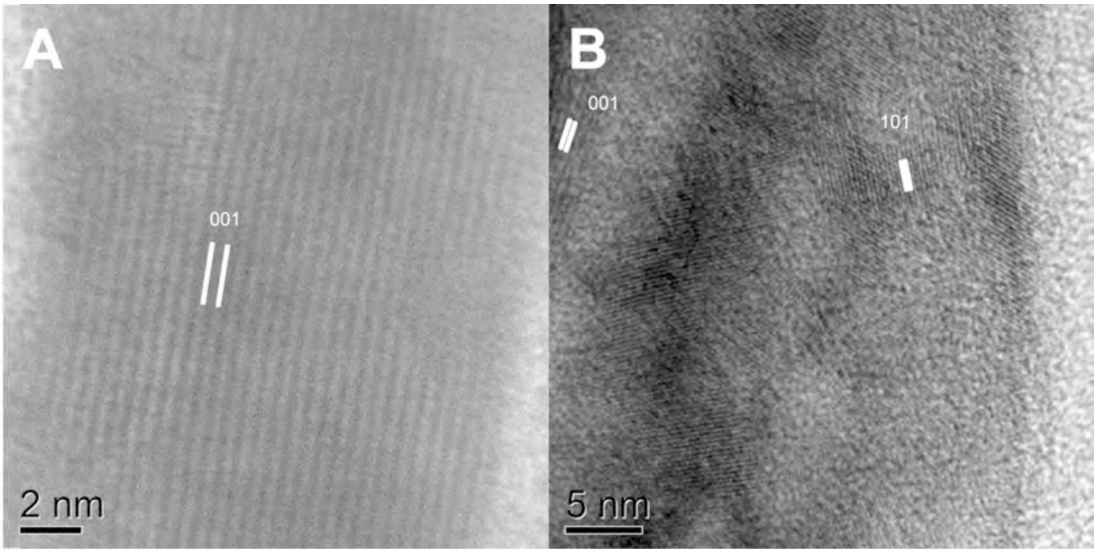

Figure 3. Fine structure of mackinawite crystals in the *D. reducens* + nZVI treatment by high resolution TEM (HRTEM). Lattice fringes with d-spacings typical of mackinawite (5.1 Å for 001 plane; 3.0 Å for 101 plane) are visible.

- XAS analysis of solid phases showed significantly different absorption structures in both XANES and EXAFS regions of the sample containing *D. reducens* + nZVI compared to the nZVI only treatment (Figure 4).
- Tc reduced by nZVI appeared to consist of Tc oxides. In the *D. reducens* + nZVI treatment, Tc was more likely to be TcS_2 (based on Fourier transform of EXAFS as Tc-S has a longer bonding distance than Tc-O).

In summary, Tc, Fe and S are present in the solid phases formed in the biotic nZVI system, and these phases are significantly different to those formed when Tc is reduced in the absence of SRB.

10.3. Characterization of the effects of sulfidation on transport processes involved in the sequestration of Tc by zerovalent iron

10.3.1. Introduction

In this section, Tc-99 mobility changed (i.e., reduction and subsequent re-oxidation) in the presence of nZVI and sulfide was investigated in the presence of subsurface sediments. Sediments add complexity to the nZVI-sulfide-pertechnetate reaction system,

because: a) ferrous iron from nZVI sorbs strongly to sediment, slowing availability for redox reactions, b) sulfide adsorbs and precipitates with available ferrous iron and other metals in the sediment as well as from the nZVI, c) sediment mineral dissolution/precipitation reactions buffer pH changes, and d) the small reductive capacity of the Hanford sediment can directly reduce a fraction of the pertechnetate. To address these complexities, some experiments in this task were conducted with just sediment and pertechnetate, and some with sediment, sulfide and pertechnetate. These results are summarized below and further described in Szecsody and others (2014) and in an unpublished manuscript (Jansik et al. 2015).

In an oxic environment, Tc(VII) is stable as pertechnetate (TcO_4^-) over a wide pH range (Icenhower et al. 2008). Under reducing conditions Tc(IV) can precipitate as either Tc hydrous oxide ($TcO_2 \cdot nH_2O$) (Icenhower et al. 2010) or Tc sulfide minerals (Tc_2S_x or $Tc_2S_{7?}$) (Lukens et al. 2003; Livens et al. 2004; Liu et al. 2007b; Liu et al. 2008; Liu et al. 2009a). While TcO_2 is readily oxidized, Tc sulfide minerals are slow to oxidize (Lukens et al., 2003), and therefore may exhibit long-term retention in reduced sediments or engineered remediation systems.

A potential approach to reductive immobilization of Tc, is the precipitation of Tc_2S_x under sulfidic conditions. The addition of sulfide (HS^-) can directly reduce Tc^{+7} to Tc_2S_7:

$$2\ TcO_4^- + 7\ HS^- + H2O \rightarrow Tc_2S_7 + 9\ OH^- \quad (1)$$

or lead to the formation of FeS (mackinawite):

$$Fe^{2+} + HS^- \rightarrow FeS_{(s)} + H^+ \quad (2)$$

which has can reduce Tc by a ligand exchange mechanism (Wolthers et al. 2005b; Wolthers et al. 2005d; Fan et al. 2013):

$$2\ TcO_4^- + 7\ FeS + n\ H_2O \rightarrow Tc_2S_7 + 7\ Fe^{3+} + n\ OH^- \quad (3)$$

The formation of FeS in the presence of aqueous Fe^{2+} and HS^-, is fast (i.e., within hours in most laboratory studies) (Rickard and Luther 2007). Recently, Liu et al (2007) reported the reduction capacity of FeS in batch systems, to be0.46 mol TcO_4^-/ mol FeS. Fan et al. (2013) found the reduction rate of TcO_4^- to increase in the presence of FeS. Liu

(Liu et al. 2007b; Liu et al. 2008) and Fan et al. (2014) found that, in the presence of FeS, Tc was precipitated as Tc_2S_7. However, Lukens (2003) used Tc K-edge extended X-ray absorption fine structure (EXAFS) analysis to identify the reduced Tc_2S_x phase as $Tc_3S_2(S_2)_4$ (or Tc_3S_{10}). Prior studies have shown that Tc_2S_x minerals oxidize slower than $TcO_2 \cdot nH_2O$ minerals. For example, Livens (2004) observed Tc_2S_x oxidation to be five times slower than $TcO_2 \cdot nH_2O$ oxidation.

Numerous prior studies have focused on the geochemistry of Tc_2S_x in aqueous solutions (Kunze et al. 1996; Livens et al. 2004; Liu et al. 2007b; Liu et al. 2009a; Fan et al. 2013), however few have evaluated the role of sediment on reduction and reoxidation of Tc. Additionally, all prior studies (Kunze et al. 1996; Livens et al. 2004; Liu et al. 2007a; Liu et al. 2009a; Fan et al. 2013) have been conducted in batch systems and have not evaluated the impact of sediment packing and advective transport on the formation and reoxidation of Tc_2S_x minerals.

The addition of nano zero-valent iron (nZVI) and HS^- could increase the Tc reduction capacity of a sediment/groundwater system and reduce the rate of reoxidation by removing potential oxidants (e.g.,. oxygen, nitrate, and sulfate). Moreover, nZVI could also potentially stimulate the growth and activity of iron- or sulfate-reducing bacteria. For example, prior studies have also shown the generation of H_2 from zero valent iron (ZVI) stimulated microbial sulfate reduction in natural sediment (Fernandez-Sanchez et al. 2004).

When added to water nZVI will hydrolyze, producing Fe^{2+}:

$$2\,Fe^0 + O_2 + 2\,H_2O \rightarrow 2\,Fe^{2+} + 4\,OH^- \quad (4)$$

$$Fe^0 + 2\,H_2O \rightarrow Fe^{2+} + H_2 + 2\,OH^- \quad (5)$$

The Fe^{2+} is expected to sorb to iron oxide surfaces forming Fe^{2+}/Fe^{3+} reaction sites, to precipitate as $Fe(OH)_2$, and/or to be removed from the system with groundwater flow. Due to increased reactive surface area on mineral surfaces and to kinetic limitations of aqueous reactions, it is expected that in sediment systems Fe^{2+}/Fe^{3+} reaction sites on iron oxides ($Fe(OH)_2$) will dominate Tc reduction in the absence of HS^-:

$$TcO_4^- + 3\,Fe(OH)_2(s) + 6\,H_2O \rightleftharpoons TcO_2 \cdot 4H_2O(s) + 3\,Fe(OH)_3(s) + OH^- \quad (6)$$

Study of Tc immobilization in systems with packed sediment and advective flow is critical for evaluating the potential effectiveness of added nZVI and/or HS^- in reducing Tc at the field scale. It is likely that the presence of sediment will increase Tc reduction rates by increasing sorbed Fe^{2+} and the number of Fe^{2+}/Fe^{3+} reaction sites. However, reactive surface area is smaller in packed sediment systems and advection may transport TcO_4^- and HS^- away (or towards) reaction sites decreasing Tc reduction rates. In addition, the stability of Tc_2S_x formed by these processes will likely depend on the sequence that reactive species are introduced into the system. For example, if TcO_4^- is introduced prior to HS^-, then the Tc is likely to be reduced by aqueous and/or sorbed Fe^{2+}. If Tc is introduced after the HS^-, then Tc will likely be reduced by FeS. If HS^- and TcO_4^- are introduced together, in a system with excess Fe^{2+}, it will result in a co-precipitation of both Tc_2S_x and FeS species.

For this portion of the study, multiple hypotheses regarding the impact of nZVI and HS^- on Tc reduction and reoxidation were evaluated. First, since the coupled Fe^{2+}/Fe^{3+} reaction sites on mineral surfaces have been shown to increase the reduction rate of Tc, it was hypothesized that a higher sediment-to-solution ratio will increase the rate of Tc reduction by nZVI. Second, it was hypothesized that the simultaneous introduction of nZVI and HS^- will result in the formation of FeS and increase the Tc reduction rate and retention of Fe^{2+}. Third, it is anticipated that HS^- concentrations may need to be in excess of the Fe^{2+}, based on the reaction stoichiometry, therefore higher concentrations of HS^- may increase Tc reduction rates. Finally, since prior studies have shown Tc_2S_x phases to be more resistant to reoxidation than $TcO_2 \cdot nH_2O$ (Liu et al. 2009b); we hypothesized that the formation of Tc_2S_x mineral phases will result in smaller Tc^{4+} oxidation rates. The rate of pertechnetate reduction (and oxidation) in Hanford sediment and Hanford sediment in the presence of sulfide was also evaluated in order to separate effects that were due to the additional presence of the nZVI.

10.3.2. Methods

Materials. A medium-to-fine grained mafic sand (Environmental Restoration Disposal Facility or ERDF Pit, 6 m deep, U.S. DOE Hanford Site, 200E area) characteristic of the Hanford formation, Eastern Washington, was used for all experiments. The sediment was

previously characterized and found to have a mineral composition of quartz (32%), plagioclase (25%), K feldspar (13%) muscovite (9%), biotite (8%), illite (2.8%), and montmorillonite and other clays (1.2%) (Serne et al. 2008). The surface area of this sediment (grain size 94.8% sand) was 31 m^2/g (Szecsody et al. 2004).

Reagent grade chemicals, including sodium sulfide ($Na_2S{\cdot}9H_2O$, Sigma-Aldrich), and 4-(2-hydroxyethyl)-1-piperazinethanesulfonic acid (HEPES, J.T. Baker) were used for all experiments. An ammonium pertechnetate stock solution (0.24 M) was used as the Tc source.

The nZVI particles were synthesized (Fan et al. 2013) using a modified version of the borohydride reduction method (Wang and Zhang 1997), where 2.43 g of $FeCl_3{\cdot}6H_2O$ were first dissolved in 500 mL of a deionized deoxygenated (DO/DI) water (70 vol %)/methanol (30 vol %) mixture (Fan et al. 2013). 1.2 g of $NaBH_4$ were dissolved in 40 mL deionized (DI) water and continuously added to the $FeCl_3$ solution via a syringe pump (KD Scientific) at a flow rate of 2 mL/min as the solution was vigorously mixed by a homogenizer (Kinematica). After introducing $NaBH_4$, the solution was allowed to sit ~ 15 minutes until H_2 generation ceased. All steps above were carried out under inert gas stream (N_2 or Ar) to avoid oxygen contact. The solution was then transferred to an anaerobic chamber (95% N_2/5% H_2, Coy Scientific). Solid nZVI particles were recovered by flash drying, as previously described (Nurmi et al. 2005). After synthesis nZVI was stored in 10 mL glass vials and capped with a 1 cm rubber septum and used with one month.

Batch Experiments. The nZVI concentration was 0.1 mg/mL in all experiments (Table 1). Two sets of batch experiments were conducted to evaluate the impact of sediment-to-solution ratio and HS^- concentration on Tc reduction rate Table 1). The first set of experiments was conducted with the sediment-to-solution ratio ranging from 0 to 1.0 g sediment/mL and initial concentrations of 10 mM HS^- and 30 mM HEPES. In the second set, the sediment-to-solution ratio was 1.0 g sediment/mL and the HS^- concentration was varied from 0 to 30 mM.

Table 1. Experimental Parameters in Sediment-Sulfide-nZVI Studies.

Experimental Objective	System Type	Matrix	HS^- Pretreat-ment (mM)	Sed. (mg/mL)	TcO_4^- (μM)	HS^- (mM)	HEPES (mM)	nZVI (mg/mL)	nZVI (mg/g sediment)	Tc Reduction Rate (hr^{-1})	Tc Reduction Rate/ mass nZVI ($hr\ mg^{-1}$)
Evaluate the effect of sediment on Tc reduction rate	Batch	--	10	0	6.01	10	30	0.1	--	4.5	4.5
	Batch	sediment	10	0.1	6.08	10	30	0.1	--	31.5	31.5
	Batch	sediment	10	1.0	6.05	10	30	0.1	--	50.8	50.8
Evaluate the effect of HS^- concentration on effects Tc reduction rate	Batch	sediment	0	1	6.24	0	0	0.1	--	48.6	48.6
	Batch	sediment	0	1	6.05	10	30	0.1	--	50.8	50.8
	Batch	sediment	0	1	5.50	30	90	0.1	--	0.57	0.57
Evaluate effect of natural sediment on Tc reduction rate	1D column	50% sediment/ 50% glass beads	0	2.6	1.37	10	30	--	0.01	1.37	14.6
	1D column	10% sediment/ 90% glass beads	0	0.52	1.30	10	30	--	0.02	0.66	3.5
Evaluate effect of HS^- concentration on Tc reduction rate	1D column	sediment	0	5.2	1.73	0	0	--	0.02	2.58	13.8
	1D column	sediment	0	5.2	0.45	2	6	--	0.02	1.52	8.1
	1D column	sediment	0	5.2	1.91	10	30	--	0.02	1.67	8.9
	1D column	sediment	0	5.2	0.76	30	90	--	0.02	3.07	16.4
Evaluate the effect of HS^- pretreatment on Tc reduction rate	1D column	sediment	2	5.2	1.75	2	6	--	0.02	0.39	2.1
	1D column	sediment	10	5.2	1.26	10	30	--	0.02	0.53	2.8
	1D column	sediment	30	5.2	1.21	30	90	--	0.02	1.08	5.8

Experiments were prepared in an anaerobic chamber (Coy Scientific). For each test, the specified amount of sediment and 9.8 mL of HS^- solution were added to 10 mL glass vials, while the vials were being briefly bubbled with helium. 20 mg nZVI were slurried with 4 mL of degassed DI and sonicated according to Fan et al. (2013). 200 µL of the nZVI slurry containing 1.0 mg were pipetted to a glass vial and capped with a 1 cm rubber stopper. The experiments were shaken for 5 min, and then set for twelve hours to allow the nZVI to hydrolyze and the Fe^{2+} to sorb to the sediment. A predetermined amount of TcO_4^- was added to each vial using a degassed syringe. Aqueous samples were collected over 24 hours using a degassed syringe, and filtered with a 0.45 m syringe filters. Tc reduction rates were determined by fitting a first order kinetic equation to measured Tc concentrations.

Column Experiments. Three sets of column experiments were conducted to evaluate the impact of natural sediment amount, sulfide pretreatment, and sulfide concentration on Tc reduction rate (Table 1). Column experiments were conducted in PEEK columns (10 cm long x 0.765 cm diameter, ~1.6 cm^3 pore volume). All columns were packed in an aerobic chamber (Coy Scientific). 8 g of sediment were degassed with helium, weighted and slurried with 8 mL of degassed DI water. In some experiments, the amount of natural sediment was varied by substituting 0.5 mm glass beads (Spheriglass, Potters Industries LLC) for sediment by mass. 20 mg of nZVI were mixed with 4 mL of degassed DI and sonicated for 5 min as previously described. 0.170 mg nZVI (in 34 L suspension) were pipetted into 8.97 g of sediment and immediately mixed using a vortex mixer for 60 seconds. The sediment slurry was then centrifuged for 10 minutes at 3000 rpm. The sediment/nZVI mixture was returned to the anaerobic chamber, excess fluid was decanted and the sediment was remixed to ensure uniform nZVI distribution.

Columns were packed using a slurry method and allowed to set for 12 hours before flow was introduced to allow nZVI and sulfide to react. For experiments pretreated with HS^-, 3.0 mL (~ 2 pore volumes) of the HS^- solution were injected into the column immediately after packing. HS^- solutions were prepared and stored in zero headspace sampling bags to minimize volatilization of the HS^-. Flow was delivered to the

columns using a HPLC pump (Hitachi, L-6200) at a pore water velocity of 150 cm hr^{-1}. Influent and effluent samples were analyzed for pH and Tc concentrations.

Columns were maintained anaerobic for 3 months to evaluate crystallization of precipitates, which may initially be partially amorphous. Reoxidation experiments were conducted by injecting oxygen saturated DI water for 100 pore volumes at a pore water velocity of 43.5 cm/hr. Effluent samples were collected with an autosampler (Isco Foxy 200) over the duration of the experiment. Stop-flow column experiments were conducted in some cases to evaluate the slow pertechnetate reduction by the low concentration of ferrous iron or other reduced metal surface phases. These stop-flow column experiments are essentially batch experiments (no flow), but at a high (5 – 6 g/mL) sediment/solution ratio of field systems. These experiments consisted of initially injecting aqueous pertechnetate into the sediment column (2.2 cm diameter by 35.5 cm length) in continuous flow experiments (described above), then for the next 4000 h there is no flow in the system. Samples are collected at selected times ranging from 10 h to 4000 h by injecting 4 mL of anaerobic groundwater into one end of the column and collect 4 mL of water that has reacted with the sediment for the elapsed time. A total of nine aqueous samples were collected given the 45 mL pore volume, then solid phase samples were collected when the sediment column was taken apart.

Tc reduction rates, k were determined by fitting:

$$k = \frac{-\ln\frac{C}{C_o}}{\tau} \tag{7}$$

to the measured Tc concentrations, where C was the effluent TcO_4^- concentration, C_o was the influent concentration, and τ was the residence time within the column. An identical series of column experiments were conducted to evaluate the transport of HS^- and Fe^{2+} in the absence of Tc.

Sequential Extractions. Sequential liquid extractions were conducted on sediments from the column experiments to evaluate changes in Tc mineral association after reduction. For these extractions, six grams of sediments of reduced sediment were placed in contact with 7.5 mL of the particular extraction solution in a centrifuge tube and shaken for a

specified time. Samples were then centrifuged at 3000 rpm for 10 min, the extraction fluid was decanted, filtered through a 0.45 μm filter, and retained for analysis. *Aqueous Tc* was defined as the portion of Tc extractable by shaking with synthetic Hanford groundwater (Szecsody et al. 2010) for 1 hr. Sorbed Tc was defined as the portion of Tc extractable by a carbonate solution (0.0114 M $NaHCO_3$, 0.0028 M Na_2CO_3, 1 h) after aqueous Tc was removed [note: while a carbonate solution makes sense for U, the anion TcO4– should desorb with a high concentration in any salt solution, including this]. Following the carbonate extraction, a series of four additional extractions were used to target: rind carbonates (1 mol/L sodium acetate, pH 5. 1 h), residual carbonates (acetic acid, pH 2.3, 5 days), iron oxides (0.1 mol/L ammonium oxalate, 0.1 mol/L oxalic acid,1 h), and aluminosilicates (8 mol/L HNO_3, 95 °C, 2 h).

Analysis. Tc-99 concentrations were analyzed using liquid scintillation counting with a 0.1 to 500 KeV energy window for 30 minutes and an 11-point quench standard set; Opti-flur (Perkin Elmer) was used for low ionic strength samples and Hionic-Fluor (Perkin Elmer) was used for high ionic strength samples.

HS^- concentrations were measured using the methylene blue method, (Hach Method 8131). Effluent samples were measured immediately after collection to minimize HS^- volatilization. Fe^{2+} concentrations were measured using the ferrozine method (Stookey 1970).

10.3.3. Results

10.3.3.1. Tc Reduction and Immobilization in Sediments or Sediments with Sulfide

In natural oxic sediments, pertechnetate migration is generally reported to move nearly unretarded because of no sorption or reduction/precipitation. In this study, slow pertechnetate reduction and immobilization was observed in columns with pertechnetate infiltration into natural (untreated) Hanford sediments with no co-contaminants under anaerobic conditions (Figure 4, open diamonds).

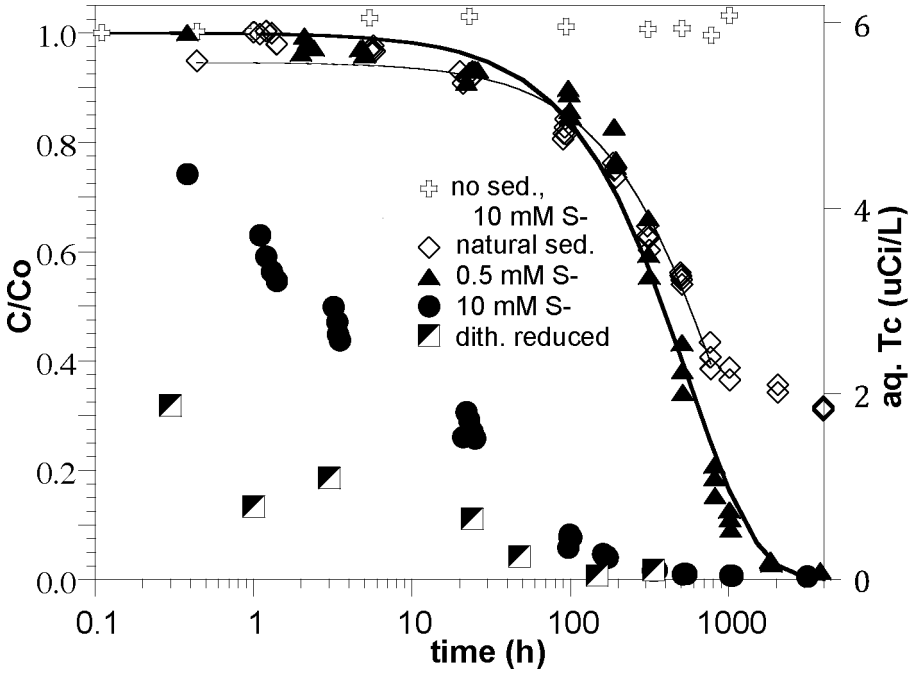

Figure 4. TcO_4 reduction in anaerobic sediment (pH 8) with no treatment (natural sediment) or with chemical (dithionite) reduction of sediment (resulting in adsorbed ferrous iron) or sulfide addition to sediments (Szecsody et al. 2014).

Pertechnetate was removed from aqueous solution in a batch system (presumed by surface reductants) with a removal half-life of 613 h. Reduction was likely due to dissolution of mafic minerals with a small reductive capacity such as biotite or magnetite, or structural ferrous iron in montmorillonite (Stucki et al. 1984). Characterization of the iron surface phases of the untreated sediment shows no adsorbed ferrous iron, but other ferrous iron surface phases present. Ferrous phases make up 35% of the total iron. This experimental system has the high sediment/water ratio of field sediment, so rates and extent of pertechnetate removal would be somewhat more representative than low sediment/water batch experiments. The pertechnetate removal rate was very slow (0.0015 to 0.002 nmol g^{-1} h^{-1}, Table 2), and the Tc accumulation on the sediment surface is low, at 1.5 nmol g^{-1}. The first 60% of the aqueous pertechnetate (4 x 10^{-6} mol L^{-1}) was removed by 1000 h, then an additional 10% between 1000 and 4000 h. Limited reductive capacity of this Hanford sediment was observed in a previous study (Stevens and McKinley 2000). The incomplete removal may be caused by a limited mass of surface

reductant, or possibly by the formation of a Tc(IV)-natural organic matter complex (fraction organic carbon averaged 0.058 ± 0.021% (Szecsody et al. 2013).

Table 2. Pertechnetate removal rates from aqueous solution

treatment	system	rxn. time (h)	sed./H_2O (g/mL)	aq. TcO_4 (mol/L)	Tc removal rate (h^{-1})	Tc removal rate (nmol g^{-1} h^{-1})	Tc surface mass (nmol/g)	Tc surface mass %*	Tc Kd (mL/g)
none, natural sediment	column	550	5.11	4.40E-06	0.0023	0.0020	1.48	0.91**	0.005
none, natural sediment	column, stop flow	0 - 4000	4.58	5.89E-06	0.0011	0.0015	0.61	0.3**	0.004
sulfide, 0.5 mM, pH 8	column, stop flow	0 - 4000	5.2	4.39E-06	0.0018	0.0015	0.56	1.7	0.04
sulfide, 10 mM, pH 8	column, stop flow	0 - 4000	4.58	3.90E-06	0.11	0.094	1.59	26.1	0.54
sulfide, 10 mM, pH 12	column, stop flow	0 - 4000	6.63	4.03E-06	1.07	0.65	3.94	42.0	1.7
0.1M dithionite pretreat	batch	0 - 350	0.10	1.10E-05	3.82	420	108	98.2	
0.1M dithionite pretreat	column	5.0	4.13	4.10E-05	1.52	15.1	148	> 99.5	
0.1M dithionite pretreat	column	5.32	4.45	1.38E-04	1.71	53.0	712	> 99.5	
0.1M dithionite pretreat	column	0.412	4.33	1.38E-04	21.9	698	1400	> 99.5	

* % of injected or initial pertechnetate **limited Tc removal observed

At field scale, pertechnetate infiltration with co-contaminants through sediments is controlled by physical processes and partially by geochemical processes such as co-contaminant dissolution of specific mineral phases, which directly or indirectly influence pertechnetate mobility, as previously observed for uranium in alkaline wastes (Wan 2004a, b, Tokunaga et al., 2004, Szecsody et al., 2013, 2014). When pertechnetate is co-disposed with 4M NaOH, the rate of pertechnetate reduction increases one to two orders of magnitude (removal rates 0.07 to 0.22 nmol g^{-1} h^{-1} or half-life 23 h (Szecsody et al. 2014). In addition, Tc precipitates could also be coated by non-Tc precipitates, given the significant mineral dissolution and precipitation that occurs with alkaline waste contact with the sediments (Szecsody et al. 2012), described in the following section). The incorporation of metal hydroxide precipitates into other insoluble mineral species over time has been reported in the literature (Ainsworth et al. 1994; Coughlin and Stone 1995; Martinez and McBride 1998). For uranium, there is clear evidence of the resistance of reduced U(IV)O_2 precipitates to oxidize/remobilize under oxic conditions (Payne et al. 1994; Szecsody et al. 1998).

For comparison to Tc reduction rates observed in natural sediments, two simple reductants (adsorbed ferrous iron and aqueous sulfide) were added to the sediment/groundwater system. With added adsorbed ferrous iron (by pretreatment with dithionite/carbonate), the pertechnetate reduction rate (15 to 700 nmol g^{-1} h^{-1}) was three to four orders of magnitude more rapid than the untreated sediment (Figure 4, squares

and Table 2). The dithionite-treated sediment contained 7.7 mol g^{-1} of adsorbed ferrous iron (and a total ferrous iron concentration of 46 mol g^{-1}, with 4 mol L^{-1} pertechnetate. Rapid pertechnetate reduction (300 - 1700 nmol g^{-1} h^{-1}) was previously observed in aqueous systems (pH 7 and 8) with 0.4 mmol L^{-1} aqueous ferrous iron and 11 mol L^{-1} pertechnetate (Zachara et al. 2007).

In contrast, addition of high concentrations of sulfide (0.5 to 10 mmol L^{-1} excess relative to 4 mol L^{-1} pertechnetate) did increase the TcO_4^- reduction rate (Figure 4, closed circles, at 10 mM S^-, pH 8) compared to natural sediments, but only if high sulfide concentration was used. Aqueous 0.5 mM sulfide alone with no sediment (pH 8) does not result in any loss of aqueous pertechnetate over 1000 h (Figure 4). The low sulfide concentration (0.5 mM S^-, pH 8) had little effect (triangles, Fig 3.1) on the pertechnetate reduction rate compared with untreated sediment. Although the 0.5 mM S– concentration is 80 times greater than the TcO_4^- concentration (Table 2), much of the S– is likely precipitating with other metals such as iron, as observed in sulfide/zero valent iron systems (see following section), in which Tc was identified associated with surface FeS. High sulfide concentration (10 mM S^-) at pH 8 increased the pertechnetate reduction rate to 0.094 nmol g^{-1} h^{-1}, similar to rates observed in NaOH–treated sediments (Table 2). The 10 mM aqueous sulfide at pH 10.6 increased the pertechnetate reduction rate an additional order of magnitude. The increase in the TcO_4^- reduction rate with 10 mM S^- addition possibly reflects precipitation of some TcS_x phases, which are more slowly oxidized compared with TcO_2.

10.3.3.2. Tc Reduction in Sediments with sulfide and nZVI.

Batch experiments were conducted with varying sediment-to-solution ratio and HS^- concentration to evaluate the effects of these parameters on Tc reduction rates. The batch experiment conducted with no sediment had the slowest Tc reduction rate (4.5 h^{-1}). Reduction rates increased with increasing sediment-to-solution ratio (Table 1); an increase in sediment-solution ratio from 0 to 0.1 mg/mL increased the Tc reduction rate to 31.5 hr^{-1}. At a sediment-to-solution ratio of 1 mg/mL the Tc reduction rate increased to 50.8 hr^{-1}. Tc reduction was rapid in batch experiments with sediment, with nearly all Tc reduced after 1 hr (Figure 4).

In batch experiments conducted with a sediment-to-solution ratio of 1 g/mL, there was only a slight difference between the Tc reduction rate at HS^- concentrations of 0 and 10 mM (Table 1). In both experiments, nearly all the Tc was reduced within 0.02 hours (Figure 5), with k ~50 hr^{-1} (Table 1). The experiment conducted with 30 mM HS^- had a smaller Tc reduction rate (0.57 hr^{-1}). After 24 hrs, nearly all the Tc was removed from solution in all experiments.

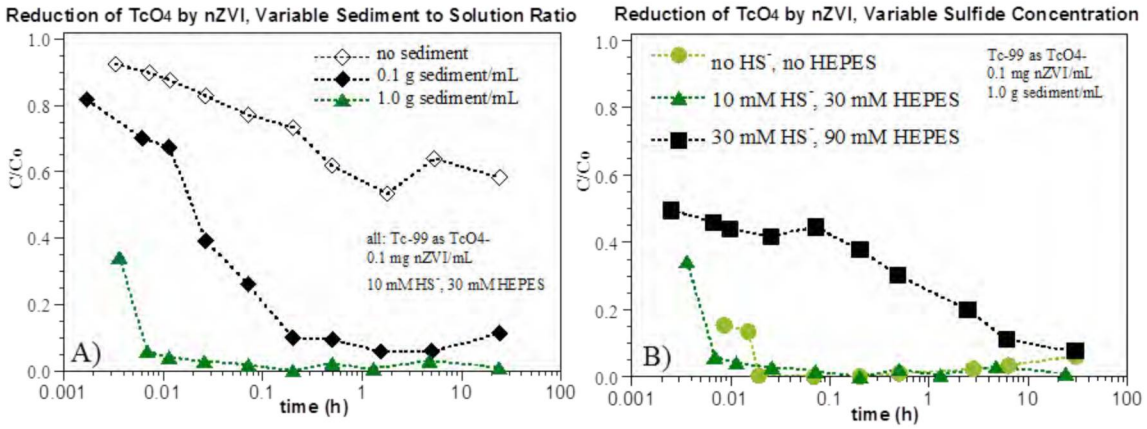

Figure 5. a) Effect of sediment-to-solution ratio on Tc reduction and b) effect of HS^- on Tc reduction by nZVI in batch experiments.

10.3.3.3. Tc Reduction in Sediments with Sulfide and nZVI during Flow

The effect of sediment on Tc reduction rate in column experiments was evaluated by replacing a portion of the natural sediment with glass beads (Table 1 and Table 3). The glass beads were used to vary the reactive surface area analogous to the variation of the sediment-solution ratio in batch experiments. The sediment surface area (for ferrous iron adsorption) was 31.6 m^2/g, whereas the 0.25 mm glass bead surface area was <0.2 m^2/g. After 9.8 pore volumes, the column with 100% sediment retained more Tc than the two columns with glass beads (Table 3). The mass of Tc retained per gram sediment was similar for the 100% sediment and the 50% sediment/50% glass bead columns (Table 3); however, the mass of Tc retained per gram sediment was higher in the 10% sediment/90% glass bead column. The Tc reduction rates (Table 1) were smaller for the column with 10% sediment/ 90% glass beads than for the column with 50% sediment/ 50% glass beads.

Table 3. Effect of sediment/glass bead ratio on Tc retention.

Material	uMol Tc Retained	uMol Tc Retained g nZVI^{-1}	uMol Tc Retained g Sediment^{-1}
100% Sediment	0.027	0.16	0.0034
10% Sediment, 90% Glass Beads	0.017	0.10	0.0192
50% Sediment, 50% Glass Beads	0.011	0.13	0.0017

HS^- pretreatment was used in some column experiments to evaluate how the prior formation of FeS minerals would effect the subsequent Tc reduction rate. The amount of Tc retained in column with no HS^- pretreatment was the highest (0.028 µmol), followed by 10 mM HS^- pretreatment (0.018 µmol), and 0 mM HS^- pretreatment (0.010 µmol) (Figure 6). Additional columns conducted with pretreatment and concentrations of 2 and 30 mM HS^- had smaller reduction rates than experiments conducted at the same HS^- concentrations without pretreatment (Table 1). As a whole, columns with HS^- pretreatment had slower Tc reduction rates than columns conducted without pretreatment.

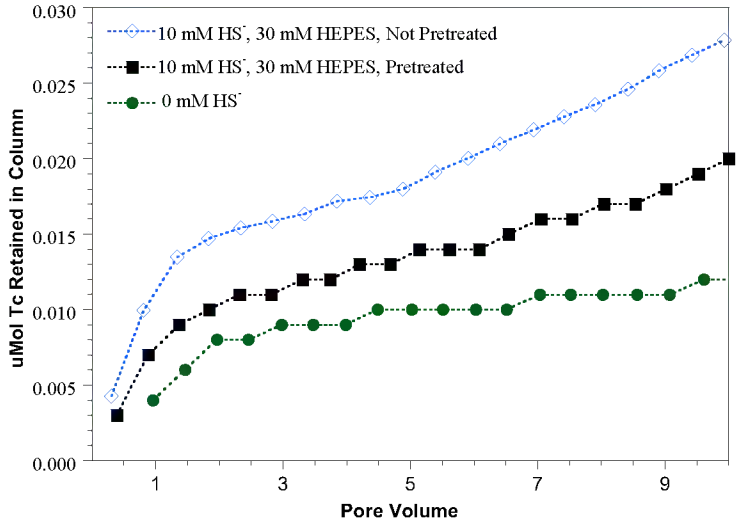

Figure 6. Effect of HS^- pretreatment on Tc retention in column experiments.

Parallel experiments conducted without Tc were used to evaluate the effect of HS^- pretreatment on Fe^{2+} adsorption. It was hypothesized that formation of FeS minerals, generated by pretreatment, would increase the retention of Fe^{2+}. The column pretreated

with 10 mM HS^- retained nearly all the introduced Fe^{2+} for 10 pore volumes (Figure 7). The experiment without pretreatment retained only 60% of the added Fe^{2+}. The 50% sediment/50% glass bead column, which was not pretreated, had <5% of the initial Fe^{2+} retained in the untreated column after 9.8 pore volumes. Additionally, sorbed Fe^{2+} measurements showed that five times more Fe^{2+} was retained in the column with pretreatment than in the column without pretreatment (Table 4).

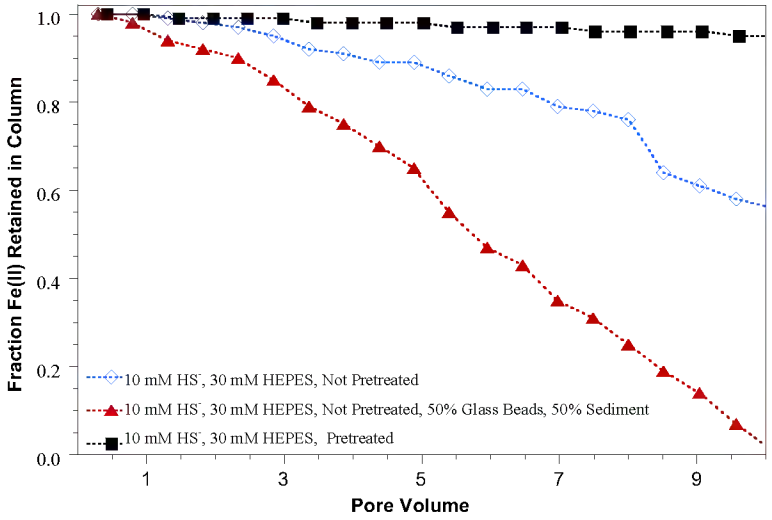

Figure 7. Effect of HS^- pretreatment on Fe^{2+} retention in column experiments.

Table 4. Absorbed Fe^{2+} in column experiments conducted without Tc.

Material	Pretreatment with HS^-	HS^- (mM)	HEPES (mM)	Percent Fe Sorbed to Surface
Sediment	No	10	30	4%
Sediment	Yes	10	30	20%
50% Sediment, 50% Glass Beads	No	10	30	3%

Experiments were also conducted in columns with no pretreatment to evaluate the impact of HS^- concentration on Tc reduction rate (Figure 8). The column pretreated with 2 mM HS^- retained less Tc than the column pretreated with 30 mM HS^-. The column pretreated with 10 mM HS^- retained the most Tc. The reduction rate in the column pretreated with 30 mM HS^-, was the highest at 3.07 hr^{-1} (Table 1).

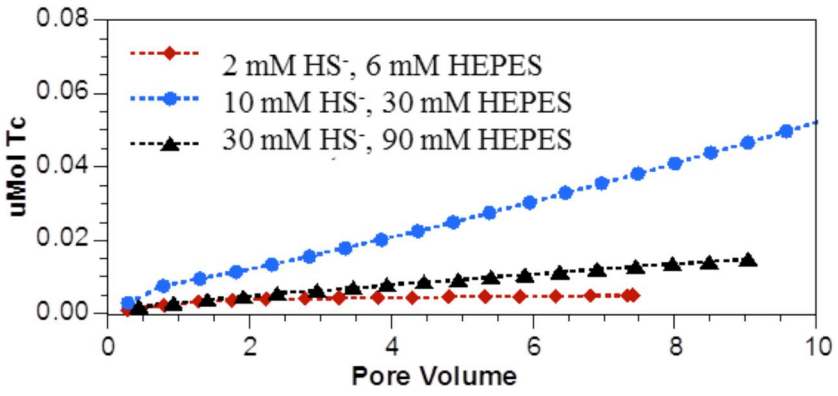

Figure 8. Effect of HS^- concentration on Tc retention in unpretreated columns.

In columns that were not pretreated, effluent samples contained black particles and were visibly cloudy. Filtered and unfiltered samples were analyzed to determine the potential effect of particulate formation on measured Tc concentrations. The column with 10 mM HS^-had 64% of the influent Tc was precipitated in the Tc particulate phase (Figure 9). For the purpose of these experiments, the Tc particulate phase was not treated as aqueous or retained, because it was highly mobile and reoxidized rapidly. Figure 10 illustrates the distribution of cumulative Tc mass in the aqueous, particulate and sediment phases over the duration of the 10 mM HS^- experiment.

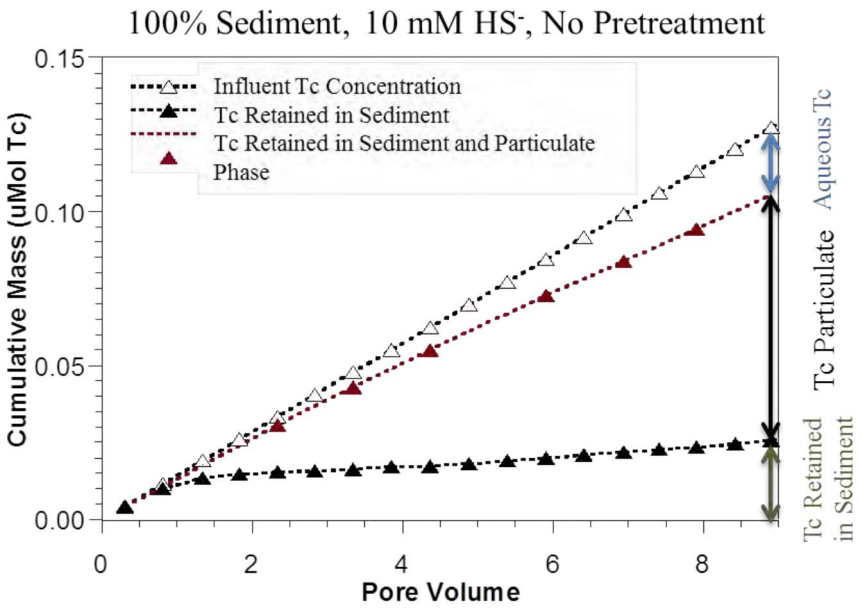

Figure 9. Tc Retention in sediment, particulate, and aqueous phases during the 10 mM HS^- experiment.

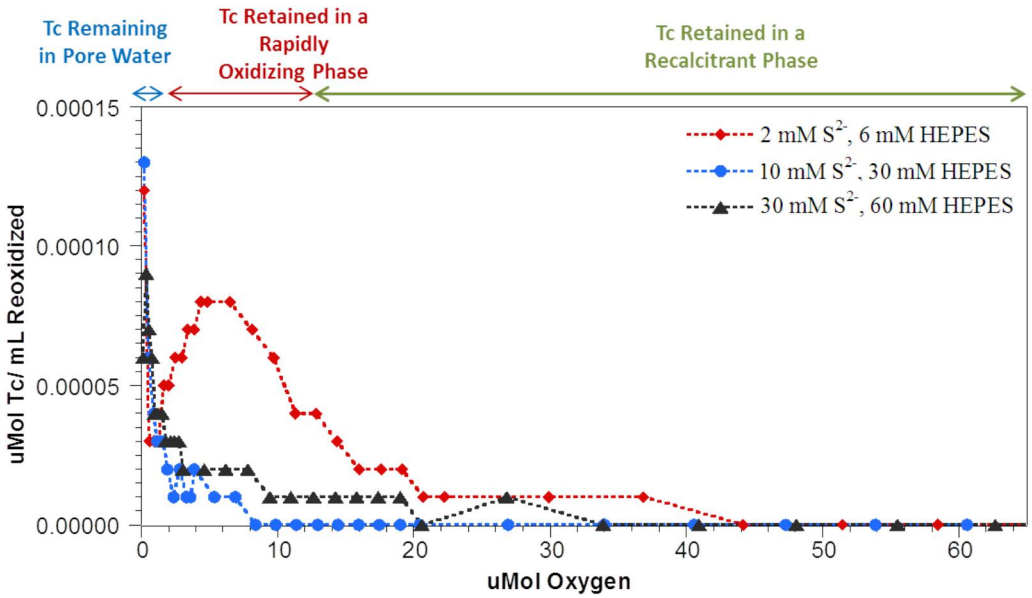

Figure 10. Effect of HS^- on reoxidation of previously reduced Tc.

10.3.3.4. Tc Oxidation in Natural Sediments or Sediments with Sulfide during flow.

Oxidation of natural untreated sediment in a flow-through column (which contains precipitated Tc) resulted in an initial rapid release of Tc (Figure 11a, open circles) within the first pore volume, followed by a slow rate of oxidation, (0.06 to 0.12 nmol g^{-1} h^{-1}, Table 5). This may reflect multiple mechanisms retaining Tc on the surface including reduced Tc as well as pertechnetate trapped in immobile pore volume. If mixed Tc^{IV}-Fe precipitates formed, one study showed these precipitates are slow to oxidize (Zachara et al. 2007). For comparison, the oxidation rate of aqueous TcO_2•nH2O (i.e., no sediment) was reported as 0.062 – 0.077 nmol L^{-1} h^{-1} (Liu et al. 2007b). Although 91 to 95% of the Tc was remobilized within 10 h (20 pore volumes of air-saturated water), additional oxidation was not conducted due to detection limits with liquid scintillation counting. Solid phase extractions were made along the length of the sediment column to quantify the mineral association of remaining Tc. Solid phase extractions showed Tc was present on the surface partially in mobile (i.e., easy to extract) phases as well as harder to extract precipitates (Figure 12a). There was also a greater concentration of technetium near the inlet of the column, which implies rapid precipitation.

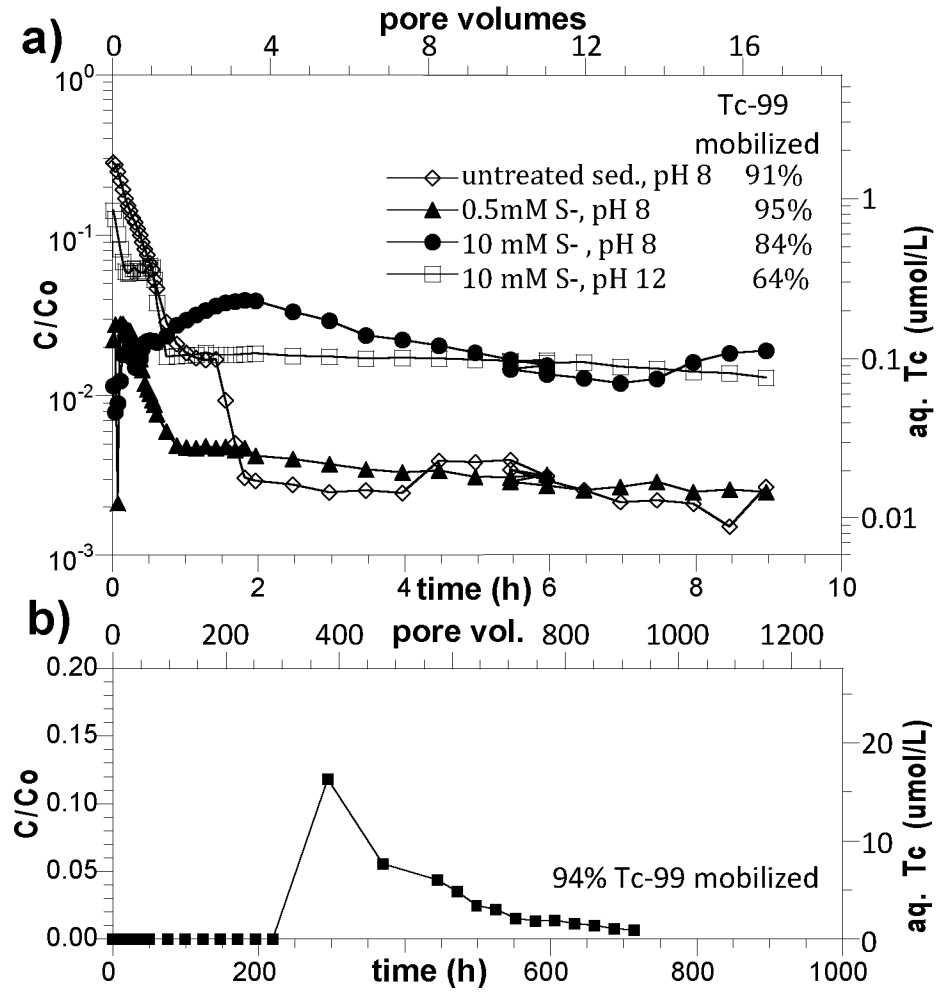

Figure 11. Surface Tc release from sediment back into aqueous solution upon system oxidation in: a) untreated and S− treated sediments in 1-D columns, and b) chemically-reduced sediment producing predominantly adsorbed ferrous iron.

Oxidation of surface Tc in two idealized systems (i.e., sediment with adsorbed ferrous iron or aqueous sulfide) was investigated for comparison of Tc oxidation rates and extent to natural sediment and NaOH-treated sediment systems. Oxidization of Tc from the sediment with adsorbed ferrous iron (i.e., dithionite-reduced) in both batch and 1-D columns resulted in a rapid oxidation rate (2.6 to 6.8 nmol g^{-1} h^{-1}, Table 5), with oxidation of nearly all surface Tc. In a batch system, 98.2% of the technetium was remobilized after 400 h of oxidation, whereas in a 1-D column system, 94.2% of the technetium was remobilized after 730 h (Figure 11b). In the 1-D column system, Tc remained immobile for the first 250 h with air-saturated water injection as there was

considerable excess surface ferrous iron that was consumed by the influent dissolved oxygen. However, once the sediment was oxidized, Tc oxidized and was remobilized quickly and nearly completely. This behavior was expected, as $Tc^{IV}O_2$ is the likely precipitate phase.

Table 5. Tc oxidation rates from sediment experiments without and with sulfide.

treatment	system	rxn. time (h)	sed./H_2O (g/mL)	aq. TcO_4 (mol/L)	Tc oxidation rate (h^{-1})	Tc oxidation rate (nmol g^{-1} h^{-1})	Tc surface mass remaining (nmol/g)	Tc surface mass remaining %**
none, natural sediment	column	450	4.47	4.10E-05	0.0063	0.058	0.69	9.1
none, natural sediment	column	8	4.58	5.89E-06	0.094	0.121	0.005	4.7
sulfide, 0.5 mM, pH 8	column, stop flow	8	5.20	4.39E-06	0.014	0.011	0.47	4.5
sulfide, 10 mM, pH 8	column, stop flow	8	4.58	3.90E-06	0.039	0.033	0.95	16
sulfide, 10 mM, pH 12	column, stop flow	8	6.63	4.03E-06	0.028	0.017	3.6	36
0.1M dithionite pretreat	batch	400	0.10	1.10E-05	0.024	2.6	0.19	1.8
0.1M dithionite pretreat	column	730	4.14	1.38E-04	0.204	6.8*	0.75	5.8

* after 400 h of no Tc oxidation ** of initial surface Tc

In the sediment system with sulfide addition, slower technetium oxidation (and remobilization) was expected, as TcS_x phases oxidize more slowly. With a low sulfide concentration (0.5 mM), the rate of Tc oxidation, was slower (0.011 nmol g^{-1} h^{-1}) than the natural sediment (0.06 to 0.12 nmol g^{-1} h^{-1}), even though the total Tc mass oxidized was similar to the natural sediment (91-95%, Figure 11a) and a similar Tc surface mass concentration remained (0.5-0.9 nmol g^{-1}, Table 5). Solid phase extractions of sediments along the column length (Figure 12b) showed surface Tc was present in different phases (similar to the natural sediment), but mass was distributed evenly along the column length, suggesting a slower reduction/precipitation rate compared to the natural sediment (Figure 12a) with greater Tc mass near the column inlet. At higher (10 mM) sulfide concentration, the Tc oxidation rate (0.014 to 0.033) was also about an order of magnitude slower than the natural sediment and the Tc concentration remaining on the surface was greater (0.5 to 3.6 nmol g^{-1}) than the natural sediment (0.005 to 0.7 nmol g^{-1}, Table 5). The fraction of Tc mass oxidized in 10 h of exposure to air-saturated water was 84% (10 mM S–, pH 8) and 64% (10 mM S^{-}, pH 10.6). Sequential liquid extractions of the sediment after oxidation showed significantly greater Tc precipitate near the column inlet for 10 mM sulfide at five times the concentration for pH 8 (Figure 12c) and eight times the concentration for pH 10.6 (Figure 12d). This may represent a more rapid TcS_x

precipitation rate under alkaline conditions, as the pH at the column inlet was higher (inlet pH 12.0, effluent pH 9.5).

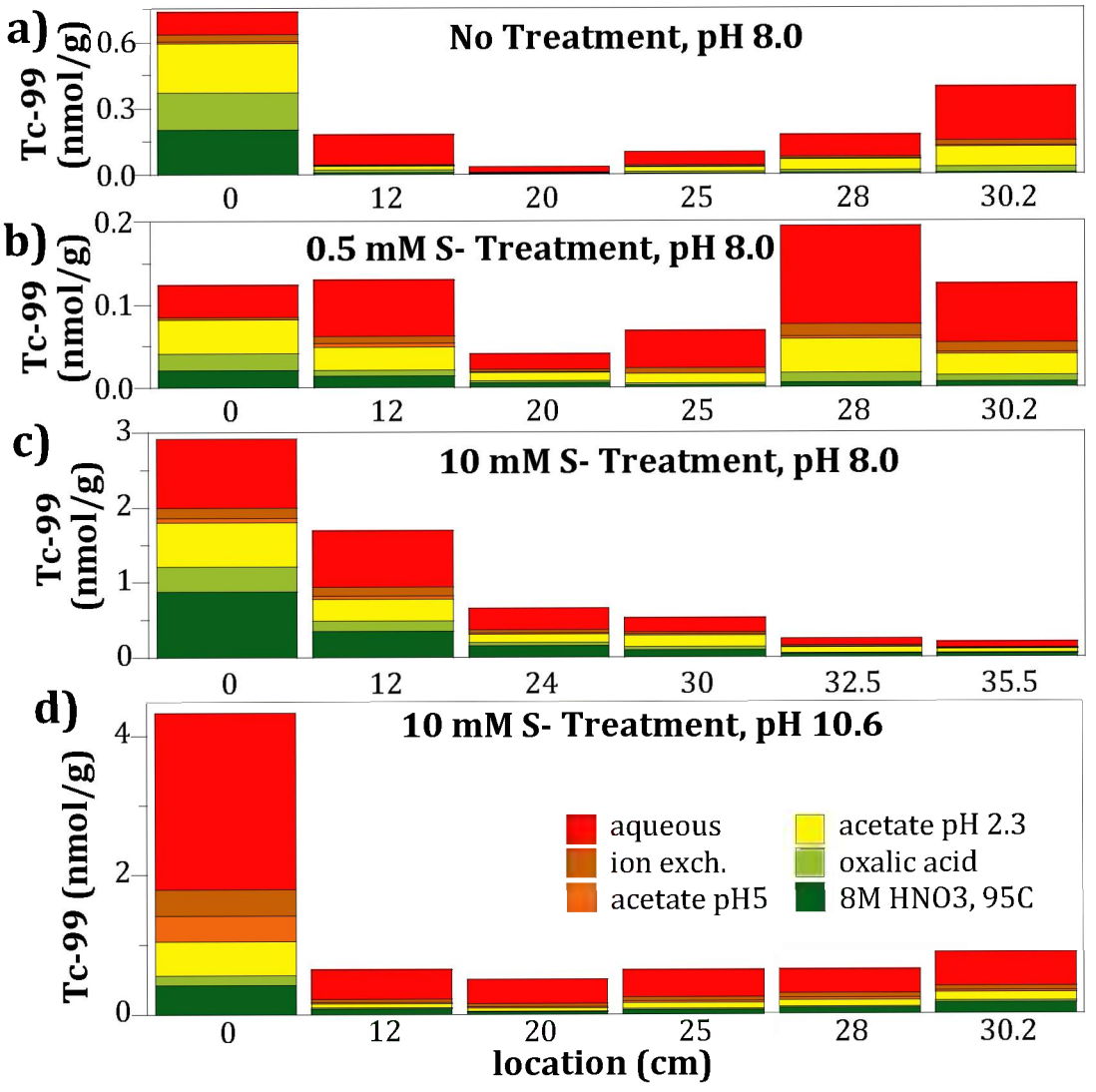

Figure 12. Tc extracted from sediments after oxidation for: a) no treatment, b) 0.5 mM S− treatment, c) 10 mM S− treatment, and d) 10 mM S− treatment at pH 10.6

10.3.3.5. Tc Oxidation in Sediments with sulfide and nZVI during flow.

Column experiments conducted with HS^- pretreatment (2, 10, and 30 mM HS^-) did not retain enough Tc to accurately measure reoxidation rates, therefore reoxidation experiments were performed only in columns conducted without HS^- pretreatment. In all

columns, the initial Tc peak in the effluent was attributed to the Tc remaining in the pore water at the conclusion of the reduction experiment (Figure 10). A secondary peak occurred after 1 µMol O_2 was introduced into the column, which is attributed to Tc reoxidation. The experiment conducted with 2 mM HS^- had the largest amount of Tc reoxidation (Figure 10). The column conducted with 10 mM HS^- had the least amount of Tc reoxidized.

Reoxidized sediments from the columns pretreated with 10 and 30 mM HS^- required low pH extraction fluids to remove the Tc associated with the sediment (Figure 13). At increasing sulfide concentration, a greater mass of Tc was retained by the sediment, even after 20 pore volumes of oxic water injection (Figure 13). This may have been caused by formation of a higher fraction TcSx precipitates (in the excess sulfide water) or formation of iron sulfide precipitates, which may have coated Tc surface phases, slowing their reoxidation.

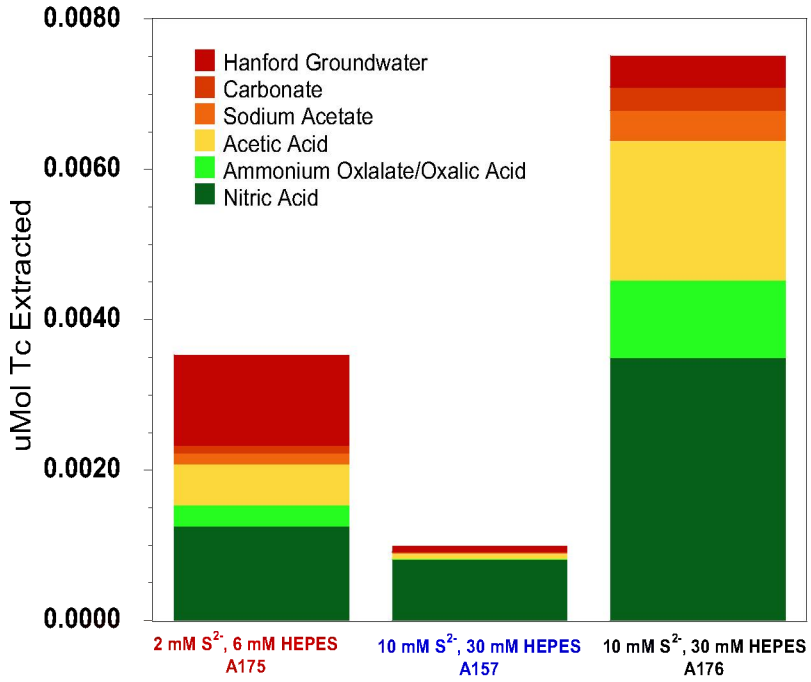

Figure 13. Tc remaining in sediments after oxidation, as shown by Tc sequential extraction after reoxidation.

10.3.3.6. Discussion

In this portion of the study, the effects of nZVI and HS^- on Tc reduction and reoxidation were evaluated in batch and column experiments. In batch experiments, Tc reduction rates increased as the sediment –to-solution ratio increased. Column experiments conducted with glass beads substituted for a portion of the sediment had more rapid Tc reduction, suggesting that sediment surfaces provide reaction sites for Tc reduction. This hypothesis is supported by others (Cui and Eriksen 1996a; Cui and Eriksen 1996b; Peretyazhko et al. 2008a; Peretyazhko et al. 2008b; Fredrickson et al. 2009), who have also shown the reduction of Tc by Fe^{2+} to be faster in sediment systems than in aqueous solutions. These results are consistent with the hypothesis that sediment is important in increasing the reduction rate of Tc.

This study hypothesized that the introduction of FeS would increase the Tc reduction rate and the retention of Fe^{2+} within the column experiments. Pretreatment of columns with HS^- was designed to generate the mineral mackinawite (FeS), which has been shown to reduce Tc (Liu et al. 2006; Liu et al. 2007b; Liu et al. 2008; Liu et al. 2009b; Fan et al. 2013). Geochemical modeling of batch systems (Geochemist's Workbench 7.0), indicated that at a pH of 8, the introduction of 10 mM HS^- with 2 mM nZVI, should facilitate the rapid (hours) formation of mackinawite (FeS). The modeling results are consistent with results in Fan *et al.* (2013) who used Mossbauer spectroscopy to show that mackinawite formed in batch systems with 10 mM HS^- and 2 mM Fe^{2+}.

The formation of FeS in pretreated columns is consistent with the retention of Fe^{2+} (Figure 7), which showed that only 95% of the Fe^{2+} was retained in the column. This was much higher than the 60% Fe^{2+} that was retained in the 10 mM HS^- column with no pretreatment (Figure 7). Extractions also directly confirmed the mass of sorbed Fe^{2+} and determined the column with HS^- pretreatment to have five times the amount of sorbed Fe^{2+} as the column without pretreatment (Table 4). These findings are congruent with the hypothesis that introducing HS^- and nZVI prior to TcO_4^- will form, mackinawite and reduce the amount of Fe^{2+} advected from the system.

Columns pretreated with HS^- prior to the introduction of Tc retained less Tc and had smaller Tc reduction rates than columns conducted without pretreatment. This

finding was contrary to our hypothesis that FeS minerals would increase the rate of Tc reduction. The difference in Tc retention is likely due to a smaller Tc reduction rate by mackinawite. Tc reduction via sorbed Fe^{2+} and aqueous HS^- may be faster than the ligand exchange mechanism thought to be responsible for Tc reduction by mackinawite (Wolthers et al. 2005a; Wolthers et al. 2005c). Additionally, it is possible that the formation of mackinawite on nZVI surfaces slowed the dissolution of Fe^{2+} from nZVI, which under other conditions would have also been utilized for Tc reduction. Overall, it appears that the co-precipitation of Tc_2S_7 with FeS is kinetically faster than Tc reduction by FeS.

The impact of HS^- concentration on Tc reduction was evaluated in column and batch experiments. Batch experiments with sediment conducted with 10 mM HS^- had a larger Tc reduction rate than experiments conducted with higher HS^- concentration. While this result was not anticipated, it appears that an increase in HS^- concentration may increase the formation of a mobile Tc_2S_x particulate phase that reduces the amount of reduced Tc retained in the sediment. This result is consistent with Fan *et al.* (2013), who also observed a decrease in Tc reduction rate at higher HS^- concentrations and also observed the formation of Tc_2S_x precipitates.

Column experiments showed that 10 mM HS^- was the most effective at reducing Tc, however 30 mM HS^- resulted in a larger Tc reduction rate. At 10 and 30 mM, the HS^- was in excess of all other reactants in the system. For 2 mM HS^-, the concentration of Fe^{2+} was stoichiometrically balanced for FeS generation, but did not leave additional HS^- in the system for the formation of Tc_2S_7. Decreased HS^- concentration may have produced a system where some of the TcO_4^- was directly reduced to $TcO_2 \bullet nH_2O$.

The formation of Tc containing particles was observed in column experiments conducted without HS^- pretreatment, when HS^- was present in stoichiometric excess. Experiments conducted with higher HS^-concentrations retained more Tc in the particulate phase than in the sediment. In the 10 mM HS^- column 64% of the influent Tc was retained in the column and particulate phases (Figure 9). Saiki *et al.* (2003), observed the formation of particulates in systems with HS^- and TcO_4^- and identified the particulate phase as a Tc_2S_7 colloid. For the purpose of this experiment, the Tc particulate was not

computed in the retained Tc mass; however, in systems with smaller pore water velocities, and finer material, the Tc particulate phase might be less mobile than TcO_4^-, depending on surface charge and reactivity

Column experiments conducted with 2 mM HS^- had the most Tc mobilized during reoxidation, which is consistent with the formation of $TcO_2 \bullet nH_2O$ and Tc_2S_x. Differences between the reoxidation of the 10 mM and 30 mM HS^- columns were small, but overall the Tc retained in the 10 mM HS^- column was more stable. This is consistent with the hypothesis that Tc oxidation being faster in Tc_2S_x phases.

Consistent differences between the reaction rates in column and batch systems were observed. Tc reduction rates in the columns were five times slower than in corresponding batch experiments when normalized by nZVI concentration (Table 1). This difference is likely due to the introduced complexities of reactant delivery in column systems. For the Tc reduction to proceed all reactive species must be present at the same location and same time, often this is more difficult to achieve in advective systems. Additionally, we must also consider the retention of the Fe^{2+} species. These experiments clearly show that advective processes decreased the reaction rates, and are an important consideration for experimental design.

The findings of this study are relevant for work currently being conducted on reductive stabilization of TcO_4^-. This study indicates that reductive immobilization in Tc_2S_x phases appears to be more stable than in $TcO_2 \bullet nH_2O$. It was also determined that the addition of sediment, is important in sustaining the reaction, thus indicating that mineral surfaces, in addition to reactive nZVI area, are important in the reduction of Tc. Additionally, it appears that the order in which reactants are introduced may be important in determining the reduction kinetics.

For the implementation of this remediation method additional research is needed to determine how the application of nZVI and HS^- could be scaled to the field. In this study we did not address the delivery of nZVI to Tc contaminated sediments. Current research indicates nZVI can be delivered to contaminated zones with a surfactant slurry (Kanel and Choi 2007), however this could complicate the subsurface chemistry and will need further study.

An additional consideration for implementation of this strategy, is the fate of the Tc particulate phase, which is likely Tc_2S_7. Since colloidal transport remains a topic of concern for long term contamination sources, it will be important to understand the transport properties of the particulate phase (Honeyman 1999). For the case of Tc, the presence of colloids will likely produce a decrease in mass movement. In unsaturated systems, it been shown that colloidal transport is slowed by the presence of air-water interfaces and high ionic strength pore waters (Bradford and Torkzaban 2008; Gao et al. 2008), nonetheless, it is an important consideration prior to field scale implementation.

Additionally, for the purpose of this study we assumed that all reduction would be abiotic, however biotic activity surrounding nZVI barriers has been shown to also generate sulfidic conditions (Fernandez-Sanchez et al. 2004).

10.3.4. Conclusions

In this section of the project, we evaluated the use of nZVI and HS^- for the remediation of TcO_4^-. Experimental results showed that the presence of sediment, sulfide, and nZVI was important in the mass removal of TcO_4^- from pore water. Batch and column experiments conducted with less sediment, retained a lower mass of Tc.

Pertechnetate was reduced in natural, untreated Hanford sediment under anaerobic conditions, which could occur in low permeability zones in the field. The observed reduction rate is slow (0.02 nmol g^{-1} h^{-1}) and extent limited (final Tc surface mass < 1.5 nmol g^{-1}), implying low ferrous iron (or other reductant) concentrations. Characterization of ferrous phases show indicate < 0.1 µmol g^{-1} adsorbed ferrous iron, but 24 µmol g^{-1} other ferrous phases, some of which may be redox reactive. Pertechnetate in sediments with NaOH co-contaminant (Szecsody et al. 2014) results in a more rapid reduction (0.07 to 0.2 nmol g^{-1} h^{-1}) to a significantly greater extent (6 to 60 nmol g^{-1} Tc surface mass). In contrast, pertechnetate reduction in a model system (sediment containing adsorbed ferrous iron as the reductant) was rapid (15 to 600 nmol g^{-1} h^{-1}) leaving high Tc on the surface (110 to 1400 nmol g^{-1}). Tc reduction in sediments containing 0.5 to 10 mM sulfide showed a significantly slower reduction rate (0.02 to 0.1 nmol g^{-1} h^{-1}) and low Tc

surface concentration (0.5 to 1.6 nmol g^{-1}) that was similar to observations in the natural sediment.

Oxidation of Tc precipitated in the natural untreated sediment resulted in a slow oxidation rate (0.06 to 0.12 nmol g^{-1} h^{-1}) of nearly all of the Tc (91 to 95%) within 10 hours. Liquid extractions of remaining surface Tc showed the presence of unidentified hard to extract precipitates. In contrast, oxidation of Tc from the model system containing only adsorbed ferrous iron resulted in rapid Tc oxidation (2.6 to 6.8 nmol g^{-1} h^{-1}) also of nearly all of the Tc (96 to 98%). Oxidation surface Tc in sulfide-laden sediment resulted in Tc oxidation rates that were slower than the natural sediment (0.01 to 0.03 nmol g^{-1} h^{-1}), and left significant Tc remaining (64% to 95% oxidized), especially the sulfide system at pH 10.6. Because surface Tc in the natural sediment is oxidized 1 to 2 orders of magnitude more slowly than the ferrous iron containing sediment, it suggests the surface Tc phase is different, as there are no other dissolution/precipitation reactions occurring in the system. There is also no sulfide in the natural sediment. Oxidation of Tc in NaOH-treated sediments (Szecsody et al. 2014) resulted in slow Tc oxidation (~0.05 nmol g^{-1} h^{-1}) of a small fraction of the surface Tc (13% to 23%). The Tc remaining on the surface was Tc^{IV} (by XANES), and autoradiography and elemental maps of Tc (by electron microprobe) showed Tc was present associated with specific minerals, rather than being evenly distributed on the surface. While Tc was not associated with total Fe, measured low concentrations of ferrous iron may be adsorbed to iron oxides and clays could have led to the observed Tc surface distribution. The surface phase of Tc was not identified by elemental analysis, but may be the readily oxidizing phase $Tc^{IV}O_2$ coated with aluminosilicate precipitates.

It was also shown, that while the introduction of nZVI and HS^- through pretreatment did likely result in the formation of FeS phases. The TcO_4^- reduction rates in these experiments were slower than experiments without the addition of sulfide, and in Tc was retained. Experiments conducted with the co-precipitation of FeS and Tc_2S_x (no pretreatment) retained larger amounts of Tc. Unpretreated columns run with a concentration of 10 mM HS^- had a higher Tc mass removal than columns with a 2 mM and 30 mM HS^- concentration. This result was attributed to a stoichiometric imbalance of

the reactants. Reoxidation of sediment-nZVI-sulfide columns containing Tc, showed that experiments conducted with higher HS^- concentrations were more effective at retaining the Tc than columns conducted with lower HS^- concentrations.

For the broader area of research, it appears that remediation of Tc under sulfidic conditions could be promising for long-term stabilization of Tc. The potential to stabilize Tc in a phase resistant to reoxidation could be applied across numerous sites contaminated with Tc, which is important for protecting groundwater resources and preventing the spread of contamination.

11. References

Beech, W. B. and J. Sunner (2004). "Biocorrosion: towards understanding interactions between biofilms and metals." Current Opinion in Biotechnology **15**(3): 181-186.

Bradford, S. A. and S. Torkzaban (2008). "Colloid transport and retention in unsaturated porous media: A review of interface-, collector-, and pore-scale processes and models." Vadose Zone Journal **7**(2): 667-681.

Cui, D. Q. and T. E. Eriksen (1996a). "Reduction of pertechnetate by ferrous iron in solution: Influence of sorbed and precipitated Fe(II)." Environmental Science & Technology **30**(7): 2259-2262.

Cui, D. Q. and T. E. Eriksen (1996b). "Reduction of pertechnetate in solution by heterogeneous electron transfer from Fe(II)-containing geological material." Environmental Science & Technology **30**(7): 2263-2269.

Da Silva, M. L. B., R. L. Johnson and P. J. J. Alvarez (2007). "Microbial characterization of a subsurface undergoing treatment with a permeable reactive iron barrier." Environ. Engineering Sci. **24**(8): 1122-1127.

Fan, D., R. P. Anitori, B. M. Tebo, et al. (2013). "Reductive sequestration of pertechnetate ($^{99}TcO_4^-$) by nano zero-valent iron (nZVI) transformed by abiotic sulfide." Environmental Science and Technology **47**(10): 5302-5310.

Fan, D., R. P. Anitori, B. M. Tebo, et al. (2014). "Oxidative remobilization of technetium sequestered by sulfide-transformed nano zerovalent iron." Environmental Science and Technology **48**(13): 7409–7417.

Fernandez-Sanchez, J. M., E. J. Sawvel and P. J. J. Alvarez (2004). "Effect of Fe-0 quantity on the efficiency of integrated microbial-Fe-0 treatment processes." Chemosphere **54**(7): 823-829.

Fredrickson, J. K., J. M. Zachara, A. E. Plymale, et al. (2009). "Oxidative dissolution potential of biogenic and ablogenic TcO_2 in subsurface sediments." Geochimica et Cosmochimica Acta **73**(8): 2299-2313.

Gao, B., T. S. Steenhuis, Y. Zevi, et al. (2008). "Capillary retention of colloids in unsaturated porous media." Water Resources Research **44**(4): -.

Honeyman, B. D. (1999). "Colloidal culprits in contamination." Nature **397**: 23-24.

Icenhower, J. P., N. P. Qafoku, W. Martin and J. M. Zachara (2008). The Geochemistry of Technetium: A Summary of the Behavior of an Artificial Element in the Natural Environment, Pacific Northwest National Lab**:** 74.

Icenhower, J. P., N. P. Qafoku, J. M. Zachara and W. J. Martin (2010). "The Biogeochemistry of Technetium: A Review of the Behavior of an Artificial Element in the Natural Environment." American Journal of Science **310**(8): 721-752.

Jansik, D., J. E. Szecsody and J. Istok (2015). "Effect of sulfide and nano zero-valent iron on pertechnetate reduction and reoxidation during saturated flow in Hanford sediments." Journal of Contaminant Hydrology: in prep.

Johnson, R. L., R. B. Thoms, R. O'Brien Johnson, J. T. Nurmi and P. G. Tratnyek (2008). "Mineral precipitation upgradient from a zero-valent iron permeable reactive barrier." Ground Water Monitoring & Remediation **28**(3): 56-64.

Johnson, R. L., P. G. Tratnyek, R. Miehr, B. B. Thoms and J. Z. Bandstra (2005). "Reduction of hydraulic conductivity and reactivity in zero-valent iron columns by oxygen and TNT." Ground Water Monitoring & Remediation **25**(1): 129-136.

Kanel, S. R. and H. Choi (2007). "Transport characteristics of surface-modified nanoscale zero-valent iron in porous media." Water Science and Technology **55**(1-2): 157-162.

Kunze, S., V. Neck, K. Gompper and T. Fanghanel (1996). "Studies on the immobilization of technetium under near field geochemical conditions." Radiochimica Acta **74**: 159-163.

Little, B. J., F. B. Mansfeld, P. J. Arps and J. C. Earthman (2003). "Microbiologically influenced corrosion." Encyclopedia of Electrochemistry **4**: 662-685.

Liu, D. J., J. Yao, B. Wang, C. Bruggeman and N. Maes (2007a). "Solubility study of Tc(IV) in a granitic water." Radiochimica Acta **95**: 523-528.

Liu, Y., J. Terry and S. Jurisson (2007b). "Pertechnetate immobilization in aqueous media with hydrogen sulfide under anaerobic and aerobic environments." Radiochimica Acta **95**(12): 717-725.

Liu, Y., J. Terry and S. Jurisson (2008). "Pertechnetate immobilization with amorphous iron sulfide." Radiochimica Acta **96**(12): 823-833.

Liu, Y., J. Terry and S. Jurisson (2009a). "Potential interferences on the pertechnetate-sulfide immobilization reaction." Radiochimica Acta **97**(1): 33-41.

Liu, Y. J., S. S. Jurisson and J. Terry (2006). "Gaseous immobilization of pertechnetate in aqueous media with hydrogen sulfide: Stoichiometry and kinetics." Abstracts of Papers of the American Chemical Society **231**.

Livens, F. R., M. J. Jones, A. J. Hynes, et al. (2004). "X-ray absorption spectroscopy studies of reaction of technetium, uranium, and neptunium with mackinawite." Journal of Environmental Radioactivity **74**: 211-219.

Lukens, W. W., J. J. Bucher, D. K. Shuh and N. M. Edelstein (2003). Evolution of technetium speciation in reducing grout. Berkeley, CA, Lawrence Berkeley National Laboratory.

Lukens, W. W., J. J. Bucher, D. K. Shuh and N. M. Edelstein (2005). "Evolution of technetium speciation in reducing grout." Environmental Science and Technology **39**(20): 8064-8070.

Nurmi, J. T., P. G. Tratnyek, V. Sarathy, et al. (2005). "Characterization and properties of metallic iron nanoparticles: Spectroscopy, electrochemistry, and kinetics." Environmental Science & Technology **39**(5): 1221-1230.

Payne, T., J. Davis and T. Waite (1994). "Uranium retention by weathered schists - the role of iron minerals." Radiochimica Acta **66/67**: 297-303.

Peretyazhko, T., J. M. Zachara, S. M. Heald, et al. (2008a). "Heterogeneous reduction of Tc(VII) by Fe(II) at the solid-water interface." Geochimica Et Cosmochimica Acta **72**(6): 1521-1539.

Peretyazhko, T., J. M. Zachara, S. M. Heald, et al. (2008b). "Reduction of Tc(VII) by Fe(II) sorbed on Al (hydr)oxides." Environmental Science & Technology **42**(15): 5499-5506.

Rickard, D. and G. W. Luther (2007). "Chemistry of iron sulfides." Chemical Reviews **107**(2): 514-562.

Saiki, Y., M. Fukuzaki, T. Sekine, Y. Kino and H. Kudo (2003). "Technetium(VII) sulfide colloid growing observed by laser-induced photoacoustic spectroscopy." Journal of Radioanalytical and Nuclear Chemistry **255**(1): 101-104.

Serne, R. J., M. J. Lindberg, M. M. Valenta, et al. (2008). Characterization of vadose zone 28 sediments below the T tank farm: boreholes C4104, C4105, 299-W10-196, and RCRA29 borehole 299-W11-39. Richland, WA, Pacific Northwest National Lab.

Stevens, T. O. and J. P. McKinley (2000). "Abiotic controls on H_2 production from basalt-water reactions and implications for aquifer biogeochemistry." Environmental Science & Technology **34**(5): 826-831.

Stookey, L. (1970). "Ferrozine - A New Spectrophotometric Reagent for Iron." Analytical Chemistry **72**(7).

Stucki, J. W., D. C. Golden and C. B. Roth (1984). "Effects of reduction and reoxidation of structural iron on the surface charge and dissolution of dioctahedral smectites." Clays Clay Miner **32**(5J): 350-356.

Szecsody, J., M. Truex, N. Qafoku, et al. (2013). "Influence of acidic and alkaline co-contaminants on uranium migration in vadose zone sediments." Journal of Contaminant Hydrology **151**: 155-175.

Szecsody, J., M. Truex, L. Zhong, et al. (2012). "Geochemical and Geophysical Changes During NH3 Gas Treatment of Vadose Zone Sediments for Uranium Remediation." Vadose Zone Journal **11**(4).

Szecsody, J., M. Truex, L. Zhong, et al. (2010). Remediation of Uranium in the Hanford Vadose Zone Using Gas-Transported Reactants: Laboratory Scale Experiments in Support of the Deep Vadose Zone Treatability Test Plan for the Hanford Central Plateau Richland, WA, Pacific Northwest National Laboratory.

Szecsody, J., M. Williams, J. Fruchter, V. Vermeul and D. Sklarew (2004). "In Situ Reduction of Aquifer Sediments: Enhancement of Reactive Iron Phases and TCE Dechlorination." Environmental Science and Technology **38**: 4656-4663.

Szecsody, J. E., A. Chilakapati, J. M. Zachara and A. L. Garvin (1998). "Influence of iron oxide inclusion shape on Co(II/III) EDTA reactive transport through spatially heterogeneous sediment." Water Resources Research **34**(10): 2501-2514.

Szecsody, J. E., D. P. Jansik, J. P. McKinley and N. J. Hess (2014). "Influence of alkaline co-contaminants on technetium mobility in vadose zone sediments." J. Environ. Radioact. **135**: 147-160.

Videla, H. A. and L. K. Herrera (2005). "Microbiologically influenced corrosion: Looking to the future." Int. Microbiol. **8**(3): 169-180.

Wang, C. B. and W. X. Zhang (1997). "Synthesizing nanoscale iron particles for rapid and complete dechlorination of TCE and PCBs." Environmental Science & Technology **31**(7): 2154-2156.

Wolthers, M., L. Charlet, P. R. Van der Linde, D. Rickard and C. H. Van der Weijden (2005a). "Surface chemistry of disordered mackinawite (FeS)." Geochimica Et Cosmochimica Acta **69**(14): 3469-3481.

Wolthers, M., L. Charlet, P. R. van Der Linde, D. Rickard and C. H. van Der Weijden (2005b). "Surface chemistry of disordered mackinawite (FeS)." Geochim. Cosmochim. Acta **69**(14): 3469-3481.

Wolthers, M., L. Charlet, C. H. Van der Weijden, P. R. Van der Linde and D. Rickard (2005c). "Arsenic mobility in the ambient sulfidic environment: Sorption of arsenic(V) and arsenic(III) onto disordered mackinawite." Geochimica Et Cosmochimica Acta **69**(14): 3483-3492.

Wolthers, M., L. Charlet, C. H. van Der Weijden, P. R. van der Linde and D. Rickard (2005d). "Arsenic mobility in the ambient sulfidic environment: Sorption of

arsenic(V) and arsenic(III) onto disordered mackinawite." Geochim. Cosmochim. Acta **69**(14): 3483-3492.

Zachara, J. M., S. M. Heald, B.-H. Jeon, et al. (2007). "Reduction of pertechnetate [Tc(VII)] by aqueous Fe(II) and the nature of solid phase redox products." Geochimica et Cosmochimica Acta **71**(9): 2137-2157.

12. List of Publications

1. Fan, D., R. P. Anitori, B. M. Tebo, P. G. Tratnyek, J. S. Lezama Pacheco, R. K. Kukkadapu, L. Kovarik, M. H. Engelhard, and M. E. Bowden. 2014. Oxidative remobilization of technetium sequestered by sulfide-transformed nano zerovalent iron. Environ. Sci. Technol. 48(13): 7409–7417. [10.1021/es501607s]

2. Fan, D., R. P. Anitori, B. M. Tebo, P. G. Tratnyek, J. S. Lezama Pacheco, R. K. Kukkadapu, M. H. Engelhard, M. E. Bowden, L. Kovarik, and B. W. Arey. 2013. Reductive sequestration of pertechnetate ($^{99}TcO_4^-$) by nano zero-valent iron (nZVI) transformed by abiotic sulfide. Environ. Sci. Technol. 47(10): 5302-5310. [10.1021/es304829z]

3. Turcio-Ortega, D., D. Fan, P. G. Tratnyek, E.-J. Kim, and Y.-S. Chang. 2012. Reactivity of Fe/FeS nanoparticles: Electrolyte composition effects on corrosion electrochemistry. Environ. Sci. Technol. 46(22): 12484-12492. [10.1021/es303422w]

4. Szecsody, J. E., D. P. Jansik, J. P. McKinley, and N. J. Hess. 2014. Influence of alkaline co-contaminants on technetium mobility in vadose zone sediments. J. Environ. Radioact. 135: 147-160. [10.1016/j.jenvrad.2014.02.003]

5. Fan, D. 2015. Reactivity of Reducing Iron Minerals in the Subsurface: Implications for Contaminant Remediation. Part I: Remediation of Technetium by Sulfidated Nano Zerovalent Iron. Ph.D. Dissertation, Oregon Health & Science University.

6. Jansik, D. P. 2013. Physiochemical Mechanisms for the Transport and Retention of Technetium. Ph.D. Dissertation, Oregon State University.

13. List of Presentations

1. Fan, D., R. Anitori, J. Nurmi, P. Tratnyek, B. Tebo, J. Szecsody, and J. McKinley. 2011. Technetium reduction and permanent sequestration by abiotic and biotic formation of low-solubility sulfide mineral phases. pp NORM-225.

7. Fan et al., Technetium Sequestration under Sulfidogenic Conditions Stimulated by Nanoscale Zerovalent Iron (nZVI), Poster Presentation, Gordon Research Conference in Environmental Science: Water, June, 2010, Holderness, NH.

8. D. Fan, R. P. Anitori, P. Tratnyek, B. Tebo, J. Szecsody, and J. McKinley (2011). Technetium Sequestration under Sulfidogenic Conditions Stimulated by Nanoscale Zero Valent Iron (nZVI), Migration conference, Sep 2011, Beijing, China. Poster
9. Fan et al., Reductive Sequestration of Pertechnetate ($^{99}TcO_4^-$) under Sulfidogenesis Stimulated by Nano Zero-valent Iron (nZVI) and Limited Remobilization, Poster Presentation, Gordon Research Conference in Environmental Science: Water, June, 2012, Holderness, NH.
10. Fan et al., Reductive Sequestration of Pertechnetate ($^{99}TcO_4^-$) under Sulfidogenesis Stimulated by Nano Zero-valent Iron (nZVI) and Limited Remobilization, Platform Presentation, 2nd International Symposium on Bioremediation and Sustainable Environmental Technologies, June, 2013 Jacksonville, FL
11. Fan et al., Reductive Sequestration of Pertechnetate ($^{99}TcO_4^-$) under Sulfidogenesis Stimulated by Nano Zero-valent Iron (nZVI) and Limited Remobilization, Platform Presentation, American Chemical Society Annual Conference, September, 2013 Indianapolis, IN.
12. Fan et al., Reductive Sequestration of Pertechnetate ($^{99}TcO_4^-$) under Sulfidogenesis Stimulated by Nano Zero-valent Iron (nZVI) and Limited Remobilization, Poster Presentation, Gordon Research Seminar in Environmental Science: Water, June, 2014, Holderness, NH.
13. Tratnyek, P.G. and D. Fan (2013) Technetium reduction and permanent sequestration by formation of low-solubility sulfide mineral phases. Goldschmidt Conferernce, Florence, Italy

14. Appendix

Two open access journal articles.

Environmental Science & Technology

Article

pubs.acs.org/est

Reductive Sequestration of Pertechnetate ($^{99}TcO_4^-$) by Nano Zerovalent Iron (nZVI) Transformed by Abiotic Sulfide

Dimin Fan, Roberto P. Anitori, Bradley M. Tebo, and Paul G. Tratnyek*

Division of Environmental and Biomolecular Systems, Oregon Health & Science University, 20000 NW Walker Road, Beaverton, Oregon 97006, United States

Juan S. Lezama Pacheco†

Stanford Synchrotron Radiation Lightsource, Menlo Park, California 94025, United States

Ravi K. Kukkadapu, Mark H. Engelhard, Mark E. Bowden, Libor Kovarik, and Bruce W. Arey

Environmental Molecular Sciences Laboratory, Pacific Northwest National Laboratory, Richland, Washington 99354, United States

Supporting Information

ABSTRACT: Under anoxic conditions, soluble pertechnetate ($^{99}TcO_4^-$) can be reduced to less soluble $TcO_2{\cdot}nH_2O$, but the oxide is highly susceptible to reoxidation. Here we investigate an alternative strategy for remediation of Tc-contaminated groundwater whereby sequestration as Tc sulfide is favored by sulfidic conditions stimulated by nano zerovalent iron (nZVI). nZVI was pre-exposed to increasing concentrations of sulfide in simulated Hanford groundwater for 24 h to mimic the onset of aquifer biotic sulfate reduction. Solid-phase characterizations of the sulfidated nZVI confirmed the formation of nanocrystalline FeS phases, but higher S/Fe ratios (>0.112) did not result in the formation of significantly more FeS. The kinetics of Tc sequestration by these materials showed faster Tc removal rates with increasing S/Fe between 0 and 0.056, but decreasing Tc removal rates with S/Fe > 0.224. The more favorable Tc removal kinetics at low S/Fe could be due to a higher affinity of TcO_4^- for FeS than iron oxides, and electron microscopy confirmed that the majority of the Tc was associated with FeS phases. The inhibition of Tc removal at high S/Fe appears to have been caused by excess HS^-. X-ray absorption spectroscopy revealed that as S/Fe increased, the pathway for Tc(IV) formation shifted from $TcO_2{\cdot}nH_2O$ to Tc sulfide phases. The most substantial change of Tc speciation occurred at low S/Fe, coinciding with the rapid increase in Tc removal rate. This agreement further confirms the importance of FeS in Tc sequestration.

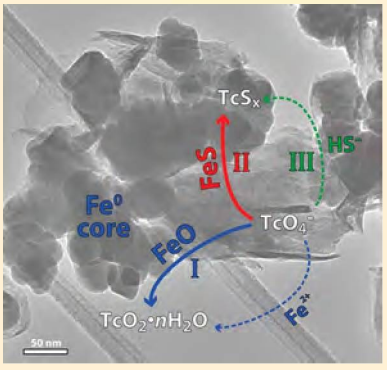

INTRODUCTION

Technetium 99 (^{99}Tc) is a weak β-emitting isotope, mainly generated from nuclear fission processes of uranium-235 and plutonium-239. Its long half-life (2.13×10^5 years) and high mobility in oxic subsurface environments (as the pertechnetate anion, $Tc^{VII}O_4^-$) make it a high priority among radionuclides that require control and remediation at U.S. Department of Energy sites.[1−4] Under anoxic conditions and in the absence of strong complexing ligands, such as carbonate and humic substances,[5,6] aqueous TcO_4^- is readily reduced to the much less soluble $Tc^{IV}O_2{\cdot}nH_2O$. This reduction can occur by various abiotic and biotic processes (reviewed by Icenhower et al.[7] and O'Loughlin et al.[8]). To date, most research has focused on using biogenic or abiogenic reactive Fe(II) species (aqueous, sorbed, or structural) as the reductants.[9−12] The rationale for this focus is partly because of the natural abundance of iron oxides, and—in particular—the concurrency of Tc reduction and iron reduction observed under natural redox gradients.[13] However, the long-term stability of Tc phases sequestered under iron reducing conditions is uncertain due to the susceptibility of $TcO_2{\cdot}nH_2O$ to reoxidation by oxygen (or nitrate) and subsequent release of TcO_4^- back into the aqueous phase.[14] Although several studies have reported that the association of Tc with iron oxide minerals by chemical adsorption[12] or structural incorporation[15] can significantly lower the rate of Tc^{IV} oxidation, the adequacy of these mechanisms for long-term stabilization of Tc in natural sediments is unproven, especially where it is likely to be limited due to heterogeneity of the sediments and other factors.

An alternative strategy to mitigate Tc reoxidation is to sequester Tc in a sulfide-rich environment that will favor the formation of Tc sulfide phases. Laboratory studies have demonstrated that Tc can be immobilized by Na_2S under

Received: November 26, 2012
Revised: April 17, 2013
Accepted: April 24, 2013
Published: April 24, 2013

simulated field conditions of nuclear waste tank repositories (high pH and ionic strength).[16−18] The resulting solid was characterized as Tc_2S_7, which was proposed to have a Tc^{IV} oxidation state, even though the stoichiometry appears to suggest Tc^{VII}. More recently, based on rigorous EXAFS fitting, Lukens et al.[16] suggested that the solid is more accurately characterized as Tc_3S_{10}. Synthetic mackinawite (FeS) can also sequester Tc via reduction and coprecipitation,[19] forming phases of which the composition is still uncertain.[19−21] Although complete understanding of these Tc/S phases is yet to be achieved, preliminary evidence from several studies suggested that Tc sequestered under sulfidic conditions is more recalcitrant to oxidation.[16,18,21]

Sulfidic conditions in a subsurface environment can be created by either direct injection of H_2S or HS^- or stimulated in situ by microbial sulfate reduction. Injection of H_2S gas has been successfully used to treat Cr(VI)-contaminated sediment,[22] but its effectiveness for sequestering Tc at groundwater pHs is low.[17,23] Stimulating in situ sulfidogenesis is potentially a more environmentally benign (sustainable) approach to this treatement. However, the formation of Tc sulfides along natural redox gradients may be limited by prior (up-gradient or earlier) Tc reduction to $TcO_2{\cdot}nH_2O$ under iron reducing conditions. This may also explain why no evidence has been reported for Tc sulfides in naturally developed sulfate reducing sediments.[13,24] Maximizing the potential for Tc sulfide formation requires a strong reducing agent to rapidly establish sulfidic conditions and thereby minimize the interference from iron reduction.

Emplacing nano zerovalent iron (nZVI) in the presence of sufficient quantities of SO_4^{2-} into the subsurface is a promising approach for achieving these conditions because (i) nZVI will abiotically scavenge alternative electron acceptors (e.g., O_2 and NO_3^-) but not SO_4^{2-}, and (ii) the H_2 generated by Fe^0 dissolution provides an electron donor that is readily utilized by many sulfate reducers.[25,26] These collateral microbiological effects of nZVI have been frequently documented in both laboratory experiments[27−30] and pilot- to field-scale applications (i.e., permeable reactive barriers (PRB)).[31−33] During microbial sulfate reduction, iron sulfides are also expected to form, and these may provide secondary phases—in addition to nZVI—that react with Tc. The most extensively studied iron sulfide phase is nanocrystalline mackinawite (amorphous FeS), commonly considered to be the first iron sulfide phase formed in sulfidic environments.[34−36] Mackinawite is highly reactive toward various heavy metals,[37,38] chlorinated solvents,[39,40] and oxyanions.[41−43] Therefore, it is expected to play an important role in contaminant degradation/sequestration in sulfidic environments.

The objective of this study was to provide the fundamental geochemical understanding of Tc sequestration during the development of sulfidogenic conditions in the presence of nZVI. Abiotic sulfide was used to simulate biotic sulfate reduction. Figure 1 presents a conceptual model of Tc sequestration pathways in three sequential scenarios: (I) the pre-sulfate reduction stage, (II) the initial stage of sulfate reduction, and (III) the end stage of sulfate reduction. We hypothesized that as sulfate reduction develops, the reactive phases (mineral or aqueous) that are responsible for Tc sequestration evolve, leading to different sequestration pathways and products. By combining wet chemical analysis with electron microscopy, synchrotron X-ray absorption spectroscopy, and other methods, we examined the change of host mineral phases during sulfidation, Tc sequestration kinetics under incremental S/Fe ratios, and further elucidated sequestration pathways, Tc distribution, phase compositions, and the local coordination environment of Tc within the final Tc−Fe−S solids.

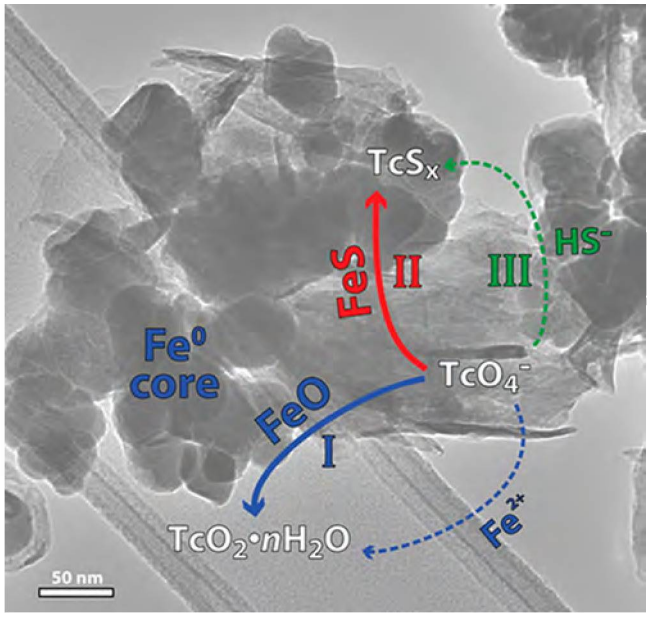

Figure 1. Conceptual model of Tc sequestration pathways under sulfidogenic conditions stimulated by nano zerovalent iron (nZVI). Processes (I), (II), and (III) represent the pre-, initial, and end stages of sulfate reduction, respectively (solid arrows: reaction with mineral phases; dashed arrows: reaction with aqueous species).

EXPERIMENTAL SECTION

Reagents. $FeCl_3{\cdot}6H_2O$, $NaBH_4$, Na_2S, and methanol were ACS grade. All reagents were used as received without further purification. ^{99}Tc was obtained as concentrated stock solution of ammonium pertechnetate (NH_4TcO_4) from Pacific Northwest National Laboratory. ^{99}Tc is a radioactive beta emitter (half-life 2.13×10^5 years; E_{max} = 294 keV) and was handled in a properly equipped radioactive laboratory.

Preparation of nZVI. Sulfur-free nZVI particles were synthesized using a modified version of the borohydride reduction method.[44] Briefly, $FeCl_3{\cdot}6H_2O$ (2.43 g) was dissolved in 500 mL of 7:3 (v/v) deionized deoxygenated (DI/DO) water/methanol. $NaBH_4$ (1.42 g) was dissolved in 40 mL of DI/DO water and continuously introduced to the $FeCl_3$ solution via a 0.5 mm I.D. plastic tubing with a syringe pump (KD Scientific, Holliston, MA) at 2 mL min^{-1}, while the resulting suspension was vigorously mixed by a homogenizer (Kinematica, Bohemia, NY). After introducing $NaBH_4$, the solution was allowed to sit for 15 min for H_2 bubbles to dissipate. All of the above steps were carried out under an inert gas stream (N_2 or Ar). The suspension was then transferred to an anaerobic chamber (95% N_2/5% H_2). Solid nZVI particles were recovered by flash drying, as previously described.[45]

Sulfidation. Pre-equilibration between nZVI and sulfide was carried out in 120-mL glass serum bottles. All procedures below were carried out in the anaerobic chamber except where otherwise mentioned. Dry nZVI particles (0.02 g) were weighed into each bottle. The bottles were then filled with 20 mL of deoxygenated Hanford synthetic groundwater

dx.doi.org/10.1021/es304829z | Environ. Sci. Technol. 2013, 47, 5302−5310

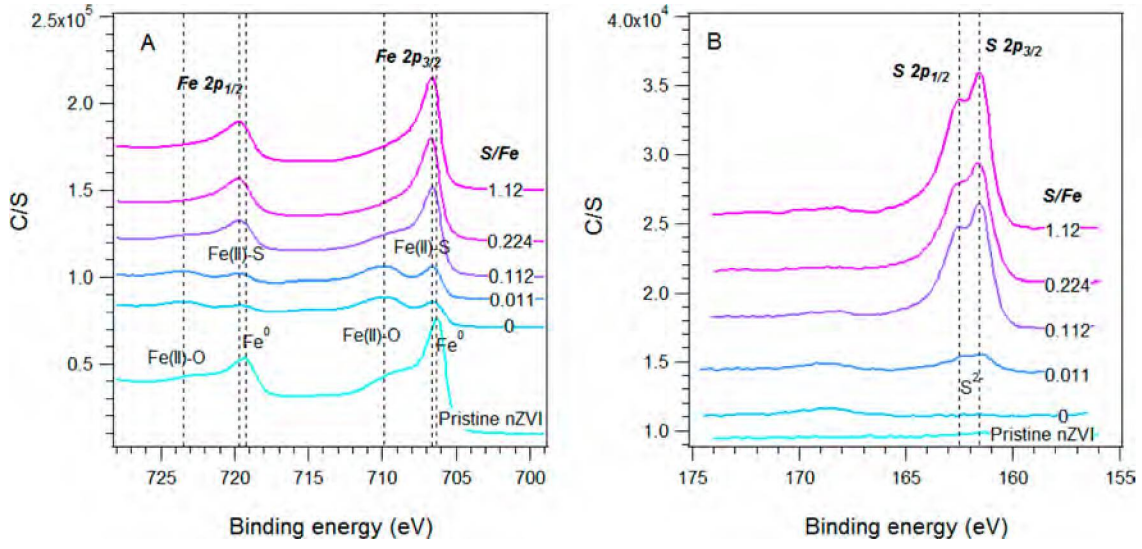

Figure 2. XPS (A) Fe 2p and (B) S 2p narrow region spectra of 0.5 g L^{-1} nZVI pre-exposed to increasing sulfide concentrations (0–10 mM) for 1 day in HS300 artificial groundwater (Fe peak assignments, represented by dashed lines, were based on literature values summarized by Mullet et al.[55] and Descostes et al.[56]).

(HS300) buffered at pH 7.9 by 30 mM HEPES (the detailed HS300 recipe is given as Table S1 in the Supporting Information (SI)). The bottles were sonicated in a water bath for 5 min to disperse the nZVI particles. The volume of HS300 was then adjusted up to 100 mL (0.2 g L^{-1} nZVI). A 0.2 M sulfide stock solution was prepared by dissolving anhydrous Na_2S in deoxygenated HS300 and aliquoted to each bottle to achieve concentrations varying incrementally from 0 to 4 mM, thus providing S/Fe molar ratios ranging from 0 to 1.12. At high sulfide doses, 6 M HCl was added to titrate the pH back to 7.9. The bottles were then sealed with grommet septum stoppers (Bellco Glass, Vineland, NJ), taken out of the anaerobic chamber, and placed in a shaker (150 rpm) at 27 ± 0.5 °C for pre-equilibration, during which time the aqueous sulfide concentration (<0.2 μm) was measured intermittently by the methylene blue colorimetric method (Hach DR700 Spectrophotometer Handbook, Loveland, CO).

Tc Reduction. After 1 day pre-equilibration, 10 mL of nZVI/sulfide suspension was withdrawn from the serum bottle and transferred to a 15-mL serum vial in the anaerobic chamber, TcO_4^- stock solution was then added to achieve a final concentration of 6 μM. The reactors were sealed by a 20-mm septum (SUN SRi, Rockwood, TN) and placed on an end-to-end rotator (20 rpm). Tc concentration in the aqueous phase (<0.2 μm) was monitored periodically by liquid scintillation counting (Beckman, Brea, CA). In selected experiments, 0.02-μm filtration was used in order to separate the colloidal phase of Tc from the dissolved phase. Controls included reactors with HS300/Tc but no sulfide, and HS300/Tc with 4 mM sulfide.

Solid Characterization. The bulk mineralogy of sulfidated nZVI was characterized by micro X-ray diffraction (μXRD) and Mössbauer spectroscopy. The near-surface composition of sulfidated nZVI during reaction with different amounts of sulfide was analyzed by X-ray photoelectron spectroscopy (XPS). To recover sufficient quantities of solids for these bulk analyses, 0.5 g L^{-1} nZVI and proportionally higher sulfide doses (to keep the S/Fe comparable with batch experiments) were used. The microscopic structure of the mineral phase was examined by scanning electron microscopy (SEM) and transmission electron microscopy (TEM) with energy dispersive X-ray spectroscopy (EDX). For SEM and TEM of Tc-containing samples, lower nZVI (0.2 g L^{-1} nZVI) and sulfide doses, but higher Tc concentrations (50 μM), were used in order to detect Tc by EDX. Details of these solid phase characterizations are given in SI Section S1.

X-ray Absorption Spectroscopy. Tc K-edge XAS for Tc sequestered by nZVI (0.5 g L^{-1}) and increasing sulfide (0–10 mM) were collected in fluorescence mode at the Stanford Synchrotron Radiation Lightsource (SSRL) on beamline 4-1 and 11-2. EXAFS spectra were analyzed using SixPack, Athena, and Artemis interfaces to the IFEFFIT package.[46] Back-scattering phase and amplitude functions required for fitting of spectra were obtained from FEFF8.[47] Details of XAS are given in SI Section S5.

RESULTS AND DISCUSSION

Characterization of Pristine and Sulfidated nZVI. The sulfur-free nZVI particles synthesized by borohydride reduction form chain-like structures, and individual particles have an average diameter of 30–60 nm with a well-defined core–shell structure (SI Figure S1A), both of which are the typical features of nZVI produced by this method.[48−50] While the core is mainly composed of Fe^0, the 2–3 nm thick shell appears to be composed of Fe oxides—based on the XPS Fe 2p narrow region spectra (Figure 2A)—and boron, which is evident in the XPS wide survey scans (SI Table S2) and presumably results from the incorporation of iron boride in the outer shell as byproducts during the synthesis.[51] Mössbauer spectroscopic data suggested that the nZVI contains little or no magnetite (Figure 3A), in contrast to nZVI synthesized by H_2 reduction (e.g., RNIP).[50] Both the μXRD (SI Figure S2A) and Mössbauer spectra of freshly prepared nZVI suggested that the pristine nZVI is largely amorphous. Finally, BET N_2-gas adsorption measurements showed that the material had a surface area of ~20 m^2 g^{-1}, which is within the typical range for this type of material.[48,52]

Sulfidation of nZVI at S/Fe = 0.112 for 1 day resulted in the emergence of poorly crystalline mackinawite phase according to μXRD (SI Figure S2C). The diffraction pattern was slightly

dx.doi.org/10.1021/es304829z | Environ. Sci. Technol. 2013, 47, 5302−5310

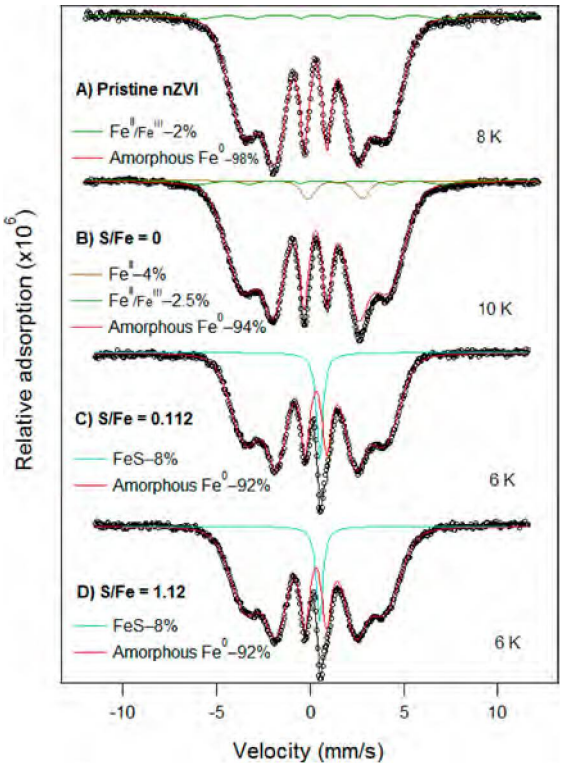

Figure 3. Experimental and modeled Mössbauer spectra of (A) pristine, (B–D) nZVI exposed to 0, 1, and 10 mM sulfide, respectively, in HS300 for 24 h.

different from that observed for bulk crystalline mackinawite, with an expanded *c* parameter that is consistent with disordered or nanocrystalline materials described previously.[36,53] Mössbauer spectra further confirmed that the bulk phases were mainly composed of residual nZVI (amorphous Fe^{0}) and secondary mackinawite (Figure 3). However, fitting the Mössbauer spectra gave a negligible increase in the percentage of mackinawite when S/Fe increased 10-fold from 0.112 to 1.12 (Figure 3). Likewise, XPS wide survey scans showed the surface atomic ratio of sulfide leveling off at S/Fe ≥ 0.112 (SI Table S2). The inhibition of sulfide uptake was further confirmed by significant aqueous sulfide detected at S/Fe = 0.224 and 0.56 even after extended exposure time (SI Figure S3). This is likely caused by a decrease in available Fe/FeO surface sites due to the formation of FeS, which is evidenced by the attenuation of broad Fe(II)–O peaks around 710 and 723 eV and evolution of sharp Fe(II)–S peaks around 706 and 719 eV when S/Fe increased from 0 to 0.112 in the XPS narrow region spectra of Fe 2p (Figure 2A). Note that the overlap of Fe(0) and Fe(II)–S peaks prevents quantifying these two species separately, but parallel S 2p spectra confirmed that the enhanced peaks were largely due to the formation of FeS (Figure 2B). Alternatively, particle aggregation—either originating with pristine nZVI or further induced by sulfidation—may also decrease the availability of surface sites to react with sulfide, and thereby possibly contribute to limiting sulfide uptake. This effect has been reported to significantly suppress sulfide uptake by aggregated Ag nanoparticles (NPs) relative to well-dispersed NPs.[54] TEMs of nZVI sulfidated at S/Fe = 0.112 revealed that FeS deposition onto the surfaces of nZVI appears to be highly nonuniform and does not leave a well-defined Fe^{0}/FeS core–shell structure. Instead, a laminar phase appears to grow out of the original nZVI particles, forming distinct phases that are closely associated with material retaining the original nZVI structure. The chemical composition and diffraction pattern further confirmed that this phase is FeS (SI Figure S1C).

Tc Sequestration Kinetics. Aqueous TcO_4^- was rapidly removed from solution at all values of S/Fe except 0 and 1.12 (Figure 4A). However, the kinetics of this reaction were not entirely pseudo-first-order because of tailing that appears to approach a limiting value after ~1 h. Therefore, the TcO_4^- removal rates were quantified using only the initial, linear portion of the *ln* (concentration) vs time plots. Figure 4B shows the initial Tc immobilization rate (left axis) and residual sulfide concentration measured before Tc addition (right axis) vs S/Fe in each experiment. As S/Fe increased from 0 to 0.045, the Tc disappearance rate increased. The reaction rate was too fast to be accurately determined from the data obtained at S/Fe = 0.056 and 0.224, but higher values of S/Fe resulted in decreased Tc removal rates. The high Tc removal rate observed at low S/Fe ratios can be explained by either enhanced nZVI corrosion due to sulfide facilitated corrosion[57] and/or increasing formation of reactive FeS. Both of these two mechanisms have been invoked to explain the enhanced

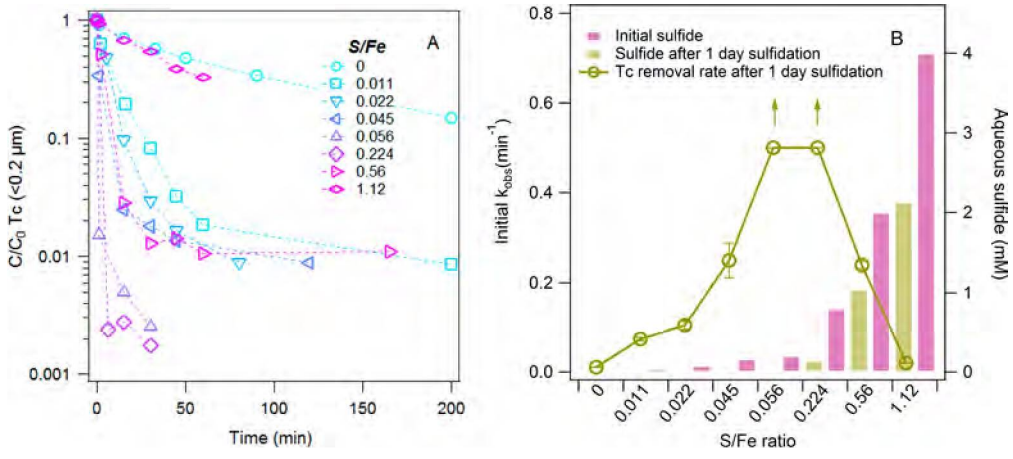

Figure 4. (A) Tc reduction kinetics at increasing S/Fe ratios after 1 day pre-exposure of nZVI to sulfide (n = 2). (B) Aqueous sulfide concentrations and initial Tc removal rate constants after 1 day pre-exposure of nZVI to various concentrations of sulfide (error bars represent standard deviations from linear regression; upward arrows represent lower limits because the reduction rate was too fast to be determined from the data).

dx.doi.org/10.1021/es304829z | *Environ. Sci. Technol.* 2013, 47, 5302–5310

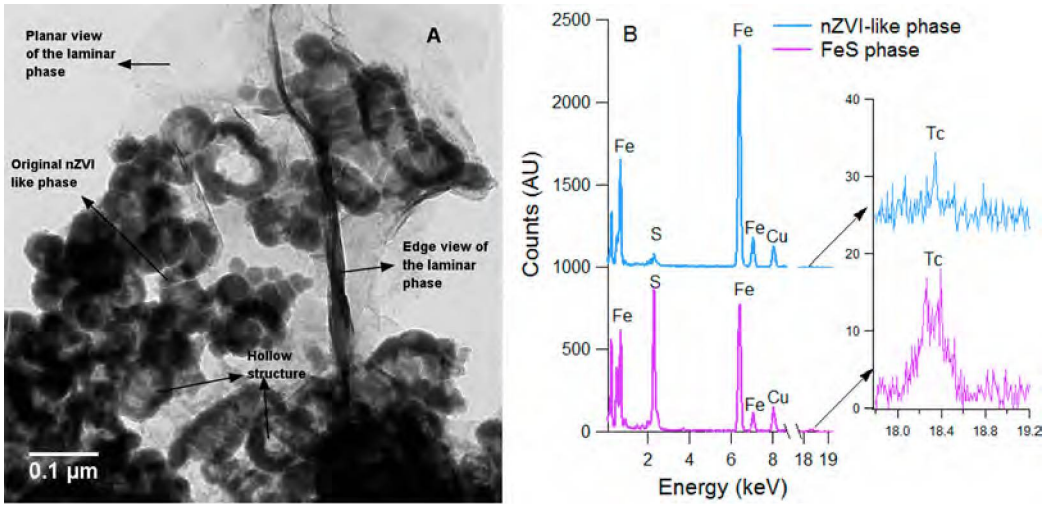

Figure 5. (A) Transmission electron micrograph of sulfidated nZVI exposed to TcO_4^-. (B) Representative EDX spectra of Fe-rich and S-rich area with enlarged spectra showing Tc ([nZVI] = 0.2 g L^{-1}; [S^{2-}] = 0.4 mM).

reactivity of sulfidated ZVI with chlorinated solvents (e.g., carbon tetrachloride and trichloroethylene).[28,39,58] In the present study, however, the latter mechanism is considered more likely because mackinawite has been shown to be a highly reactive phase with a wide range of inorganic oxyanions, including TcO_4^-. This hypothesis is also backed by the correlation between enhanced Tc removal rate and the increasing amount of surface FeS observed by XPS (Figure 2) as S/Fe increased from 0 to 0.112. Further evidence for this interpretation is provided by the XAS data presented below.

At high S/Fe, the inhibition of Tc removal varies with the residual aqueous sulfide concentration. As S/Fe increased from 0.224 to 1.12, the reaction rate decreased significantly while the aqueous sulfide concentration increased from ~0.2 to ~2 mM (Figure 4B), indicating that the inhibition is likely caused by aqueous sulfide. To verify this, additional experiments were performed that showed removal of excess aqueous sulfide before Tc addition restored faster Tc removal (SI Figure S5). Inhibition by sulfide has been previously observed for adsorption of molybdate onto pyrite (FeS_2),[59] which was interpreted as a result of sulfide competing for adsorption sites and/or the formation of Mo−S complexes. Direct interaction between TcO_4^- and aqueous sulfide has been reported to form Tc_2S_7 (or Tc_3S_{10}) solids at acidic or basic pHs.[17,23] However, at neutral pHs similar to our experimental conditions, it was found that Tc removal—in a way that is consistent with our observations—was negligible.[17,23]

We note that these studies quantified "aqueous Tc" by measuring Tc in either supernatant after centrifugation[23] or 0.45-μm filtrate,[17] both of which may not be sufficient to differentiate truly dissolved TcO_4^- from colloidal Tc_2S_7.[60] To test this, we compared Tc concentration after 0.2- and 0.02-μm filtration when TcO_4^- was reacted with 0 and 4 mM sulfide (SI Figure S6). In the absence of sulfide, Tc activity was kept unchanged in 0.2-μm filtrate and only slightly decreased in 0.02-μm filtrate after 96 h reaction. By contrast, in the presence of 4 mM sulfide, Tc activity decreased by 15% in 0.2-μm filtrate and by 35% in 0.02-μm filtrate, which indicates the formation and growth of Tc sulfide, most likely Tc_2S_7, colloids. However, it is worth noting that the time required to form significant quantities of colloidal Tc is considerably longer than the batch reaction time presented in Figure 4A. Therefore, the contributions of this reaction to the overall TcO_4^- removal, even at high S/Fe, might be limited, and the possibility that other factors contributed to the observed inhibition of Tc removal, such as sulfide competing for reaction sites, cannot be excluded.

Microscopy. The Tc distribution between the mineral phases was examined by TEM at S/Fe = 0.112. This ratio was chosen for two reasons. (i) Characterizations on sulfidated nZVI suggest that at S/Fe = 0.112, a significant amount of FeS is formed, but it is still much less abundant than residual nZVI phases. In addition, the majority of nZVI is not occluded by FeS coating (therefore, if FeS is indeed more important for Tc sequestration, as indicated by kinetic data, Tc should be partitioned preferentially to FeS). (ii) At S/Fe = 0.112, no excess aqueous sulfide was present (SI Figure S3), and therefore interference by reaction between Tc and HS^- was minimized. Figure 5A shows the morphology of sulfidated nZVI after reacting with TcO_4^-. Consistent with microscopy on sulfidated nZVI that was not reacted with Tc (SI Figure S1C), two morphologically distinct phases were present: aggregated particles that retain structure similar to pristine nZVI and a laminar phase that is most likely mackinawite. A third type of structure that was frequently encountered, but not observed in samples without Tc, was the hollow structures. Similar looking structures have been observed when Cu^0 NPs transform to sulfide-deficient Cu_xS NPs under bench-simulated sulfate reducing conditions.[61] Dispersed copper sulfide NPs that are more sulfide-rich were also observed. The authors suggested that the hollow structures might be a result of direct transformation of the zerovalent metal NPs due to a counter-diffusion phenomenon known as nanoscale Kirkendall effect,[62] whereas the dispersed NPs probably form by aqueous phase precipitation. Similar mechanisms might apply in the present study, given that the EDX spectra suggest that the laminar phase is more sulfide-rich than the hollow particles (data not shown). The absence of the hollow structures in the samples not exposed to Tc might be related to the lack of "aging" (Tc samples were kept in aqueous suspension for 2 months before being prepared for TEM, whereas samples without Tc were recovered as solid powder immediately after 1 day of sulfidation).

dx.doi.org/10.1021/es304829z | Environ. Sci. Technol. 2013, 47, 5302−5310

Despite the highly heterogeneous morphology formed upon nZVI sulfidation, Tc appears to be mainly associated with the FeS phase. Figure 5B shows the representative EDX spectra for nZVI-like and FeS phases. It can be seen that the FeS phase contains substantially more Tc than the nZVI-like phase. Although the level of Tc in the FeS phase was found to vary, up to 4% of Tc (atomic ratio) was detected in several locations. The preferential association of Tc with FeS further supports the hypothesis that FeS formed during sulfidation is mainly responsible for the increasing trend in Tc removal rates observed at low S/Fe ratios.

X-ray Absorption Spectroscopy. To better characterize the state of the sequestered Tc, Tc K-edge XAS data were obtained on solids recovered for each S/Fe ratio. The XANES spectra did not show the diagnostic pre-edge peak of TcO_4^- in any of the samples, suggesting that TcO_4^- was reduced to below detection. The Tc absorption edge decreased steeply from ca. 21.060 to ca. 21.054 keV as S/Fe increased from 0 to 0.056, but gradually leveled off above 0.056 (Figure 6). Given

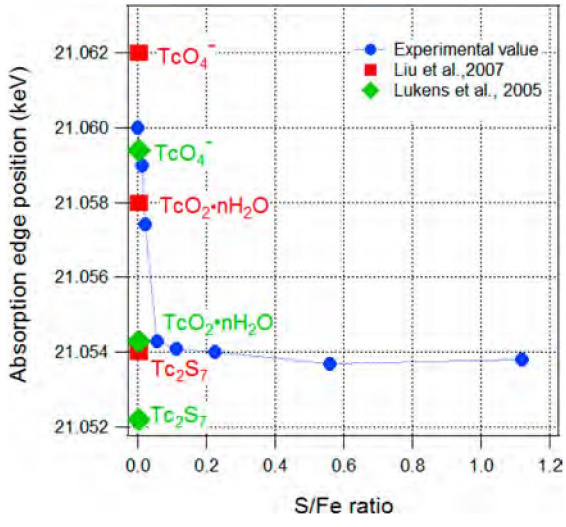

Figure 6. Tc K-edge adsorption edge position of Tc immobilized at incremental S/Fe ratios (blue solid dots) vs the first inflection point of TcO_4^-, TcO_2, and Tc_2S_7 reported in previous studies[16,18] (TcS_2 is not included because TcS_2 was reported only in Wharton et al.[21] and the value of its edge position (and the values of other comparable Tc compounds) is about 20 eV lower than values reported in other studies).

that the position of Tc K-edge absorption edge does not always correspond to the oxidation state of this element[63,64] and Tc_2S_7 has been reported to have a lower adsorption edge than TcO_2,[16,18] this two-phase trend most likely reflects changes in Tc speciation rather than its oxidation state. This interpretation is further supported by the EXAFS data in Figure 7, which shows a clear progression of Tc speciation from one pattern to the other with increasing S/Fe. The shell-by-shell EXAFS fit was further conducted for Tc reduced at S/Fe = 0 and 1.12, respectively, as two end-members (at S/Fe = 1.12, we only consider the speciation of Tc reacted with mineral phases because the contribution from colloidal Tc to the overall speciation of reduced Tc is small). The fitting results are summarized in SI Table S4. In the absence of sulfide, Tc has an inner shell coordination with 6 O atoms at a distance of 2.02 Å, which agrees well with the structure of $Tc^{IV}O_2{\cdot}nH_2O$. Different from previously reported EXAFS fit for Tc reduced by different

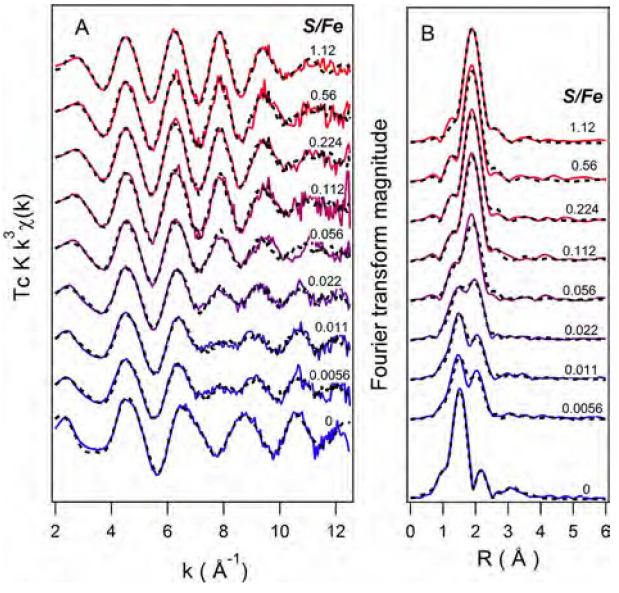

Figure 7. (A) Tc K-edge EXAFS and (B) the respective Fourier transform of Tc reduced at increasing S/Fe ratios. Experimental data are represented with circles. Fits are shown as solid lines (shell-by-shell fit for S/Fe = 0 and 1.12 and linear combination fit for all other S/Fe ratios in-between).

nZVI under simulated waste conditions,[65] the best fit to our data was obtained with Tc (instead of Fe) as neighboring metal atoms in the second shell. At S/Fe = 1.12, Tc is surrounded by 6 S atoms, 2 at 2.30 Å and the other 4 at 2.47 Å. The fit is similar to the crystallographic data for TcS_2,[66] although the S coordination number and distance are not entirely consistent. Compared with previous studies on Tc speciation after reacting with synthetic FeS, our finding generally agrees with the TcS_2-like phases reported by Wharton et al.[21] but not the $TcO_2{\cdot}nH_2O$ reported by Liu et al.[19] The reason for the inconsistency requires further investigation, but likely involves the high loading of TcO_4^- used by Liu et al. (150 μM) and differences in the surface properties of FeS.

By taking the two spectra at S/Fe = 0 and 1.12 as principal components (or "end-members"), the relative proportions of $TcO_2{\cdot}nH_2O$ to TcS_2 can be estimated by linear combination fitting (LCF) to the EXAFS spectra of different S/Fe ratios (Figure 7). Figure 8 plots the LCF results at incremental S/Fe ratios. As S/Fe increased, the portion of the high S/Fe end-member (TcS_2) generally increased while the portion of low S/Fe end-member ($TcO_2{\cdot}nH_2O$) decreased. At S/Fe = 0.011, about one-third of the reduced Tc speciation can be accounted for by the TcS_2, despite only trace amounts of surface FeS detected by XPS (Figure 2A). Taken together, these data suggest that FeS has a higher affinity for TcO_4^- than do nZVI/Fe oxides. In light of this result, it is noteworthy that the most substantial change in Tc speciation (by EXAFS)—the steep drop in the Tc absorption edge (by XANES)—occurred concurrently with the rapid increase of initial Tc removal rates at low S/Fe ratios. The agreement between the XAS and kinetic data again supports the conclusion that the increasing Tc removal rate during the initial stage of sulfidation is due to the rapid shift of Tc sequestration pathway from reduction by nZVI to reduction by FeS (Figure 1). As sulfidation proceeds, surface FeS apparently becomes the dominant mineral phase for Tc sequestration because Tc EXAFS spectra from above S/Fe = 0.112 were nearly identical to the high S/Fe end-member.

dx.doi.org/10.1021/es304829z | Environ. Sci. Technol. 2013, 47, 5302−5310

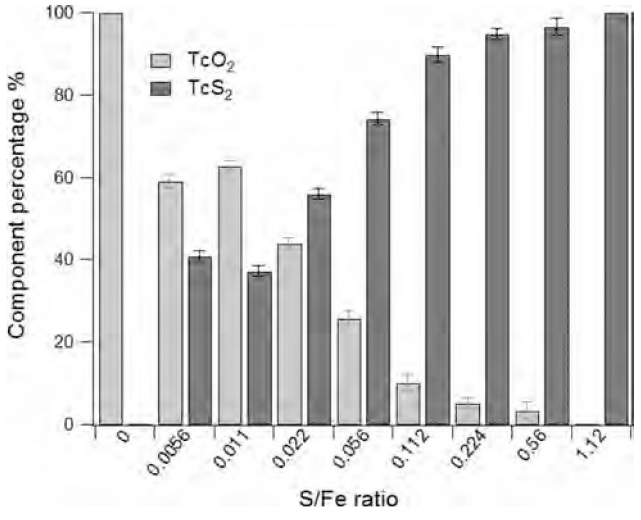

Figure 8. Tc speciation at different S/Fe ratios based on linear combination fitting of Tc EXAFS (Figure 7) using the spectra at S/Fe = 0 and 1.12 as two end-members.

Implications for Tc Sequestration in the Subsurface. The results presented here demonstrate that sulfidation of nZVI, although forming highly heterogeneous mineral surfaces, can direct TcO_4^- sequestration products from Tc^{IV} oxide (pathway I in Figure 1) to Tc^{IV} sulfide phases (pathway II in Figure 1) under groundwater conditions. Given the typically low TcO_4^- concentration in groundwater (even as a contaminant $<10^{-5}$ M), and that TcO_4^- has a higher affinity for FeS, it can be expected that sulfidic conditions will favor sequestration of Tc as Tc sulfides rather than Tc oxides, even at the early stage of microbial sulfate reduction. Other reducing iron phases—such as residual nZVI or secondary Fe(II) minerals formed from reaction of nZVI with groundwater constituents—reduce TcO_4^- readily, but nevertheless are outcompeted by FeS. As sulfate reduction proceeds, these iron phases (and possibly other naturally abundant Fe oxide minerals) will undergo further sulfidation to provide additional FeS capacity for Tc sequestration. At the same time, the formation of iron sulfides will lower the free aqueous sulfide concentration, thereby decreasing the possibility of forming potentially mobile colloidal Tc sulfide phases (pathway III in Figure 1).

In contrast to conventional (n)ZVI applications, where the Fe^0 directly reduces target contaminants, this study demonstrates a scenario where the main goal of adding nZVI is conditioning and sustaining a sufficiently reducing environment to favor microbial sulfate reduction. In actual remedial practice, however, direct reduction of TcO_4^- to TcO_2 by nZVI could be the dominant sequestration pathway before microbial sulfate reduction is established (pathway I in Figure 1). Additional EXAFS spectra showed that Tc reduced by nZVI and then exposed to 1 mM sulfide for 3 days is nearly identical to Tc reduced under S/Fe = 0.011 (SI Figure S11), indicating partial transformation from $TcO_2{\cdot}nH_2O$ to TcS_2. The rate of transformation, however, is considerably slower than the kinetics of Tc removal shown in Figure 4, even though geochemical modeling indicated that the transformation is thermodynamically possible (SI Figure S12). Therefore, field-scale application of nZVI for the remediation of Tc may require some direct introduction of sulfide to minimize the initial formation of TcO_2, such as by pretreating nZVI with aqueous sulfide. This study shows that a small amount of added sulfide may be sufficient to alter the dominant sequestration pathway, and at the same time, not substantially inhibit the ability of the nZVI to condition the subsurface to a sufficiently reducing environment.

There are many additional uncertainties to be addressed before up-scaling such a remediation strategy, including how to effectively deliver nZVI in the subsurface environment,[67] the effects of physical heterogeneity of the subsurface on Tc sequestration, and the effects of interactions between Tc and natural organic matter (especially thiol moieties) on Tc sequestration in sulfidic environments.[68] Many of these topics have been examined previously or are under investigation currently, but are beyond the scope of this study. Regardless, the present study suggests an effective alternative for Tc sequestration.

■ ASSOCIATED CONTENT

Supporting Information

Details on the characterization and properties of original and sulfidated nZVI, batch Tc reduction kinetics under high Fe dose, evidence of formation of colloidal Tc phases, additional SEM/TEM results of solids exposed to Tc, additional XAS information, and geochemical speciation modeling for Fe/S/Tc under relevant groundwater conditions. This material is available free of charge via the Internet at http://pubs.acs.org.

■ AUTHOR INFORMATION

Corresponding Author

*E-mail: tratnyek@ebs.ogi.edu; phone: 503-748-1023; fax: 503-748-1464.

Present Address

[†]School of Earth Sciences, Environmental Earth System Science Department, Stanford University Stanford, CA, 94305-4216.

Notes

The authors declare no competing financial interest.

■ ACKNOWLEDGMENTS

This material is based on work supported by the Subsurface Biogeochemical Research Program of the U.S. Department of Energy, Award DE-SC0001376. This report has not been subject to review by the DOE and therefore does not necessarily reflect agency views and no official endorsements should be inferred. Mössbauer, XPS, μXRD, SEM, and TEM/EDS were performed using the Environmental Molecular Sciences Laboratory (EMSL), a national scientific user facility sponsored by the Department of Energy's Office of Biological and Environmental Research and located at Pacific Northwest National Laboratory. XAS was carried out at the Stanford Synchrotron Radiation Lightsource, a Directorate of SLAC National Accelerator Laboratory and an Office of Science User Facility operated for the U.S. Department of Energy Office of Science by Stanford University. We thank Alice Dohnalkova and Charles Resch for EM sample preparation, Sung-Woo Lee for preliminary XAS data collection and discussion, Ninian Blackburn for fitting preliminary XAS data, Danielle Jansik and James Szecsody for general discussions, and Wayne Lukens for providing XAS spectra for Tc model compounds and advice regarding the XAS fitting.

REFERENCES

(1) Hartman, M.; Barnett, D.; Chou, C. et al.. *Hanford Site Groundwater Monitoring for Fiscal Year 1999*; PNNL-12086; Pacific Northwest National Laboratory: Richland, WA, 2000.

(2) Jones, T. E.; Khaleel, R.; Myers, D. A.; Shade, J. W.; Wood, M. I. *A Summary and Evaluation of Hanford Site Tank Farm Subsurface Contamination*; HNF-2603; Lockheed Martin Hanford: Richland, WA, 1998.

(3) Beasley, T. M.; Dixon, P. R.; Mann, L. J. ^{99}Tc, ^{236}U, and ^{237}Np in the Snake river plain aquifer at the Idaho National Engineering and Environmental Laboratory, Idaho Falls, Idaho. *Environ. Sci. Technol.* **1998**, *32*, 3875−3881.

(4) Haase, C.; Dreier, R.; McMaster, W.; Moore, G.; Solomon, D. Characteristics and modes of occurrence of groundwater contaminants on the U.S. Department of Energy reservation in Oak Ridge, Tennessee. *Geo. Soc. Am. Abs.* **1991**, *23*, 7−77.

(5) Maes, A.; Geraedts, K.; Bruggeman, C.; Vancluysen, J.; Rossberg, A.; Hennig, C. Evidence for the interaction of technetium colloids with humic substances by X-ray absorption spectroscopy. *Environ. Sci. Technol.* **2004**, *38*, 2044−2051.

(6) Rard, J. A. Current status of the thermodynamic data for technetium and its compounds and aqueous species. *J. Nucl. Radiochem. Sci.* **2005**, *6*, 197−204.

(7) Icenhower, J. P.; Qafoku, N. P.; Zachara, J. M.; Martin, W. J. The biogeochemistry of technetium: A review of the behavior of an artificial element in the natural environment. *Am. J. Sci.* **2010**, *310*, 721−752.

(8) O'Loughlin, E. J.; Boyanov, M. I.; Antonopoulos, D. A.; Kemner, K. M. Redox processes affecting the speciation of technetium, uranium, neptunium, and plutonium in aquatic and terrestrial environments. In *Aquatic Redox Chemistry*; Tratnyek, P. G., Grundl, T. J., Haderlein, S. B., Eds.; American Chemical Society: Washington, DC, 2011; ACS Symposium Series Vol. *1071*, pp 477−517.

(9) Cui, D.; Eriksen, T. E. Reduction of pertechnetate in solution by heterogeneous electron transfer from Fe(II)-containing geological material. *Environ. Sci. Technol.* **1996**, *30*, 2263−2269.

(10) Peretyazhko, T.; Zachara, J. M.; Heald, S. M.; Jeon, B.-H.; Kukkadapu, R. K.; Liu, C.; Moore, D.; Resch, C. T. Heterogeneous reduction of Tc(VII) by Fe(II) at the solid-water interface. *Geochim. Cosmochim. Acta* **2009**, *72*, 1521−1539.

(11) Plymale, A. E.; Fredrickson, J. K.; Zachara, J. M.; Dohnalkova, A. C.; Heald, S. M.; Moore, D. A.; Kennedy, D. W.; Marshall, M. J.; Wang, C.; Resch, C. T.; Nachimuthu, P. Competitive reduction of pertechnetate ($^{99}TcO_4^-$) by dissimilatory metal reducing bacteria and biogenic Fe (II). *Environ. Sci. Technol.* **2011**, *45*, 951−957.

(12) Zachara, J. M.; Heald, S. M.; Jeon, B.; Kukkadapu, R. K.; Liu, C.; McKinley, J. P.; Dohnalkova, A. C.; Moore, D. A. Reduction of pertechnetate [Tc(VII)] by aqueous Fe(II) and the nature of solid phase redox products. *Geochim. Cosmochim. Acta* **2007**, *71*, 2137−2157.

(13) Burke, I. T.; Boothman, C.; Lloyd, J. R.; Mortimer, R. J. G.; Livens, F. R.; Morris, K. Effects of progressive anoxia on the solubility of technetium in sediments. *Environ. Sci. Technol.* **2005**, *39*, 4109−4116.

(14) McBeth, J. M.; Lear, G.; Lloyd, J. R. Technetium reduction and reoxidation in aquifer sediments. *Geomicrobiol. J.* **2007**, *24*, 189−197.

(15) Um, W.; Chang, H.; Icenhower, J. P.; Lukens, W. W.; Serne, R. J.; Qafoku, N. P.; Westsik, J., J. H.; Buck, E. C.; Smith, S. C. Immobilization of 99-technetium (VII) by Fe(II)-goethite and limited reoxidation. *Environ. Sci. Technol.* **2011**, *45*, 4904−4913.

(16) Lukens, W. W.; Bucher, J. J.; Shuh, D. K.; Edelstein, N. M. Evolution of technetium speciation in reducing grout. *Environ. Sci. Technol.* **2005**, *39*, 8064−8070.

(17) Kunze, S.; Neck, V.; Gompper, K.; Fanghanel, T. Studies on the immobilization of technetium under near field geochemical conditions. *Radiochim. Acta* **1996**, *74*, 159−163.

(18) Liu, Y.; Terry, J.; Jurrison, S. Pertechnetate immobilization in aqueous media with hydrogen sulfide under anaerobic and aerobic environments. *Radiochim. Acta* **2007**, *95*, 717−725.

(19) Liu, Y.; Terry, J.; Jurrison, S. Pertechnetate immobilization with amorphous iron sulfide. *Radiochim. Acta* **2008**, *96*, 823−833.

(20) Watson, J. H. P.; Croudace, I. W.; Warwick, P. E.; James, P. A. B.; Charnock, J. M.; Ellwood, D. C. Adsorption of radioactive metals by strongly magnetic iron sulfide nanoparticles produced by sulfate-reducing bacteria. *Sep. Sci. Technol.* **2001**, *36*, 2571−2607.

(21) Wharton, M. J. A., B.; Charnock, J. M.; Livens, F. R.; Pattrick, R. A. D.; Collision, D. An X-ray absorption spectroscopy study of the copreipitation of Tc and Re with mackinawite (FeS). *Appl. Geochem.* **2000**, *15*, 347−354.

(22) Thornton, E. C.; Amonette, J. E. Hydrogen sulfide gas treatment of Cr(VI)-contaminated sediment samples from a plating-waste disposal site: Implications for in-situ remediation. *Environ. Sci. Technol.* **1999**, *33*, 4096−4101.

(23) Liu, Y.; Terry, J.; Jurisson, S. Pertechnetate immobilization in aqueous media with hydrogen sulfide under anaerobic and aerobic environments. *Radiochim. Acta* **2007**, *95*, 717−725.

(24) Keith-Roach, M. J.; Morris, K.; Dahlgaard, H. An investigation into technetium binding in sediments. *Mar. Chem.* **2003**, *81*, 149−162.

(25) Scherer, M. M.; Richter, S.; Richard, L. V.; Alvarez, P. J. Chemistry and microbiology of permeable reactive barriers for in situ groundwater clean up. *Crit. Rev. Environ. Sci. Technol.* **2000**, *30*, 363−411.

(26) Liamleam, W.; Annachhatre, A. Electron donors for biological sulfate reduction. *Biotechnol. Adv.* **2007**, *25*, 452−463.

(27) Gu, B.; Phelps, T. J.; Liang, L.; Dickey, M. J.; Roh, Y.; Kinsall, B. L.; Palumbo, A. V.; Jacobs, G. K. Biogeochemical dynamics in zero-valent iron columns: Implications for permeable reactive barriers. *Environ. Sci. Technol.* **1999**, *33*, 2170−2177.

(28) Van Nooten, T.; Lieben, F.; Dries, J.; Pirard, E.; Springael, D.; Bastiaens, L. Impact of microbial activities on the mineralogy and performance of column-scale permeable reactive iron barriers operation under two different conditions. *Environ. Sci. Technol.* **2007**, *41*, 5274−5230.

(29) Kirschling, T. L.; Gregory, K. B.; Minkley, E. G., Jr.; Lowry, G. V.; Tilton, R. D. Impact of nanoscale zero valent iron on geochemistry and microbial populations in trichloroethylene contaminated aquifer materials. *Environ. Sci. Technol.* **2010**, *44*, 3474−3480.

(30) Van Nooten, T.; Springael, D.; Baktiaens, L. Positive impact of microorganisms on the performance of laboratory-scale permeable reactive iron barriers. *Environ. Sci. Technol.* **2008**, *42*, 1680−1686.

(31) Van Nooten, T.; Springael, D.; Bastiaens, L. Microbial community characterization in a pilot-scale permeable reactive iron barrier. *Environ. Eng. Sci.* **2010**, *27*, 287−292.

(32) Phillips, D. H.; Van Nooten, T.; Bastiaens, L.; Russell, M. I.; Dickson, K.; Plant, S.; Ahad, J. M. E.; Newton, T.; Elliot, T.; Kalin, R. M. Ten year performance evaluation of a field-scale zero-valent iron permeable reactive barrier installed to remediate trichloroethene contaminated groundwater. *Environ. Sci. Technol.* **2010**, *44*, 3861−3869.

(33) Gu, B.; Watson, D. B.; Wu, L.; Phillips, D. H.; White, D. C.; Zhou, J. Microbiological characteristics in a zero-valent iron reactive barrier. *Environ. Monit. Assess.* **2002**, *77*, 293−309.

(34) Morse, J. W.; Millero, F. J.; Cornwell, J. C.; Rickard, D. The chemistry of the hydrogen sulfide and iron sulfide systems in natural waters. *Earth-Sci. Rev.* **1987**, *24*, 1−42.

(35) Rickard, D.; Luther, G. W., III Chemistry of iron sulfides. *Chem. Rev.* **2007**, *107*, 514−562.

(36) Jeong, H. Y.; Lee, J. H.; Hayes, K. F. Characterization of synthetic nanocrystalline mackinawite: Crystal structure, particle size and specific surface area. *Geochim. Cosmochim. Acta* **2008**, *72*, 493−505.

(37) Jeong, H. Y.; Sun, K.; Hayes, K. F. Microscopic and spectroscopic characterization of Hg(II) immobilization by mackinawite. *Environ. Sci. Technol.* **2010**, *44*, 7476−7683.

(38) Coles, C. A.; Rao, S. R.; Yong, R. N. Lead and cadmium interactions with mackinawite: Retention mechanisms and the role of pH. *Environ. Sci. Technol.* **2000**, *34*, 996−1000.

(39) Bulter, E. C.; Hayes, K. F. Factors influencing rates and products in the transformation of trichloroethylene by iron sulfide and iron metal. *Environ. Sci. Technol.* **2001**, *35*, 3884−3891.
(40) He, Y. T.; Wilson, J. T.; Wilkin, R. T. Impact of iron sulfide transformation on trichloroethylene degradation. *Geochim. Cosmochim. Acta* **2010**, *74*, 2025−2039.
(41) Scheinost, A. C.; Charlet, L. Selenite reduction by mackinawite, magnetite and siderite: XAS characterization of nanosized redox products. *Environ. Sci. Technol.* **2008**, *42*, 1984−1989.
(42) Hyun, S. P.; Davis, J. A.; Sun, K.; Hayes, K. F. Uranium(VI) reduction by iron(II) monosulfide mackinawite. *Environ. Sci. Technol.* **2012**, *46*, 3369−3376.
(43) Wolthers, M.; Charlet, L.; Van Der Weijden, C. H.; Van Der Linde, P. R.; Rickard, D. Arsenic mobility in the ambient sulfidic environment: sorption of arsenic(V) and arsenic(III) onto disordered mackinawite. *Geochim. Cosmochim. Acta* **2005**, *69*, 3483−3492.
(44) Wang, C.; Zhang, W. Synthesizing nanoscale iron particles for rapid and complete dechlorination of TCE and PCBs. *Environ. Sci. Technol.* **1997**, *31*, 2154−2156.
(45) Nurmi, J.; Sarathy, V.; Tratnyek, P.; Baer, D.; Amonette, J.; Karkamkar, A. Recovery of iron/iron oxide nanoparticles from solution: Comparison of methods and their effects. *J. Nanopart. Res.* **2011**, *13*, 1937−1952.
(46) Ravel, B.; Newville, M. ATHENA, ARTEMIS, HEPHAESTUS: Data analysis for X-ray absorption spectroscopy using IFEFFIT. *J. Synchrotron Radiat.* **2005**, *12*, 537−541.
(47) Rehr, J. J.; Albers, R. C.; Zabinsky, S. I. High-order multiple-scattering calculations of X-ray-absorption fine structure. *Phys. Rev. Lett.* **1992**, *69*, 3397−3400.
(48) Li, X.-Q.; Elliott, D. W.; Zhang, W.-X. Zero-valent iron nanoparticles for abatement of environmental pollutants: Materials and engineering aspects. *Crit. Rev. Solid State Mater. Sci.* **2006**, *31*, 111−122.
(49) Baer, D. R.; Tratnyek, P. G.; Qiang, Y.; Amonette, J. E.; Linehan, J.; Sarathy, V.; Nurmi, J. T.; Wang, C.; Anthony, J. Synthesis, characterization, and properties of zero-valent iron nanoparticles. In *Environmental Applications of Nanomaterials: Synthesis, Sorbents, and Sensors*; Fryxell, G. E., Ed.; Imperial College Press: London, 2007; pp 49−86.
(50) Nurmi, J. T.; Tratnyek, P. G.; Sarathy, V.; Baer, D. R.; Amonette, J. E.; Pecher, K.; Wang, C.; Linehan, J. C.; Matson, D. W.; Penn, R. L.; Driessen, M. D. Characterization and properties of metallic iron nanoparticles: Spectroscopy, electrochemistry, and kinetics. *Environ. Sci. Technol.* **2005**, *39*, 1221−1230.
(51) Glavee, G. N.; Klabunde, K. J.; Sorensen, C. M.; Hadjipanayis, G. C. Chemistry of borohydride reduction of iron(II) and iron(III) ions in aqueous and nonaqueous media - Formation of nanoscale Fe, FeB, and Fe_2B powders. *Inorg. Chem.* **1995**, *34*, 28−35.
(52) Wang, Q.; Snyder, S.; Kim, J.; Choi, H. Aqueous ethanol modified nanoscale zerovalent iron in bromate reduction: Synthesis, characterization, and reactivity. *Environ. Sci. Technol.* **2009**, *43*, 3292−3299.
(53) Wolthers, M.; Van der Gaast, S. J.; Rickard, D. The structure of disordered mackinawite. *Am. Mineral.* **2003**, *88*, 2007−2015.
(54) Reinsch, B. C.; Levard, C.; Li, Z.; Ma, R.; Wise, A.; Gregory, K. B.; Brown, G. E.; Lowry, G. V. Sulfidation of silver nanoparticles decreases *Escherichia coli* growth inhibition. *Environ. Sci. Technol.* **2012**, *46*, 6992−7000.
(55) Mullet, M.; Boursiquot, S.; Abdelmoula, M.; Genin, J.; Ehrhardt, J. Surface chemistry and structural properties of mackinawite prepared by reaction of sulfide ions with metallic iron. *Geochim. Cosmochim. Acta* **2002**, *66*, 829−836.
(56) Descostes, M.; Mercier, F.; Thromat, N.; Beaucaire, C.; Gautier-Soyer, M. Use of XPS in the determination of chemical environment and oxidation state of iron and sulfur samples: Constitution of a data basis in binding energies for Fe and S reference compounds and applications to the evidence of surface species of an oxidized pyrite in a carbonate medium. *Appl. Surf. Sci.* **2000**, *165*, 288−302.
(57) Turcio-Ortega, D.; Fan, D.; Tratnyek, P. G.; Kim, E.-J.; Chang, Y.-S. Reactivity of Fe/FeS nanoparticles: Electrolyte composition effects on corrosion electrochemistry. *Environ. Sci. Technol.* **2012**, *46*, 12484−12492.
(58) Kim, E.-J.; Kim, J.-H.; Azad, A.-M.; Chang, Y.-S. Facile synthesis and characterization of Fe/FeS nanoparticles for environmental applications. *ACS Appl. Mater. Interfaces* **2011**, *3*, 1457−1462.
(59) Bostick, B. C.; Fendorf, S.; Helz, G. R. Differential adsorption of molybdate and tetrathiomolybdate on pyrite (FeS_2). *Environ. Sci. Technol.* **2002**, *37*, 285−291.
(60) Saiki, Y.; Fukuzaki, M.; Sekine, T.; Kino, Y.; Kudo, H. Technetium(VII) sulfide colloid growing observed by laser-induced photoacoustic spectroscopy. *J. Radioanal. Nucl. Chem* **2003**, *255*, 101−104.
(61) Weber, F.-A.; Voegelin, A.; Kaegi, R.; Kretzschmar, R. Contaminant mobilization by metallic copper and metal sulphide colloids in flooded soil. *Nat. Geosci.* **2009**, *2*, 267−271.
(62) Yin, Y.; Rioux, R. M.; Erdonmez, C. K.; Hughes, S.; Somorjai, G. A.; Alivisatos, A. P. Formation of hollow nanocrystals through the nanoscale Kirkendall effect. *Science* **2004**, *304*, 711−714.
(63) Almahamid, I.; Bryan, J. C.; Bucher, J. J.; Burrell, A. K.; Edelstein, N. M.; Hudson, E. A.; Kaltsoyannis, N.; Lukens, W. W.; Nitsche, H. Electronic and structural investigations of technetium compounds by X-ray absorption spectroscopy. *Inorg. Chem.* **1995**, *34*, 193−198.
(64) Terry, J.; Grzenia, B.; Papagiannopoulou, D.; Kyger, J.; Jurisson, S.; Robertson, J. D. Structural determination of Tc radiopharmaceuticals and compounds using X-ray absorption spectroscopy. *J. Radioanal. Nucl. Chem* **2005**, *263*, 531−537.
(65) Darab, J. G.; Amonette, A. B.; Burke, D. S. D.; Orr, R. D.; Ponder, S. M.; Schrick, B.; Mallouk, T. E.; Lukens, W. W.; Caulder, D. L.; Shuh, D. K. Removal of pertechnetate from simulated nuclear waste streams using supported zerovalent iron. *Chem. Mater.* **2007**, *19*, 5703−5713.
(66) Lamfers, H. J.; Meetsma, A.; Wiegers, G. A.; De Boer, J. L. The crystal structure of some rhenium and technetium dichalcogenides. *J. Alloys Compd.* **1996**, *241*, 34−39.
(67) Johnson, R. L.; Nurmi, J. T.; O'Brien Johnson, G.; Fan, D.; O'Brien Johnson, R.; Shi, Z.; Salter-Blanc Alexandra, J.; Tratnyek, P. G.; Lowry, G. V. Field-scale transport and transformation of carboxymethylcellulose-stabilized nano zero-valent iron. *Environ. Sci. Technol.* **2013**, *47*, 1573−1580.
(68) Liu, Y.; Terry, J.; Jurisson, S. S. Potential interferences on the pertechnetate-sulfide immobilization reaction. *Radiochim. Acta* **2009**, *97*, 33−41.

SUPPORTING INFORMATION

Reductive Sequestration of Pertechnetate (TcO_4^-) by Nano Zero-valent Iron Transformed by Abiotic Sulfide

*Dimin Fan, Roberto P. Anitori, Bradley M. Tebo, Paul G. Tratnyek**
Division of Environmental and Biomolecular Systems
Oregon Health & Science University
20000 NW Walker Road, Portland, OR 97006

Juan S. Lezama Pacheco
Stanford Synchrotron Radiation Lightsource
Menlo Park, CA 94025
Current Address
School of Earth Sciences, Environmental Earth System Science Department,
Stanford University
Stanford, CA 94305-4216

Ravi K. Kukkadapu, Mark H. Engelhard, Mark E. Bowden,
Libor Kovarik, Bruce W. Arey
Environmental Molecular Sciences Laboratory, Pacific Northwest National Laboratory
Richland, WA 99354

*Corresponding author:
Email: tratnyek@ebs.ogi.edu, Phone: 503-748-1023, Fax: 503-748-1464

Contents

1. Characterization and Properties of Pristine nZVI and Sulfidated nZVI

Composition of Hanford artificial groundwater (HS300)

Table S1. Recipe for Hanford artificial groundwater (HS300a)

Component	Concentration (mM)
$NaHCO_3$	1.44
$KHCO_3$	0.16
$MgCl_2 \bullet 6H_2O$	0.51
$CaCl_2 \bullet 2H_2O$	0.37
$CaSO_4 \bullet 2H_2O$	0.63
NaH_2PO_4	1.50
NH_4Cl	4.70
HEPES	30.00[b]

[a] Modified from SGW1 medium in Lee et al.[1]
[b] 30 mM HEPES provides additional buffer capacity to neutralize pH increase from sodium sulfide.

Methods

Micro X-ray Diffraction.

Powders for diffraction analysis were loaded into 0.5 mm glass capillaries (Charles Supper Co., MA) under nitrogen atmosphere and sealed with wax. Diffraction data were recorded by the 2D image plate of a Rigaku D/Max Rapid II diffractometer. Cr Kα radiation (λ = 2.2910 Å) focused through a 300 μm diameter collimator was used, which avoids the high background produced from fluorescence of Fe-containing samples. The 2-dimensional diffraction data were integrated between 10 and 160° 2θ to give powder traces. Backgrounds were removed using the JADE software (Materials Data Inc. CA) by subtracting a trace from an empty capillary and additionally fitting a smooth spline curve.

Mössbauer Spectroscopy.

Sample preparation for Mössbauer spectroscopy is identical to the procedures reported in Peretyazhko et al.[2] Mössbauer spectra of the samples were collected using either a WissEl Elektronik (Germany) or Web Research Company (St. Paul, MN) instruments that included a closed-cycle cryostat SHI-850 obtained from Janis Research (Wilmington, MA), a Sumitomo CKW-21 He compressor unit (Wilmington, MA), and an Ar-Kr proportional counter detector

with WissEl setup or a Ritverc (St. Petersburg, Russia) NaI detection system. A ^{57}Co/Rh source (50 mCi to 75 mCi, initial strength) was used as the gamma energy source. With the WissEl setups, the transmitted counts were stored in a multichannel scalar (MCS) as a function of energy (transducer velocity) using a 1024-channel analyzer. The setups data were folded to 512 channels to provide a flat background and a zero-velocity position corresponding to the center shift (CS) of a metal Fe foil at room temperature (RT). Calibration spectra were obtained with a 25 μm thick Fe foil (Amersham, England) placed in the same position as the samples to minimize any geometry errors. The Mössbauer data were modeled with Recoil^{TM} software (University of Ottawa, Canada) using a Voigt-based structural fitting routine.

X-Ray Photoelectron Spectroscopy.

The XPS analyses were conducted using a Physical Electronics Quantera Scanning ESCA Microprobe with a focused monochromatic Al Ka X-ray source (1486.7 eV) source and a spherical section analyzer. The mineral powder sample was mounted inside a nitrogen recirculated glove box operated at <0.5 ppm O_2. The samples were pressed onto double sided Scotch tape (#34-8507-5367-3) and supported by 1 cm x 3 cm clean flat Si (100) wafers. The individual Si wafer pieces were then mounted onto the standard Physical Electronics 75 mm x 75 mm sample holder using 2-56 stainless steel screws. The sample holder was then placed into the XPS vacuum introduction system and pumped to $<1 \times 10^{-6}$ Torr using a turbomolecular pumping system prior to introduction into the main ultra high vacuum system. The main vacuum system pressure is maintained at $<5 \times 10^{-9}$ Torr during analysis and pumped using a series of sputter ion pumps and turbo-molecular pumps. For large collections of mineral particles, the X-ray beam was operated at approximately 100 W, focused to 100 μm diameter, and rastered over a 1.3 mm x 0.1 mm rectangle on the sample. The X-ray beam is incident normal to the sample and the photoelectron detector is at 45° off-normal. High energy resolution spectra were collected using a pass-energy of 69.0 eV with a step size of 0.125 eV. For the Ag 3d5/2 line, these conditions produced a FWHM of 0.91 eV. The sample experienced variable degrees of charging. Low energy electrons at ~1 eV, 20 μA and low energy Ar^+ ions were used to minimize this charging. The spectra were aligned to a carbon peak energy of 285.0 eV (adventitious carbon). The compositional results were obtained using the standard sensitivity factors in the Phi Multipak software package using peak area intensities after a Shirley background substation.

Transmission Electron Microscopy (TEM).

The samples without exposure to Tc were prepared for TEM observations by dispersing a dry powder on a lacey-carbon coated 200 mesh Cu TEM grids under anaerobic conditions. In a subsequent step of loading the sample into the TEM, however, the samples were exposed to aerobic conditions for a period of few minutes. TEM conventional and high-resolution images were performed with spherical aberration corrected FEI Titan 80-300 operated at 300kV. The elemental analysis was performed with EDAX Si (Li) EDS detector and a subsequent analysis was performed with TIA software.

BET Surface Area Measurements

100 to 200 mg of material was placed in a sealed BET vial and weighed (pre-drying weight). The sample in the BET vial was then placed in the VacPrep 061 in which the samples were heated under flowing UHP N_2 at 200°C. At selected times, the samples were allowed to cool and then weighed (after-drying weight). After samples were dried, surface area was measured by N_2 adsorption using a Micrometrics Gemini V surface area and pore size analyzer.

Results

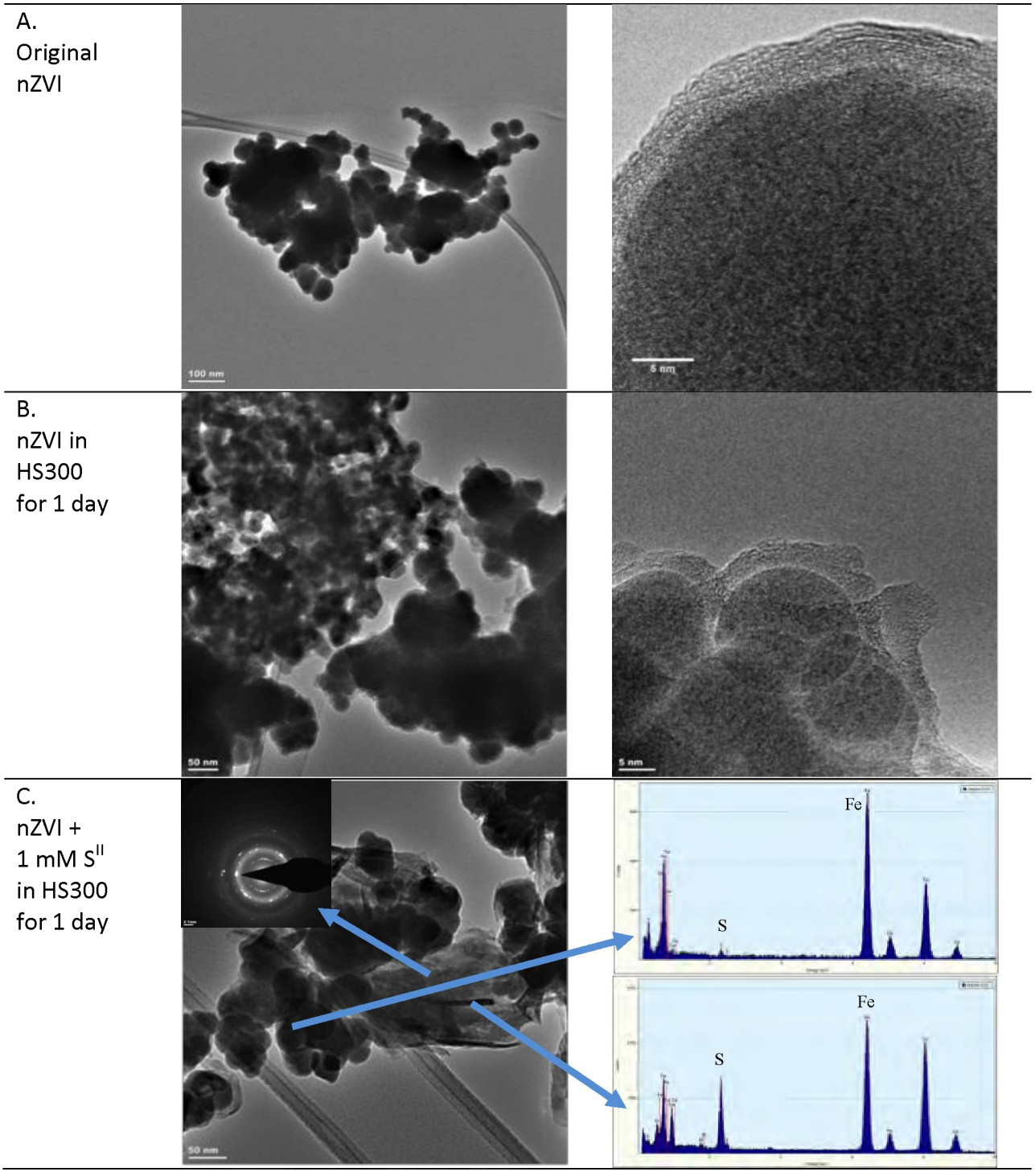

Figure S1. Transmission electron micrographs of (***A***) freshly prepared nZVI: long chain structure connecting primary particles (left), primary particle with core-shell structure (right); (***B***) nZVI exposed in HS300 for 1 day: aggregated particles (left), core-shell structure upon exposure to HS300 (right); (***C***) nZVI exposed in 1 mM sulfide (S/Fe = 0.112) and HS300 for 1

day: co-presence of residual nZVI and FeS (left), EDX of residual nZVI (right top), and EDX of FeS (right bottom).

Table S2. Surface element atomic percentage of pristine nZVI and nZVI exposed to incremental sulfide concentrations in HS300 for 1 day by XPS wide survey scan.

S/Fe ratio	Atomic ratio %									
	Fe2p	O1s	S2p	B1s	C1s	Ca2p	P2p	Si2p	Cu2p3	MgKLL
0 (Pristine nZVI)	27.8	27.4	N/D	19.2	25.6	N/D	N/D	N/D	N/D	N/D
0 (nZVI + HS300)	13.8	45.7	0.4	N/D	25.3	4.4	6.8	1.7	N/D	0.8
0.011 (nZVI + HS300 + 0.1 mM S^{2-})	15.1	42.0	0.8	N/D	29.7	4.0	6.4	1.1	N/D	0.8
0.112 (nZVI + HS300 + 1 mM S^{2-})	42.9	37.7	10.5	N/D	N/D	3.5	3.4	N/D	1.0	1.0
0.224 (nZVI + HS300 + 2 mM S^{2-})	51.5	26.6	10.9	N/D	N/D	3.8	2.4	N/D	1.1	1.9
1.12 (nZVI + HS300 + 10 mM S^{2-})	53.9	25.2	12.9	N/D	N/D	2.7	2.2	N/D	1.4	1.6

N/D: Not detectable above the signal background.

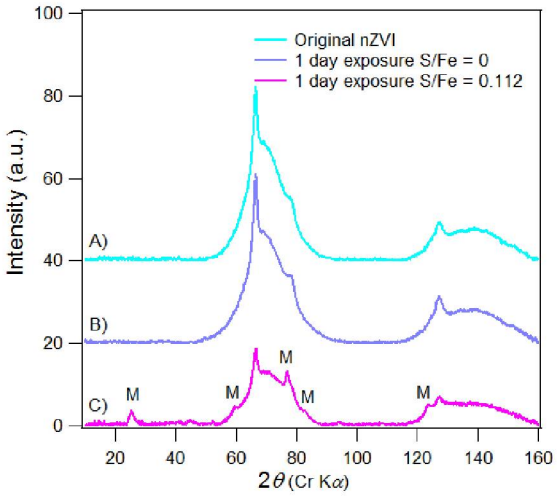

Figure S2. Micro-XRD pattern of (***A***) pristine nZVI, (***B***) nZVI in HS300 for 1 day (S/Fe = 0) and (***C***) nZVI exposed to 1 mM sulfide in HS300 for 1 day (M stands for mackinawite).

Table S3. Summary of μXRD and Mössbauer data of pristine nZVI with comparisons to previously reported studies.

Sources	This study	Prior studies[b] of related nZVI (Fe^{BH} [a])	Prior studies[c] of Fe-boron alloys
(μ)XRD	Less than 10% of the phase matches face cubic center (FCC) γ-iron best (represented by sharp peak in **Figure S2**). Broad humps represent poorly crystalline phase, which as smaller cell parameter than the sharp peak.	Predominantly body cubic center (BCC)-α iron	Amorphous
Mössbauer	Most consistent with amorphous iron[3]	BCC-α iron	Amorphous

[a] Fe^{BH} represents nZVI synthesized by borodydride reduction, adapted from Nurmi et al.[4]; [b] [5-7]; [c] [8-10].

Discussion

Figure S1B shows that the nZVI exposed to HS300 media for 1 day retains the chainlike morphology similar to pristine nZVI (**Figure S1A**). The core-shell structure of individual

particle is also preserved. However, the thickness of the shell is much less uniform and generally thicker compared to the pristine nZVI, evidently due to more extensive growth of the FeO passive layer. This interpretation is supported by XPS survey scan that shows the increasing oxygen amount in sample exposed to HS300 only (**Table S2**). XPS survey scans also showed no boron in samples that were exposed to aqueous media, which can be attributed to the hydrolysis of Fe boride.[9]

Table S3 summarizes differences in the μXRD and Mössbauer results between the present study and prior work. The μXRD pattern of the pristine nZVI contained sharp peaks that were most consistent with an FCC lattice (**Figure S2A**). By contrast, most of the prior XRD characterizations of nZVI synthesized by $NaBH_4$ reduction suggest BCC α-iron.[5, 7] In this study, it was estimated that the sharp peaks that match FCC lattice best (**Figure S2A**) account for less than 10% of the total signal. The majority of the signal represented by the broad peaks cannot be identified with certainty, and could be amorphous or poorly crystalline material. Previous studies on Fe^{BH} also suggest that the XRD peak of Fe^{BH} is broader compared to typical α-iron, representing a distribution of crystallite size.[4, 5] Although the FCC lattice is typically found in γ-iron that is formed at high pressure and temperatures, FCC-modified iron may also arise as a result of alloying elements, most commonly carbon, at ambient conditions, especially when the particle size is small.[11] For the present nZVI samples, we speculate that boron incorporated into the nZVI shell has stabilized the FCC Fe lattice. The Mössbauer spectrum of the pristine nZVI exhibits broad features that are most consistent with amorphous Fe metal,[3] which are clearly distinct from previously published Mössbauer spectra of nZVI made by borohydride reduction.[6, 7] However, in these two previous studies, the samples were prepared either by heat- or freeze-drying, which could easily be responsible for changing the crystallinity of the material.[12] In fact, several earlier studies using borohydride reduction to synthesize ultrafine particles of Fe-metal (metalloid) alloys with recovery by filtration have reported broad Mössbauer features similar to this study, and they also interpreted their results as indication that the freshly prepared material was amorphous.[8, 10] After annealing at high temperature, however, the spectra obtained in these studies[8, 10] showed features indicating transformation to more crystalline α-iron. Given that the flash drying protocol used in this study is essentially an anaerobic filtration,[12] the amorphous nature of the pristine nZVI observed here is reasonable.

In addition to post synthesis treatment, other experimental differences during the synthesis between our methods and those of previous studies could contribute to differences in the final product. One distinctive aspect of our method is the strong homogenization used during the introduction of $NaBH_4$ to $FeCl_3$ aqueous solution. This was done to mix the reagents rapidly and minimize aggregation of newly formed particles without the complications created by using a magnetic stir bar with magnetic nanoparticles. A variety of subjective, preliminary tests indicated that mixing with a homogenizer produced more reproducible dispersions of nZVI, but the specific effects of this on the particle composition and structure were not studied further.

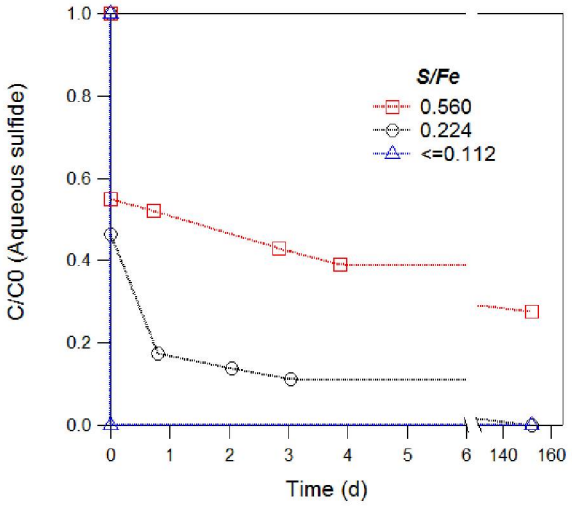

Figure S3. The kinetics of sulfide uptake by nZVI at various S/Fe ratios in HS300 (nZVI concentration: 0.2 g L^{-1}, sulfide dose: 0, 0.04, 0.08, 0.16, 0.2, 0.4, 0.8, and 2 mM, pH = 7.9, temperature = 27±0.5 ºC, aqueous sulfide concentrations in batches with sulfide dose below 0.8 mM were all below detection).

Control experiments without nZVI showed negligible changes of aqueous sulfide concentration over the sampling course (data not shown). At low S/Fe (≤ 0.112), aqueous sulfide was removed to below the detection limit within 5 min after sulfide addition (**Figure S3**). However, at relatively high S/Fe (0.224 and 0.56), the kinetics of sulfide removal from solution exhibited two phases, with about half of the input sulfide removed rapidly followed by a gradual decrease over a much longer period (**Figure S3**). The initial, fast stage likely corresponds to instantaneous sulfide adsorption onto the surface Fe oxides coating on nZVI, forming a surface

complex of Fe(II)–HS^-.[13] A similar process has been postulated to be the initial step in mackinawite formation on iron oxides in natural sulfidic environments.[14, 15] The later stage of sulfide removal reflects relatively slow formation of FeS precipitates. At S/Fe = 0.56, significant residual aqueous sulfide was detected even after 150 days of exposure, indicating incomplete transformation of nZVI to FeS.

2. Batch Tc Reduction Kinetics under High Fe dose (0.5 g/L)

Results

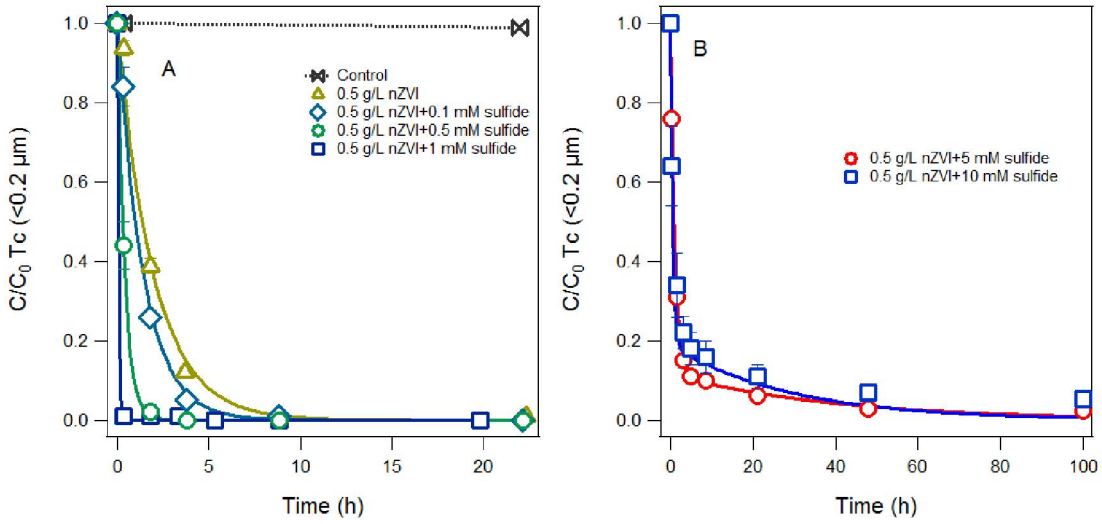

Figure S4. Tc sequestration kinetics at high nZVI dose (0.5 g L^{-1}): (***A***) low S concentration (0.1 mM to 1 mM) and (***B***) high sulfide concentration (5 and 10 mM) (S/Fe ratio has the same range as **Figure 2**. Error bars represent the standard error from duplicates).

In these high nZVI dose experiments, the batch reactors were kept still without external mixing. Therefore, the reaction rate was significantly slower than the reaction rate presented in **Figure 4**, even though the nZVI and sulfide doses were higher. However, it is important to note that the general observation of these experiments is consistent with what was shown in **Figure 4**: at low S/Fe ratios, the reaction rate increased as S/Fe increased but higher S/Fe resulted inhibition of Tc removal. The higher residual Tc concentration (< 0.2 µm) observed at 5 and 10 mM sulfide concentrations were probably due to higher residual sulfide concentration.

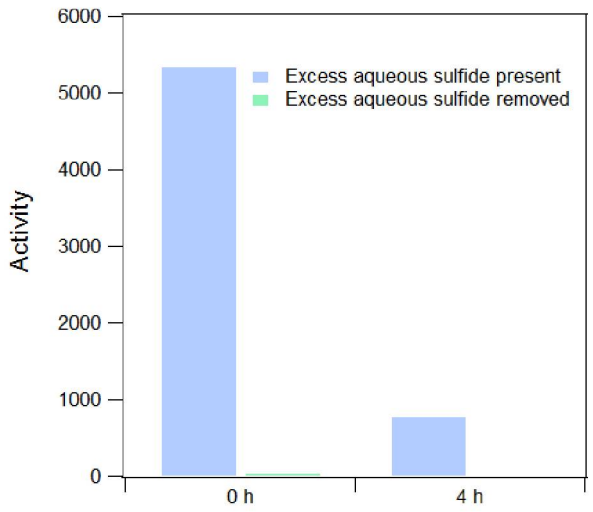

Figure S5. Tc remaining in solution in the presence and absence of excess aqueous sulfide (Tc concentration is represented by counts per minute from liquid scintillation; Two batch reactors were prepared by exposing 0.5 g L^{-1} nZVI to 10 mM sulfide in HS300 for 1 day at pH = 7.9; Before Tc addition, excess of aqueous sulfide was removed in one of the bottles by filtration and the recovered solid was resuspended in HS300).

Figure S5 shows the preliminary results where Tc removal rate was compared in the presence and absence of excess aqueous sulfide. Tc (< 0.2 μm) was quantified by using direct reading of the radioactivity (CPM). It clearly shows that when excess of aqueous sulfide was removed, Tc removal (blue bars) was much faster compared to the batch where excess of aqueous sulfide was present (green bars), and the removal rate is comparable to the lower S/Fe ratio cases (**Figure 4** and **Figure S4A**). This suggests that the inhibition of Tc removal resulted from excess aqueous sulfide.

3. Evidence of Colloidal Tc Formation

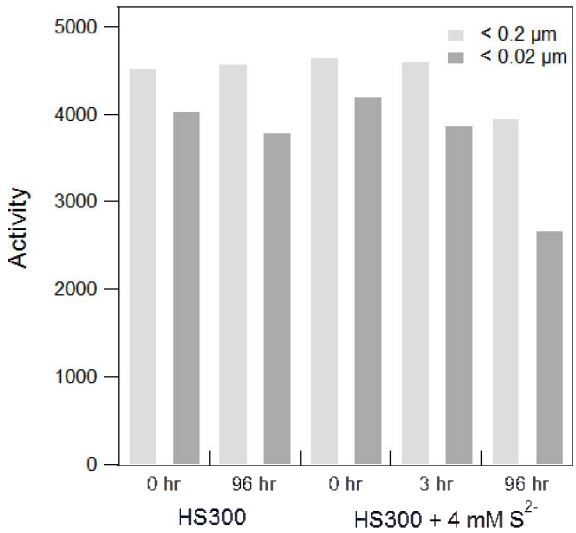

Figure S6. Tc concentration in the presence and absence of sulfide (activity in 0.2 and 0.02 µm filtrate was compared to differentiate colloidal Tc from dissolved TcO_4^-).

4. SEMs and TEMs of Sulfidated nZVI Exposed to TcO_4^-

Method

Scanning Electron Microscopy (SEM).

For Tc-containing material, a 5 µL drop was placed onto a silicon wafer and then anaerobically dried in the glove bag for scanning electron microscopy. The samples were coated using the Poloran carbon coater, and ~5−10 nm carbon coating was applied to each sample. Samples were analyzed in a FEI Quanta 3DFEG scanning electron microscope equipped with an Oxford 80 mm^2 SDD detector and INCA software. Initially 20 keV was used to analyze the samples but later changed to 30 keV to pick up the Tc L 18.2 line to confirm Tc was present since the M line overlaps with sulfur which is between 2.3−2.5 keV. Surface tomography of the samples was obtained at 5 keV since 20−30 keV destroys any surface tomography of the material.

Transmission Electron Microscopy (TEM).

For Tc-containing material, the sample preparation involved applying a 5 μL drop of material aqueous suspension to a 200-mesh copper TEM grid with carbon-coated formvar support film, (Electron Microscopy Sciences, Hatfield, PA). After 1 min, the excess liquid was removed by wicking, and the sample on a grid was anaerobically dried in the glove bag atmosphere (Coy Laboratories, Grass Lake, MI). The sample was anaerobically transferred to the TEM laboratory. Final loading of the sample on the holder required short period exposure to aerobic conditions. The prepared samples were imaged with JEOL 2010F transmission electron microscope operating at 200kV, coupled with INCA energy-dispersive spectroscopy (EDS) system (Oxford Instruments, UK) for elemental analysis.

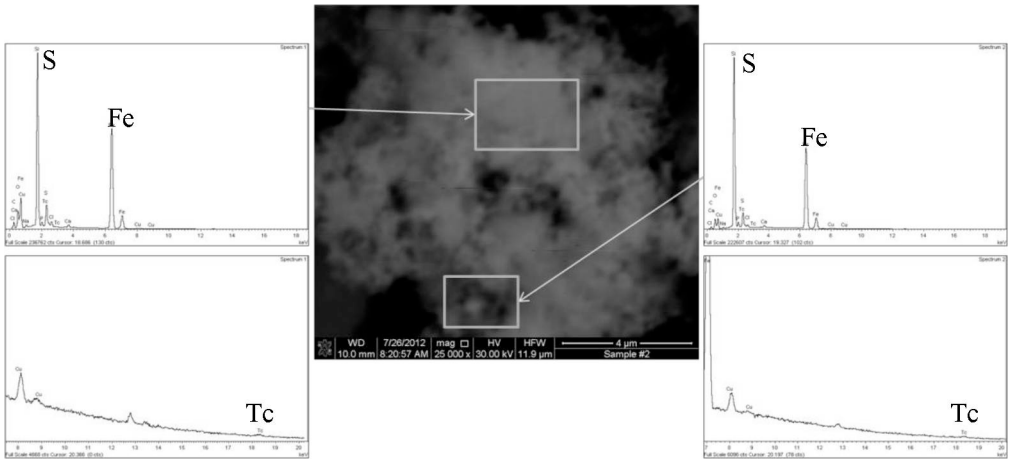

Figure S7. A Back scattered scanning electron micrograph (middle) of sulfidated nZVI (S/Fe = 0.112) exposed to 50 μM TcO_4^- and corresponding energy dispersive x-ray spectra (EDX) (top left: spectra 1; bottom left: enlarged spectra 1; top right: spectra 2; bottom right: enlarged spectra 2).

The chemical heterogeneity shown at the scale of SEM was not as significant as that seen by TEM (**Figure 5**). S/Fe ratios measured at multiple areas by EDX (**Figure S7** and other spectra (data not shown)) were around the input S/Fe ratio, which equals to 0.112. As a result, SEM did not show a significantly different Tc distribution pattern.

Isolated nZVI-like structure	Co-presence of nZVI-like and FeS-like structures	Hollow structures

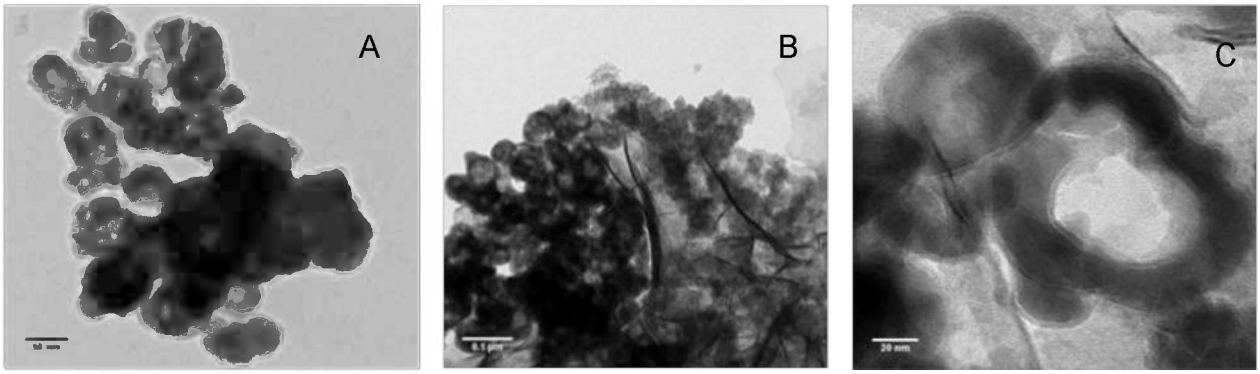

Figure S8. Transmission electron micrographs of representative morphologies of sulfidated nZVI exposed to TcO_4^- (images were collected on the same sample in **Figure 5**: $[TcO_4^-]$ = 50 μM, [nZVI] = 0.2 g L^{-1}, $[S^{2-}]$ = 0.4 mM, S/Fe = 0.112, pH = 7.9).

5. Additional XAS information

Method

Tc XAS samples were prepared by reacting 8.4 μM TcO_4^- with 0.5 g L^{-1} nZVI pre-exposed to 0–10 mM sulfide. After greater than 99% Tc (< 0.2 μm) removal, Tc-containing solids were centrifuged and loaded as a concentrated slurry/paste into single slot Teflon holders. The holders were then sealed with a single layer of Kapton tape and further contained inside a heat-sealed polypropylene bag. Samples were kept in an anaerobic chamber prior to the measurements and under a continuous He purge while collecting the XAS spectra. XAS measurements were taken at the Tc K-edge and were collected at the Stanford Synchrotron Radiation Lightsource (SSRL) on beamline 4-1 and 11-2. Spectra were measured at room temperature in fluorescence mode using a 13 (30) element solid state detector (Ge), and a N_2-cooled Si (220) double crystal monochromator, detuned for 20% for harmonic rejection. Energy calibration was internally measured during each scan using a Mo metal foil (Mo K-edge energy 20 KeV).

Linear combination fitting of EXAFS was performed in ATHENA for samples with S/Fe ratios ranging from 0.0056 to 0.56 using samples with S/Fe = 0 and 1.12 as two end members, respectively. The values of each component were normalized to the total spectral weight sum

from the components used in the linear combination. The total spectral weight sum ranged from 0.85 to 1 (without any constraining of the sum).

Additional results

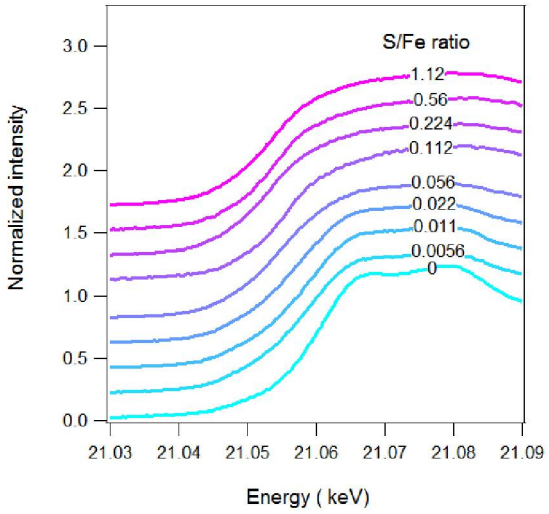

Figure S9. Tc K-edge XANES of Tc immobilized at incremental S/Fe ratios (The spectra were collected on the same set of samples as in **Figure 7**).

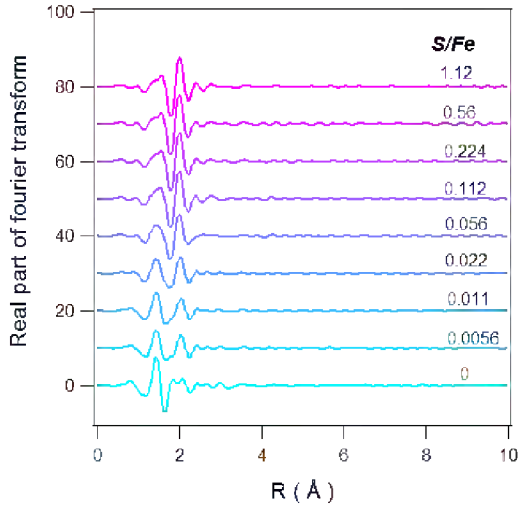

Figure S10. Real part of Fourier transform of EXAFS of Tc reduced at incremental S/Fe ratios (The spectra were collected on the same set of samples in **Figure 7**).

Table S4. Tc-EXAFS shell by shell fit for Tc reduced at S/Fe = 0 and 1.12 (*N*: coordination number; *D*: interatomic distance; σ^2: Debye-Waller factor; Standard deviation is in parenthesis)

		nZVI + Tc + 0 mM S^{2-}			nZVI + Tc + 10 mM S^{2-}
Tc-O1	*N*	†6	*Tc-S1*	*N*	‡2
	D (Å)	2.02(1)		*D* (Å)	2.30(2)
	σ^2 (Å^2)	0.006(1)		σ^2 (Å^2)	0.003(2)
Tc-Tc1		†1	*Tc-S2*		‡4
		2.44(3)			2.47(1)
		0.011(1)			0.003(2) [A]
Tc-Tc2		†1	*Tc-Tc1*		‡2
		3.19(4)			2.39(1)
		0.011(3) [a]			0.005(2) [†]
Tc-O2		†4	*Tc-Tc2*		‡1
		3.17(4)			2.58(2)
		0.009(2)			0.005(2) [B]
Tc-O3		†4	*Tc-S3*		‡2
		3.56(8)			3.13(1)
		0.009(2) [b]			0.005(2) [C]
Tc-Tc3		†4	*Tc-S4*		‡1
		3.71(2)			3.78(1)
		0.025(6)			0.005(2) [C]
Tc-O1-O1-Tc		6 [d]	*Tc-S5*		‡1
		4.06(2) [d]			3.98(3)
		0.011(2) [d]			0.005(2) [C]
Tc-Tc4		†4	*Tc-Tc3*		‡2
		4.01(2)			3.63(1)
		0.025(6) [c]			0.007(2) [D]
			Tc-Tc4		‡1
					3.81(2)
					0.007(2) [D]

† Coordination numbers maintained to crystallographic value of TcO_2.

‡ Coordination numbers maintained to crystallographic value of TcS_2

[a] $\sigma_{Tc\text{-}Tc1} = \sigma_{Tc\text{-}Tc2}$, [b] $\sigma_{Tc\text{-}O3} = \sigma_{Tc\text{-}O3}$, [c] $\sigma_{Tc\text{-}Tc4} = \sigma_{Tc\text{-}Tc3}$,

[d] Multiple scattering N, σ, and d constrained to Tc-O1 shell distances.

[A] $\sigma_{Tc\text{-}S1} = \sigma_{Tc\text{-}S2}$, [B] $\sigma_{Tc\text{-}Tc1} = \sigma_{Tc\text{-}Tc2}$, [C] $\sigma_{Tc\text{-}S} = \sigma_{Tc\text{-}Tc1+0.002}$, [D] $\sigma_{Tc\text{-}Tc} = \sigma_{Tc\text{-}Tc1+0.002}$

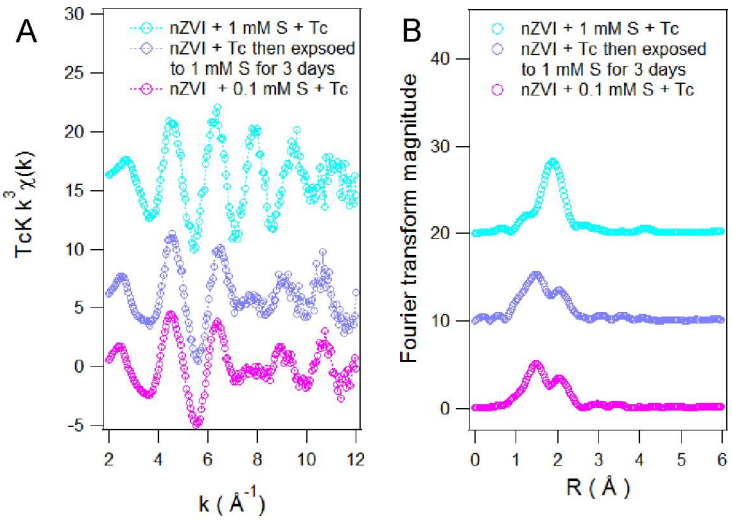

Figure S11. (***A***) Tc K-edge EXAFS and (***B***) the respective Fourier transform of Tc reduced by nZVI first then exposed to 1 mM sulfide for 3 days (spectra for Tc reduced under S/Fe = 0.011 and 0.112 were used for comparison).

6. Geochemical Speciation Modeling of Tc/Fe/S system

Methods

Geochemical speciation modeling was performed using the ACT subset of the Geochemist's Workbench modeling package, release 8.0 (RockWare Inc., Golden, CO) with the thermodynamic constants given in the thermo.com.v8.r6+ dataset. Additional data for FeS was adapted from Davison et al.[16] and input into the dataset. Speciation diagrams for Fe/Tc/S in artificial Hanford groundwater system (HS300) were generated using the concentrations listed in **Table S1**. In the generation and interpretation of these diagrams, it was assumed that activity (α) was equal to concentration.

Results

The Fe/Tc speciation diagram was constructed in a way that is similar to the experimental design. [HS^-] instead of [H^+] was used as x-axis variable in order to represent the evolution of sulfidogenic conditions. Equilibrium approach was used to calculate Fe and Tc speciation and elucidate possible Tc sequestration pathways in the presence of nZVI and sulfide. The diagram suggested that the hypothetical Tc sequestration pathways presented in **Figure 1** are thermodynamically possible. $TcO_2 \bullet nH_2O$ is the predominant reduced Tc phase when log $a[HS^-]$

is less than -23. Beyond that value, TcS_2 becomes the dominant reduced Tc phases. The boundary line between Tc_2S_7 and TcS_2 has a negative slope with respect to log $a[HS^-]$. As sulfide concentration further increases to the range of this study (shaded area), both TcS_2 and Tc_2S_7 are the dominant Tc phases, and this area coincidentally overlaps with the stability region of FeS. The diagram also indicates the possibility of transformation from $TcO_2 \bullet nH_2O$ to TcS_2 or from Tc_2S_7 to TcS_2. The first pathway is especially important in real remedial practice because $TcO_2 \bullet nH_2O$ is expected to be the dominant Tc reduced phase before sulfate reduction develops. This pathway has also been confirmed by XAS results (See **Figure S11**).

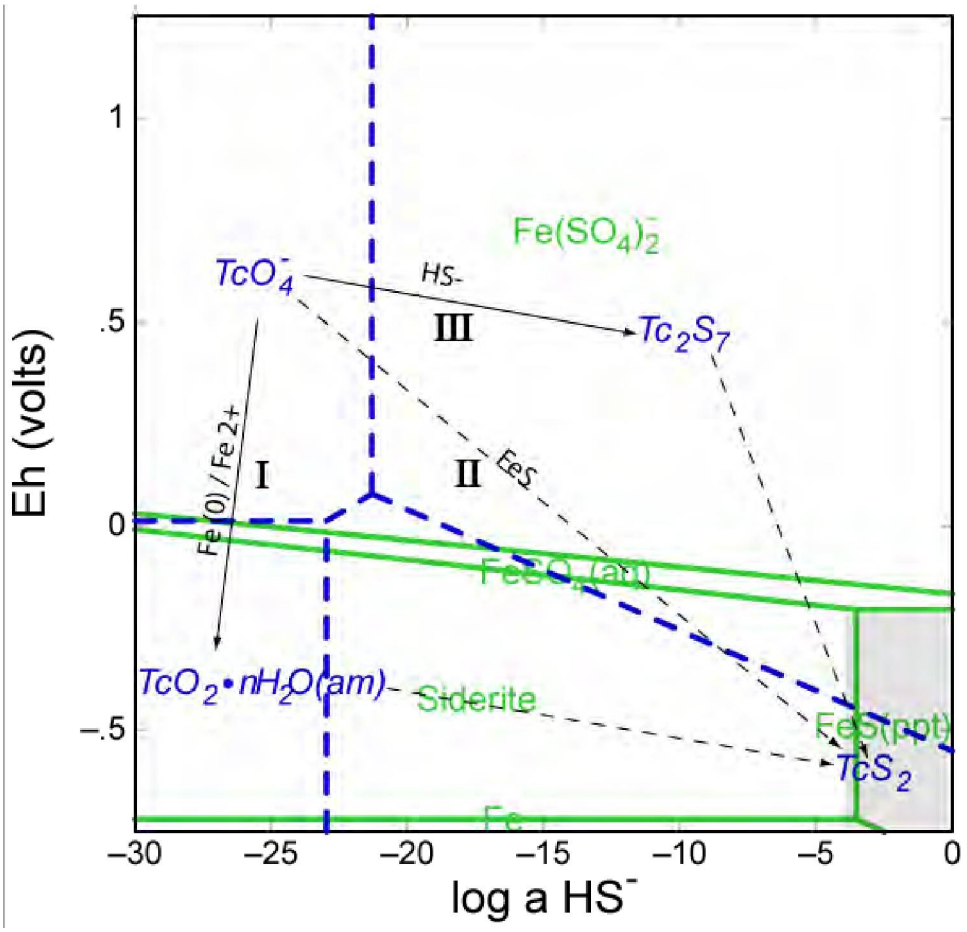

Figure S12. Eh vs. log a(HS^-) of Fe/S/Tc speciation diagram in HS300 (Fe and Tc speciation diagrams were independently constructed and overlaid with each other: areas with green boundaries are the Fe stability regions and areas with blue boundaries are the Tc stability regions; shaded area represents the experimental conditions in terms of sulfide concentration and expected Eh range; Solid arrows represent the known reaction pathways whereas dashed arrows represents hypothetical reaction pathways; Process **I**, **II**, and **III** correspond to the reaction pathways in **Figure 1**; Model input: [TcO_4^-] = 10 μM, pH = 7.9, T = 25 ºC).

References in supporting information

(1) Lee, J.-H.; Fredrickson, J. K.; Kukkadapu, R. K.; Boyanov, M. I.; Kemner, K. M.; Lin, X.; Kennedy, D. W.; Bjornstad, B. N.; Konopka, A. E.; Moore, D. A.; Resch, C. T.; Phillips, J. L. Microbial reductive transformation of phyllosilicate Fe(III) and U(VI) in fluvial subsurface sediments. *Environ. Sci. Technol.* **2012**, *46*, 3721-3730.

(2) Peretyazhko, T. S.; Zachara, J. M.; Kukkadapu, R. K.; Heald, S. M.; Kutnyakov, I. V.; Resch, C. T.; Arey, B. W.; Wang, C. M.; Kovarik, L.; Phillips, J. L.; Moore, D. A. Pertechnetate (TcO_4^-) reduction by reactive ferrous iron forms in naturally anoxic, redox transition zone sediments from the Hanford Site, USA. *Geochim. Cosmochim. Acta* **2012**, *92*, 48-66.

(3) Long, G. J.; Hautot, D.; Pankhurst, Q. A.; Vandormael, D.; Grandjean, F.; Gaspard, J. P.; Briois, V.; Hyeon, T.; Suslick, K. S. Mössbauer-effect and x-ray absorption spectral study of sonochemically prepared amorphous iron. *Phys. Rev. B* **1998**, *57*, 10716-10716.

(4) Nurmi, J. T.; Tratnyek, P. G.; Sarathy, V.; Baer, D. R.; Amonette, J. E.; Pecher, K.; Wang, C.; Linehan, J. C.; Matson, D. W.; Penn, R. L.; Driessen, M. D. Characterization and properties of metallic iron nanoparticles: spectroscopy, electrochemistry, and kinetics. *Environ. Sci. Technol.* **2005**, *39*, 1221-1230.

(5) Wang, Q.; Snyder, S.; Kim, J.; Choi, H. Aqueous ethanol modified nanoscale zerovalent iron in bromate reduction: synthesis, characterization, and reactivity. *Environ. Sci. Technol.* **2009**, *43*, 3292-3299.

(6) Kanel, S. R.; Grenèche, J.-M.; Choi, H. Arsenic(V) removal from groundwater using nano scale zero-valent iron as a colloidal reactive barrier material. *Environ. Sci. Technol.* **2006**, *40*, 2045-2050.

(7) Glavee, G. N.; Klabunde, K. J.; Sorensen, C. M.; Hadjipanayis, G. C. Chemistry of borohydride reduction of iron(II) and iron(III) ions in aqueous and nonaqueous media - formation of nanoscale Fe, FeB, and Fe_2B powders. *Inorg. Chem.* **1995**, *34*, 28-35.

(8) Forster, G. D.; Fernández Barquín, L.; Bilsborrow, R. L.; Pankhurst, Q. A.; Parkin, I. P.; Steer, W. A. Sodium borohydride reduction of aqueous iron–zirconium solutions: chemical routes to amorphous and nanocrystalline Fe–Zr–B alloys. *J. Mater. Chem.* **1999**, *9*, 2537-2544.

(9) Corrias, A.; Ennas, G.; Musinu, A.; Marongiu, G.; Paschina, G. Amorphous transition metal-boron ultrafine particles prepared by chemical methods. *Chem. Mater.* **1993**, *5*, 1722-1726.

(10) Van Wonterghem, J.; MØrup, S.; Koch, C. J. W.; Charles, S. W.; Wells, S. Formation of ultra-fine amorphous alloy particles by reduction in aqueous solution. *Nature* **1986**, *322*, 622-623.

(11) Wei, B.; Shima, M.; Pati, R.; Nayak, S. K.; Singh, D. J.; Ma, R.; Li, Y.; Bando, Y.; Nasu, S.; Ajayan, P. M. Room-temperature ferromagnetism in doped face-centered cubic fe nanoparticles. *Small* **2006**, *2*, 804-809.

(12) Nurmi, J.; Sarathy, V.; Tratnyek, P.; Baer, D.; Amonette, J.; Karkamkar, A. Recovery of iron/iron oxide nanoparticles from solution: comparison of methods and their effects. *J. Nanopart. Res.* **2011**, *13*, 1937-1952.

(13) Hansson, E. B.; Odziemkowski, M. S.; Gillham, R. W. Formation of poorly crystalline iron monosulfides: surface redox reactions on high purity iron, spectroelectrochemical studies. *Corros. Sci.* **2006**, *48*, 3767-3783.

(14) Rickard, D.; Luther III, G. W. Chemistry of iron sulfides. *Chem. Rev.* **2007**, *107*, 514-562.

(15) Morse, J. W.; Millero, F. J.; Cornwell, J. C.; Rickard, D. The chemistry of the hydrogen sulfide and iron sulfide systems in natural waters. *Earth-Sci. Rev.* **1987**, *24*, 1-42.

(16) Davison, W.; Phillips, N.; Tabner, B. J. Soluble iron sulfide species in natural waters: reappraisal of their stoichiometry and stability constants. *Aquat. Sci.* **1999**, *61*,

Environmental Science & Technology

Article

pubs.acs.org/est

Oxidative Remobilization of Technetium Sequestered by Sulfide-Transformed Nano Zerovalent Iron

Dimin Fan, Roberto P. Anitori,[†] Bradley M. Tebo, and Paul G. Tratnyek*

Institute of Environmental Health, Oregon Health & Science University, 3181 SW Sam Jackson Park Road, Portland, Oregon 97239, United States

Juan S. Lezama Pacheco

School of Earth Sciences, Environmental Earth System Science Department, Stanford University Stanford, Stanford, California 94305-4216, United States

Ravi K. Kukkadapu, Libor Kovarik, Mark H. Engelhard, and Mark E. Bowden

Environmental Molecular Sciences Laboratory, Richland, Washington 99354, United States

Supporting Information

ABSTRACT: Our previous study showed that formation of TcS_2-like phases is favored over TcO_2 under sulfidic conditions stimulated by nano zerovalent iron. This study further investigates the stability of Tc(IV) sulfide upon reoxidation by solution chemistry, solid phase characterization, and X-ray absorption spectroscopy. Tc dissolution data showed that Tc(VII) reduced by sulfide-transformed nZVI has substantially slower reoxidation kinetics than Tc(VII) reduced by nZVI only. The initial inhibition of Tc(IV) dissolution at S/Fe = 0.112 is due to the redox buffer capacity of FeS, which is evidenced by the parallel trends in oxidation−reduction potentials (ORP) and Tc dissolution kinetics. The role of FeS in inhibiting Tc oxidation is further supported by the Mössbauer spectroscopy and micro X-ray diffraction data at S/Fe = 0.112, showing persistence of FeS after 24-h oxidation but complete oxidation after 120-h oxidation. X-ray absorption spectroscopy data for S/Fe = 0.011 showed significantly increasing percentages of TcS_2 in the solid phase after 24-h oxidation, indicating stronger resistance of TcS_2 to oxidation. At S/Fe = 0.112, the XAS results revealed significant transformation of Tc speciation from TcS_2 to TcO_2 after 120-h oxidation. Given that no apparent Tc dissolution occurred during this period, the speciation transformation might play a secondary role in hindering Tc oxidation. Collectively, the results indicate that sequestrating Tc as TcS_2 under stimulated sulfate reduction is a promising strategy to improve the long-term stability of reduced Tc in subsurface remediation.

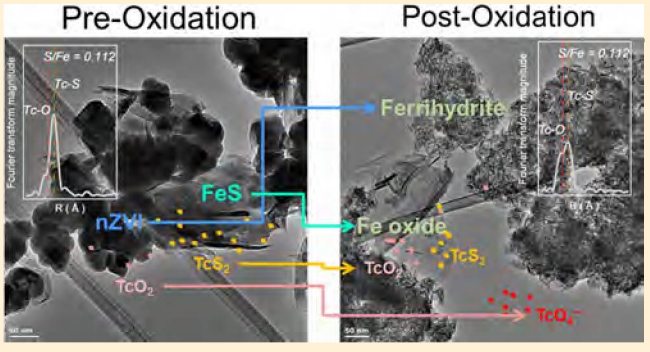

INTRODUCTION

Technetium-99 (^{99}Tc) is a common radioactive contaminant of groundwater at nuclear waste reprocessing sites.[1,2] The environmental risk of Tc arises primarily from its long half-life and high mobility as pertechnetate oxyanion ($Tc^{VII}O_4^-$) under oxic groundwater conditions.[3] Under anoxic conditions, the solubility and mobility of Tc are much less because $Tc^{VII}O_4^-$ is readily reduced to the relatively insoluble oxide, $Tc^{IV}O_2{\cdot}nH_2O$ (log K_{sp} = −8.4[4]) by a variety of abiotic and biotic processes. Many studies have suggested that dissimilatory iron reduction is the predominant biogeochemical process mediating the reductive sequestration of Tc[5−8] and that enhanced rates of Tc sequestration can be achieved with abiotic reductants like adsorbed Fe(II)[9−13] or Fe^0.[14] The resulting $Tc^{IV}O_2{\cdot}nH_2O$ can be sequestered by adsorption onto mineral surfaces,[10] incorporation into mineral lattice structures,[15] or association with organic matter.[16]

The long-term benefit of Tc sequestration by reduction, however, remains uncertain due to the high susceptibility of $Tc^{IV}O_2{\cdot}nH_2O$ to reoxidation. The reoxidation of reduced Tc oxide occurs when oxic groundwater or seawater intrudes into anoxic aquifers contaminated with Tc,[17] or when Tc-bound sediments are resuspended above the oxic-anoxic interface during seasonal redox cycling of the subsurface.[18] Although oxygen is generally considered to be the major cause of Tc

Received: April 1, 2014
Revised: May 31, 2014
Accepted: June 2, 2014
Published: June 2, 2014

reoxidation, other naturally occurring oxidants can also oxidize Tc(IV). Such oxidants include nitrate,[18,19] which is a common cocontaminant with Tc, and Mn(IV) oxides, which is an oxidant mainly of biogenic origin that recently has received substantial interests for its role in oxidizing UO_2.[20−24] The former process is coupled with microbial nitrate reduction with Tc(IV) oxide as the electron donor, while the latter reaction is mediated via solid-phase electron transfer.[22,23] Nevertheless, the rate of Tc reoxidation driven by these processes—at least as observed at the laboratory scale—is much slower than O_2-promoted oxidation.[19]

Enhanced stability of reduced Tc oxides against reoxidation has been observed when they are closely associated with host minerals.[10,15,25] This benefit was attributed to (i) formation of a protective layer that physically blocks oxygen diffusion to $Tc^{IV}O_2{\cdot}nH_2O$ and (ii) additional redox buffer capacity provided by host minerals (e.g., scavenging potential oxidants of Tc by structural Fe(II)), and (iii) incorporation of Tc(IV) into the lattice structures of the host minerals. However, the extent of stabilization varies substantially among different studies and appears to depend on the physical and chemical properties of host minerals and the specific experimental conditions under which reduced Tc is formed. For example, Frederickson et al.[25] compared the reoxidation rates of Tc reduced by two different iron-reducing sediments, and found a significantly slower Tc reoxidation rate for one material. They postulated that the slower and incomplete Tc oxidation was due to limited oxygen diffusion to Tc protected within aggregates that were only present in the less reactive sediment. In another study, Um et al.[15] reported that Tc(IV) reduced by Fe(II)-sorbed goethite exhibited strong resistance to reoxidation. However, in their experiments, the Tc-goethite mixture was annealed at 80 °C for 7 days to promote Tc substitution and incorporation into goethite structure. In general, Tc reduced by anaerobic sediments in microcosm studies seems to be more susceptible to oxidation than Tc reduced by pure or synthetic minerals. It is likely that the heterogeneity of natural sediments may favor the prevalence of labile Tc-mineral associations (e.g., physical adsorption) as opposed to relatively more stable associations with pure mineral phases (e.g., chemical adsorption or incorporation).

Given the high susceptibility of Tc oxides to oxidation, we have investigated an alternative strategy to sequester Tc as Tc sulfide by stimulating sulfidic conditions with nano zerovalent iron (nZVI). We recently showed that the sequestered Tc formed in this way is mainly composed of TcS_2-like phase.[26] Another recent study also reported the presence of TcS_2-like phases in microbially reduced hyporheic zone sediment, demonstrating the presence of Tc sulfide under less extreme environmental conditions.[27] On the basis of previous studies conducted under various conditions (mostly high pH and ionic strength to simulate waste leachate), reduced Tc sulfide phases, including TcS_2 and Tc_2S_7, appeared to be more resistant against oxidation.[28−31] The reoxidation rates of Tc_2S_7 by O_2 reported by Lukens et al.[30] and Liu et al.[28] are substantially slower than that of $TcO_2{\cdot}nH_2O$ reported elsewhere.[18,25] It was also shown that the TcS_2-like phases formed by coprecipitation with FeS transformed to $TcO_2{\cdot}nH_2O$ without being further oxidized to Tc(VII) in damp air.[31] Given the similar size of Tc(IV) and Fe(III) and the octahedral binding structure of both atoms to oxygen, the authors suggested that possible incorporation of Tc(IV) into the lattice structure of goethite—the oxidation product of FeS—stabilizes Tc(IV).

As a follow up to our previous work showing facile reductive sequestration of Tc by nZVI under sulfidic conditions, this study was performed to investigate the stability of the sequestration products with respect to oxidative dissolution. The primary goal was to characterize the changes in speciation of Tc during the reoxidation process under environmentally relevant conditions. However, because our prior work had demonstrated that secondary FeS (formed during sulfidation) is an important sink for Tc sequestration, this study also addressed changes in the host mineral composition (e.g., FeS) during oxygenation of the sample and its effects on Tc remobilization. The results confirm that reduced S containing phases of Tc and Fe contribute to the stability of Tc sequestration products, and therefore that this might form the basis for an improved strategy for remediation of technetium contaminated groundwater.

EXPERIMENTAL SECTION

Chemical Reagents. All reagents were reagent grade and used as received without further purification. ^{99}Tc was obtained as concentrated stock solution of ammonium pertechnetate (NH_4TcO_4) from Pacific Northwest National Laboratory. ^{99}Tc is a radioactive β emitter (half-life = 2.13×10^5 years; E_{max} = 294 keV) and was handled in a properly equipped radioactive laboratory.

Tc Reoxidation Experiments. Tc reoxidation was conducted following the conclusion of Tc reduction experiments. The latter were carried out as described previously.[26] Briefly, freshly prepared nZVI (0.2−0.5 g L^{-1}) was pre-equilibrated with various concentrations of sulfide (S/Fe molar ratio = 0−1.12) in 10 mL deoxygenated artificial Hanford groundwater HS300[32] (pH buffered at 7.8 with 30 mM HEPES, Chemical compositions shown in Table S1 in the Supporting Information (SI)) under anaerobic conditions for 24 h. TcO_4^- was then added to a final concentration of 6 μM. After >99% removal of aqueous Tc (<0.2 μm fraction), the reactors were left aging for different periods of time (7 days or 9 months) before reoxidation was initiated.

The reoxidation experiments were carried out by bubbling 0.2 μm filtered air into a water trap bottle, which then passed to the suspension via a 21 gauge needle through a butyl rubber septum (Bellco Glass; Vineland, NJ). The air bubbling rate (~2−3 bubbles/sec) was adjusted to provide gentle mixing of the solid and aqueous phases. No additional mixing was applied. For sampling, 0.3 mL of suspension was withdrawn from the reactor and passed through a 0.2 μm filter preflushed with N_2, and the Tc concentration in the filtrate was measured by liquid scintillation counter (Beckman; Brea, CA). Water loss due to evaporation was monitored by weighing reactors between each sampling and was found to be negligible.

Reoxidation of Host Minerals. To understand the evolution of host mineral phases during reoxidation, parallel Tc-free reoxidation experiments were conducted after 0.5 g L^{-1} nZVI was equilibrated with 0 and 1 mM sulfide for 7 days (S/Fe = 0 and 0.112). The procedure was the same as for the Tc reoxidation experiments, except that a large volume 50 mL reactor was used in order to provide a sufficient quantity of solids for material characterizations. During oxidation, the oxidation−reduction potential (ORP) of the suspension was measured intermittently with a Pt microelectrode with Ag/AgCl as a reference electrode. After 0, 24, 120, and 312 h of oxidation, the reactors were sacrificed, and the solids were recovered by vacuum filtration inside an anaerobic chamber

dx.doi.org/10.1021/es501607s | Environ. Sci. Technol. 2014, 48, 7409−7417

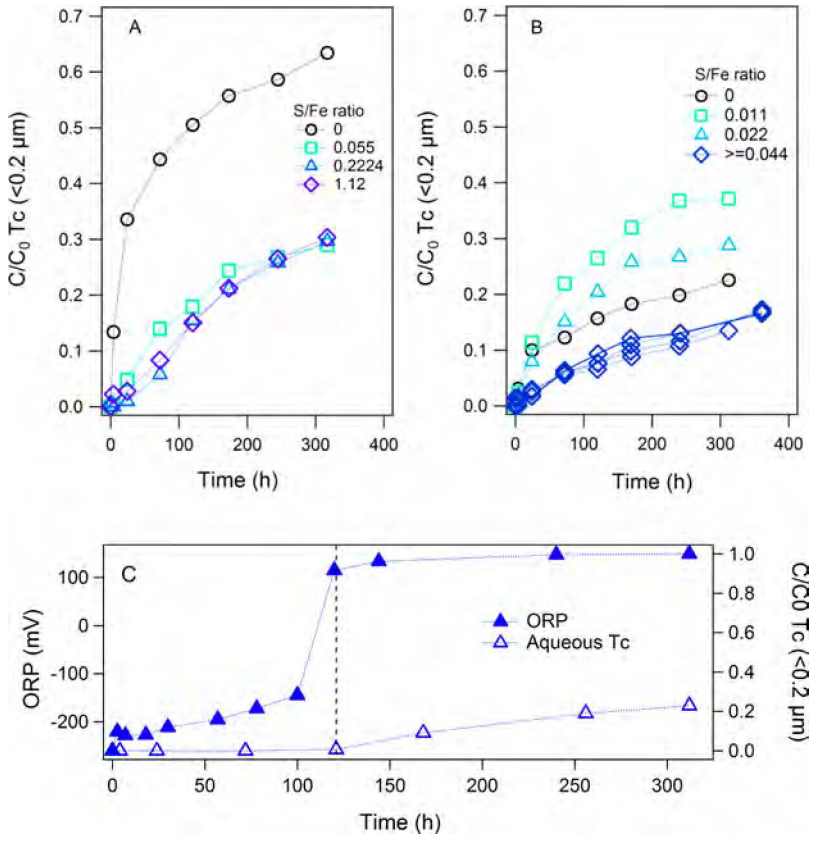

Figure 1. (A) Aqueous Tc reappearance kinetics of 7-day aged samples in 10 mL batches; (B) Tc reoxidation kinetics of 9-month aged samples in 10 mL batches; and (C) ORP and aqueous Tc concentration vs time during reoxidation in the 50 mL batch reactor at S/Fe = 0.112 aged for 7 days.

following the procedure described elsewhere.[33] The solids were then sealed under N_2 atmosphere and delivered to the Environmental Molecular Sciences Laboratory (EMSL, Richland, WA) for characterization.

Solid Phase Characterization. Preliminary characterization by Mössbauer spectroscopy on oxidized samples, with or without exposure to Tc, showed that Tc at the concentration used in this study has no detectable effect on the oxidation products of the host minerals. Therefore, further solid phase analysis was done with Tc-free samples for convenience. The bulk mineralogy of sulfidated nZVI throughout the oxidation process was characterized by micro X-ray diffraction (μXRD) and Mössbauer spectroscopy. The near-surface composition of the material was analyzed by X-ray photoelectron spectroscopy (XPS). The microscopic structures of the mineral phase were examined by transmission electron microscopy (TEM) with energy dispersive X-ray spectroscopy (EDS). Details for these methods are given in the SI.

X-ray Absorption Spectroscopy. Samples were prepared with the solids containing Tc freshly reduced by 0.5 g L^{-1} nZVI that was pretreated with 0, 0.1, and 1 mM sulfide (S/Fe: 0, 0.011, and 0.112) in 50 mL batch reactors. The reduced solids were further oxidized for 0, 24, 120, and 312 h, 7 days after Tc reduction completed. After oxidation, the solids were recovered by centrifugation and then loaded as a concentrated slurry/paste into single slot Teflon holders. The holders were then sealed with a single layer of Kapton tape and further contained inside a heat-sealed polypropylene bag. Additional samples that were aged in solution were also prepared for XAS following the same procedure. Details of those samples are given in SI. Loaded samples were kept in an anaerobic chamber prior to the measurements.

Tc K-edge XAS data were collected at the Stanford Synchrotron Radiation Lightsource (SSRL) on beamline 4−1 and 11−2. Spectra were measured at room temperature under a continuous He purge in fluorescence mode using a 13 (30) element solid state detector (Ge), and a N_2-cooled Si (220) double crystal monochromator, detuned 20% for harmonic rejection. Energy calibration was internally measured during each scan using a Mo metal foil (Mo K-edge energy 20000.0 eV). EXAFS spectra were analyzed using SixPack, Athena, and Artemis interfaces to the IFEFFIT package. Backscattering phase and amplitude functions required for fitting individual scattering contributions of spectra were obtained from FEFF8.

RESULTS AND DISCUSSION

Tc Reoxidation Kinetics. The reoxidation kinetics of freshly reduced Tc in 10 mL batch reactors is shown in Figure 1A. In the absence of sulfide, aqueous Tc rapidly increased during the initial 20-h oxygenation, presumably due to oxidative dissolution. After 20-h oxidation, the aqueous Tc appearance rate slowed, and appeared to gradually approach a plateau by 312-h oxidation. By the end of the experiments, approximately 30% of the Tc still remained associated with the solid phases, possibly because residual Tc phases that were more resistant to oxidation formed as oxidation progressed. This could be due to either Tc incorporation into the lattice structures of oxidized Fe mineral phases[15,31] or formation of secondary iron minerals that protect reduced Tc from oxidation. In the presence of sulfide, the Tc reappearance rate was significantly slower compared to the absence of sulfide. However, among three

dx.doi.org/10.1021/es501607s | Environ. Sci. Technol. 2014, 48, 7409−7417

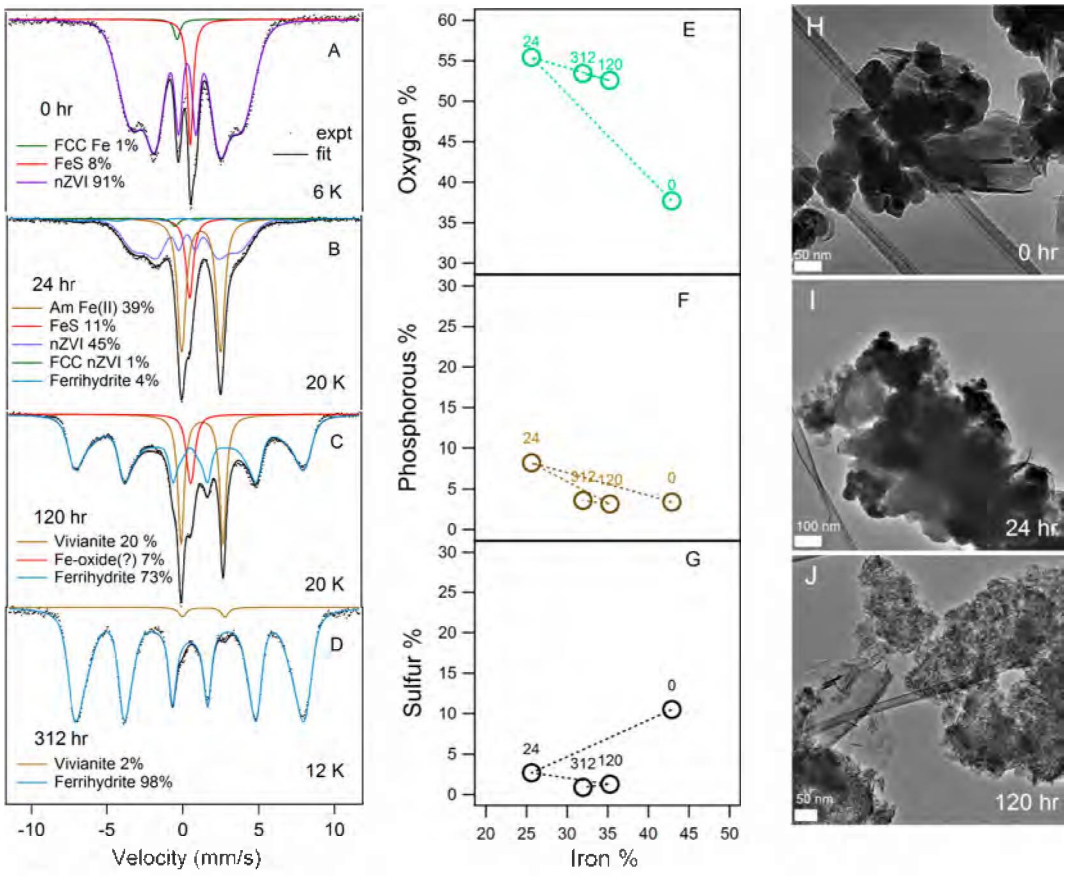

Figure 2. Solid phase characterizations of sulfidated nZVI (S/Fe = 0.112) during oxidation. Left panel: Experimental and modeled Mössbauer spectra of sulfidated nZVI after (A) 0, (B) 24, (C) 120, and (D) 312-h oxidation (FCC: face cubic center); Middle panel: XPS wide survey plot of surface atomic percentage of (E) oxygen, (F) phosphorus, (G) sulfur vs Fe during oxidation (numbers in E, F and G represent oxidation time; Sulfur refers exclusively to S^{2-}); Right panel: transmission electron micrographs of sulfidated nZVI after (H) 0, (I) 24, and (J) 120-h oxidation (associated EDS spectra are presented together with TEMs in SI Figure S5). All data for the 0-h oxidized sample are adopted from Fan et al.[26]

different S/Fe ratios (0.055, 0.224, and 1.12) that were tested initially, no appreciable difference of aqueous Tc concentration after 312-h oxidation was observed.

The trend in reoxidation kinetics observed in the presence and absence of sulfide is consistent with the speciation of reduced Tc produced across a range of S/Fe ratios that was reported in our reduction study.[26] In that work, we showed that TcO_4^- was directly reduced by nZVI to $TcO_2{\cdot}nH_2O$ in the absence of sulfide. With increasing sulfide doses—even at relatively low S/Fe ratios—a TcS_2-like phase quickly became the dominant reduced Tc species due to the high affinity of FeS for TcO_4^-. The slower kinetics of Tc reoxidation in the presence of sulfide appears to confirm the hypothesis that TcS_2-like phases are more resistant to oxidation than TcO_2. The lack of difference in Tc reoxidation kinetics at three S/Fe ratios also agrees with the finding that TcS_2 is the major component of reduced Tc species above S/Fe = 0.05.[26]

To test the effects of aging, reoxidation was also conducted on reduced Tc that was aged for 9 months (Figure 1B). Similar to freshly reduced samples, no appreciable difference in reoxidation kinetics was observed at S/Fe ratios above 0.044. However, at the two lowest S/Fe ratios tested (0.011 and 0.022)—where the percentage of TcO_2 formed was significantly higher[26]—Tc reoxidation was correspondingly faster and the kinetics seems to be positively correlated with the S/Fe ratio. This further indicates that TcS_2 is less labile to oxidation compared to TcO_2. It is noteworthy that the nZVI only sample aged for 9 month had slower reoxidation kinetics than S/Fe = 0.011 and 0.022. This result was not replicated and the reasons for it were not investigated, but it could arise from geochemical stabilization developed during the aging process. In fact, all of the 9-month aged samples at S/Fe > 0.044 had considerably slower reoxidation kinetics (Figure 1B) than their freshly reduced counterparts (Figure 1A).

Close inspection of the reoxidation kinetics of fresh samples (Figure 1A) shows that at relatively high S/Fe ratios (S/Fe = 0.22 and 1.12), there was an initial lag period of about 24 h during which little aqueous Tc was detected. By contrast, a relatively large fraction of reduced Tc was remobilized within 2 h after O_2 introduction in the absence of sulfide. A lag phase was also observed for uraninite oxidation in the presence of FeS,[34] and was attributed mainly to FeS being a redox buffer that scavenged dissolved O_2 (although the possibility of oxidized U being rereduced by Fe(II) was not excluded). Given that our previous study demonstrated that FeS is formed and this phase is responsible for sequestration of Tc as TcS_2,[26] the observed lag in initial Tc oxidation is most likely caused by FeS. It is also worth noting that the two highest S/Fe ratios did not result in longer lag phases, which is consistent with our prior finding[26] that FeS formation was inhibited at higher S/Fe ratios, presumably due to limited nZVI surface sites.

Parallel measurements of ORP and Tc dissolution in the 50 mL batch reactor (for the purpose of preparing XAS samples) at S/Fe = 0.112 further confirms the role of FeS in inhibiting

dx.doi.org/10.1021/es501607s | Environ. Sci. Technol. 2014, 48, 7409−7417

initial Tc oxidation by showing that (i) the lag period where Tc dissolution was inhibited was extended to ~120 h (compared to ~20 h in 10 mL batches), presumably because of the higher quantity of FeS in the larger reactor (Figure 1C); and (ii) the onset of active Tc dissolution occurred after a sharp rise in ORP from −150 to 100 mV around 120 h (Figure 1C). Although interpreting ORP data in our system is complicated by the presence of both dissolved and solid phase redox-active species,[35] the steep ORP rise at 120 h most likely reflects the depletion of reducing capacity contributed by nZVI and FeS due to reaction with dissolved oxygen. In fact, analogous ORP profiles have been observed in other studies where FeS was oxidized by oxygen,[34,36] and a similar concurrency between sharply increased ORP and uranium remobilization has been observed.[34]

Oxidation of Host Mineral Phases. Further investigation into the mineralogical transformations of the host minerals during oxidation was conducted at S/Fe = 0 and 0.112. Because the main focus of this study was on sulfidated nZVI, all characterizations of unsulfidated nZVI (S/Fe = 0) for comparison are presented in the SI (Figure S1−S2). The S/Fe ratio of 0.112 was chosen because our reduction study showed that this is the optimal S/Fe ratio in batch experiments to maximize FeS formation (higher S/Fe ratio did not result in more FeS formation) and to sequester Tc primarily as TcS_2.[26]

The μXRD of all oxidized samples was dominated by broad and indistinct features (SI Figure S1), in agreement with amorphous nature of the fully reduced starting material.[26] Minor peaks due to the following phases were also evident (SI Figure S1B): (i) mackinawite in 0, and 24 h samples, (ii) vivianite in 120 h sample (due to 1.5 mM phosphate in HS300), and (iii) broad peaks due to ferrihydrite-like mineral in 24, 120, and 312 h samples (ferrihydrite-like mineral content increased with oxidation time). Mössbauer spectroscopy measurements were used to quantify *bulk* changes in both nZVI and FeS components, together with evolved oxidized Fe mineral phases, during oxidation (Figure 2A−D). Prior to oxidation, the bulk solid was composed of ~8% mackinawite—the low spin (LS) Fe(II)-tetrahedral-compound shown as red singlet—and 92% nZVI, based on the Mössbauer characterization in our previous study (also shown in Figure 2A).[26]

After 24-h oxidation, the FeS singlet retained in the 20-K Mössbauer spectrum (Figure 2B), and the presence of FeS was further confirmed by multiple peaks that match mackinawite in μXRD (SI Figure S1B) and by TEM-EDS, showing the presence of typical FeS morphology with a S/Fe ratio close to 1 (SI Figure S5A). Nevertheless, XPS survey scan data on the 24-h oxidized sample indicated significant decrease of S^{2-} intensity (Figure 2E) and the Fe 2p narrow spectra (SI Figure S4A) also showed strong attenuation of the Fe(II)-S peak around 706.6 eV, both of which suggest the disappearance of reduced sulfide near the mineral surface. These results are consistent with prior studies showing significant FeS dissolution at the beginning of oxidation around acidic to neutral pH values.[37] A qualitative Mössbauer modeled fit (SI Figure S3) further revealed possible Fe(III) structures that might result from structural and surface oxidation of FeS.[34]

The main oxidized Fe species emerged after 24-h oxidation was high spin (HS) Fe(II), represented by a broad Fe(II) doublet in the 20-K Mössbauer spectrum (Figure 2B). The formation of Fe(II) primarily resulted from oxidation of nZVI as the reduction in the percentage of nZVI (from 92% to 45%) corresponded well with the formation of HS Fe(II) (39%), although a small fraction of Fe(II) could also have resulted from FeS oxidation. The nature of this HS Fe(II) phase, however, remains unclear. The XPS survey scan of the 24-h oxidation sample showed a large increase of P and O near the surface with decreased Fe (Figure 2E and F). Additionally, TEM (Figure 2I) showed that the exterior of mineral aggregates was mostly composed of less electron dense materials, which are enriched in P and Ca relative to the interior regions that are Fe rich (see EDS spectra, SI Figure S5A). However, no vivianite ($Fe_3(PO_4)_2{\cdot}8H_2O$) peaks were identified by μXRD (SI Figure S1). It is possible that at the early stage of oxidation, secondary mineral phases formed by dissolution, oxidation, and reprecipitation still mostly preserve the amorphous or nanocrystalline nature of the starting material. A small percentage of ferryhydrite (4%) was also identified by the modeled Mössbauer spectrum (the broad sextet in Figure 2B), presumably due to oxidation.

Further oxidation to 120 h resulted in more complete oxidation of host minerals. The fitting of the Mössbauer 20-K spectrum indicated that the percentage of ferrihydrite increased to 73% while the HS Fe(II) percentage decreased to 20% (Figure 2C). The residual high spin Fe(II) underwent further crystallization to form vivianite, which is supported by Mössbauer fitting parameters (SI Table S2) and μXRD (SI Figure S1B). A third component resembled the singlet feature of low spin Fe(II)S, but FeS peaks were not evident in the μXRD pattern (SI Figure S1B). Further examination of the Mössbauer fitting parameters showed slight deviations from the FeS component in the 0 and 24-h oxidized samples (SI Table S2). TEM (Figure 2J) showed that apart from the major structure that is composed of poorly crystalline small particles (presumably ferrihydrite based on the μXRD data), a small fraction of the solid materials exhibit the distinctive ribbon-like structure that is typical of mackinawite (Figure 2J and SI Figure S5C). The EDS, however, showed only Fe and O as the main elements with no or very low levels of sulfur (SI Figure S5B). It is possible that these structures were some transient phases of FeS oxidation (which likely caused the unidentified Mössbauer component with similar singlet shape to FeS in the 120-h oxidation sample) and had yet to be transformed to more stable phases. This might also indicate that the Fe atoms in nZVI and FeS were oxidized to different phases. By 312-h oxidation, the solid phase was nearly completely transformed to ferrihydrite, based on Mössbauer (Figure 2D) and μXRD data (SI Figure S1B).

Despite FeS only being a minor component of sulfidated nZVI (8% of the total solid based on Mössbauer fitting of the 0-h oxidation sample), its oxidation plays an important role in Tc remobilization because it is the major mineral phase that associated with Tc sulfide.[26] The effect of the oxidation of iron sulfide minerals on contaminant remobilization, including heavy metals and oxyanions, has been the subject of many studies.[34,37−41] Among various biotic and abiotic oxidizing agents, oxygen is of particular interest due to its ubiquitous role in chemical oxidation. The general consensus on the mechanism of abiotic oxidation of FeS by oxygen is that iron and sulfur undergo independent oxidations to form Fe (oxyhydr)oxide and elemental sulfur (polysulfide) as the main products, respectively. At neutral pHs, the oxidation of FeS was suggested to proceed via solution phase oxidation and solid phase mediated oxidation mechanisms.[34,37] Given that our study was conducted under comparable conditions (e.g., near neutral pH), it is expected that the oxidation of FeS component

dx.doi.org/10.1021/es501607s | Environ. Sci. Technol. 2014, 48, 7409−7417

in the current study follows the same pathway, despite the lack of complementary solution chemistry data. The absence of a strong polysulfide/elemental sulfur signal in our S2p XPS narrow scan (SI Figure S4B) could be because these spectra were collected at room temperature, which can cause sublimation of S^0 under high vacuum.[42] The difference in the iron mineralogy of the final oxidation product between this study and prior work might be largely due to variations in geochemical conditions (e.g., aqueous constituents).

Evolution of Tc Speciation. Both Tc reappearance kinetics and mineral characterizations suggest that the redox buffer capacity of sulfidated nZVI plays a key role in inhibiting initial Tc reoxidation. However, slower Tc reoxidation was also observed at the final stage of the batch experiments with sulfidated nZVI, even when the redox buffer capacity should have been depleted by extended exposure to oxygen (Figure 1A). Recalling that the reduction study showed that Tc was sequestered mainly as TcS_2 in the presence of sulfide,[26] it is possible that Tc speciation might be another reason for slower Tc reoxidation in the presence of sulfidated nZVI.

To further investigate the factor(s) that regulates Tc remobilization, X-ray absorption spectroscopy (XAS) measurements were performed to probe the change in speciation of reduced Tc during reoxidation. Tc K-edge data were collected on the solids of S/Fe = 0, 0.011, and 0.112 recovered after 0, 24, 120, and 312-h oxidation. In the absence of sulfide, both XANES (SI Figure S6A) and EXAFS (SI Figure S6B) showed that solid Tc speciation (S/Fe = 0) remained nearly unchanged throughout the oxidation process. Because the aqueous phase was mostly removed during XAS sample preparation, no oxidized Tc ($Tc(VII)O_4^-$) was observed (in contrast to the results described in Lukens et al.[30]). The Tc speciation was consistent with $TcO_2{\cdot}2H_2O$ shown in the reduction study,[26] along with many prior studies.[10,14,43]

The Tc reduction study showed that the speciation of reduced Tc at different S/Fe ratios can be represented by a mixture of TcO_2 and TcS_2, and that the Tc absorption edge position can be used as an indicator to qualitatively assess the respective content of TcS_2 and TcO_2 in a given mixture (because the former has about 6 eV lower absorption edge than the latter, even though both are Tc(IV) species).[26] In this study, at S/Fe = 0.011, the Tc absorption edge decreased from ca. 21059.2 to ca. 21056.6 eV after 24-h oxidation (Figure 3). This shift in the absorption edge position suggests an increasing percentage of TcS_2 after 24-h oxidation. This was further confirmed by increasing intensity for Tc—S binding in the Fourier transformed EXAFS (Figure 4B) and higher TcS_2 content based on linear combination fitting (Figure 4C). Given that little inhibition of Tc dissolution was observed at low S/Fe ratios—presumably due to minimal FeS formation—the increase in the TcS_2 percentage likely suggests that more TcO_2 relative to TcS_2 was oxidized to aqueous Tc(VII). After 120-h oxidation, the absorption edge, however, increased back to the level similar to that seen in the 0-h oxidation sample and the Tc—S peak attenuated in the Fourier transformed EXAFS spectrum (Figure 4B), indicating that TcS_2 was gradually oxidized (or transformed), leaving higher TcO_2 percentage in the solid phase.

At S/Fe = 0.112, the fully reduced Tc was mainly present as TcS_2 (>90% based on LCF of EXAFS data in Figure 4C). The initial 24-h oxidation resulted in little change of the overall Tc speciation as the absorption edge position remained at 21053 eV (Figure 3) and the EXAFS of the 0-h and 24-h oxidation

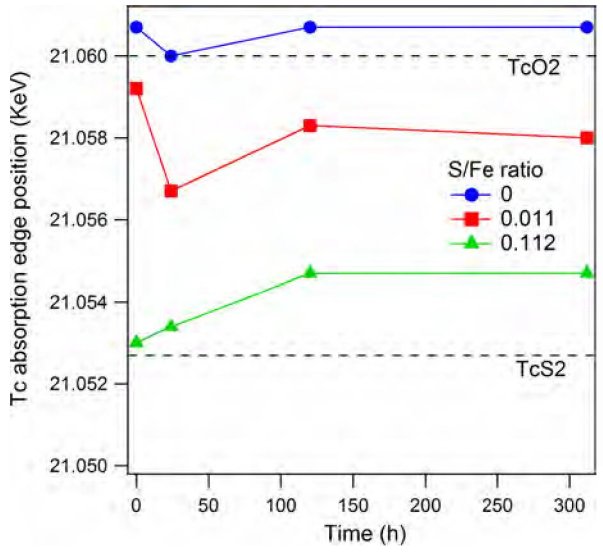

Figure 3. Tc XANES absorption edge positions during oxidation at S/Fe = 0, 0.011, and 0.112 (The values for the 0-h oxidized samples, TcO_2, and TcS_2 (dashed lines) are adopted from our Tc reduction study[26]).

samples were almost identical (Figure 4A). Because no significant Tc dissolution occurred during the initial 24 h (Figure 1C), little or no speciation change indicates that the presence of redox buffer capacity protected reduced Tc from oxidation. This is consistent with the solid phase characterization, showing substantial surface oxidation of the host minerals during the initial 24 h (Figure 2E–G). After 120-h oxidation, a significant change of solid Tc speciation was evident by XAS: (i) the absorption edge position increased by ~2 eV (Figure 3) and (ii) the Fourier transformed EXAFS showed notable enhancement of the Tc—O peak at the expense of a decreasing Tc—S peak (Figure 4B). Recall that the kinetic data still did not show elevated aqueous Tc concentration by this time point. Therefore, the substantially increasing percentage of TcO_2 in the solid phase could only have resulted from a change of Tc speciation in TcS_2 to TcO_2. A similar transformation from Tc sulfide to Tc oxide was reported for the oxidation of TcS_2-like phases in damp air in the presence of FeS.[31] However, in contrast with that study, where Tc(IV) was shown to be eventually incorporated into goethite structure, we found little evidence of Tc incorporation into the iron oxide or ferrihydrite mineral in this study (including Fe(II) in the second shell did not significantly improved the overall fitting). In addition, the EXAFS data showed a significant level of TcS_2 present in the solid phase after 312-h oxidation (data not shown), which implies that the transformation in speciation provided only a secondary barrier that partially inhibited Tc oxidation. Once the transformation began, TcO_2 became readily available for further oxidation.

Implications. Under the batch experimental conditions of this study, oxygenation of materials containing reduced Tc resulted in considerably lower release of $Tc^{VII}O_4^-$ when the Tc had been sequestered under sulfidic conditions. However, the practical benefit of creating sulfidic conditions to sequester Tc as TcS_2 will depend on whether recalcitrance of TcS_2 to oxidation can be maintained over the long-term under field-scale remediation conditions. It should be recognized that the batch experiments used in this study represented a worst case scenario in which Tc oxidation is favored by (i) unlimited

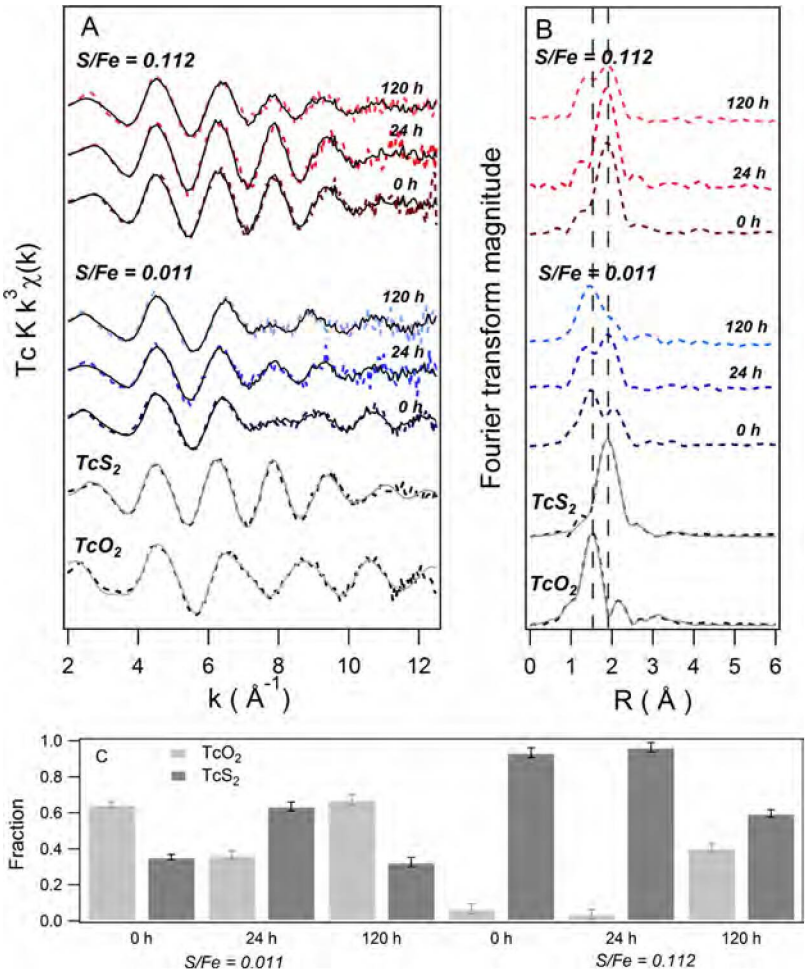

Figure 4. Tc K-edge (A) EXAFS and (B) the Fourier transformed EXAFS after 0, 24, and 120 h oxidation at S/Fe ratio = 0.011 and 0.112. Experimental data are shown by dashed lines and EXAFS fits are shown by solid lines. Vertical dashed lines in 4B denote the positions of first shell Tc—O and Tc—S binding. (C) Fraction of Tc speciation during oxidation at S/Fe = 0.011 and 0.112 based on linear combination fitting of EXAFS data (Tc reduced at S/Fe = 0 (TcO_2) and Tc reduced at S/Fe = 1.12 (TcS_2) and their respective shell-by-shell fitting were used as reference spectra.[26] Data for 0-h oxidized sample are adopted from the Tc reduction study.[26] Linear combination fitting of EXAFS of oxidized Tc at S/Fe = 0.011 and 0.112 was done using TcS_2 and TcO_2 as principle components.).

oxygen supply, (ii) no mass transport limitations, and (iii) limited redox buffer capacity of FeS. These conditions usually do not apply in the subsurface, which might make sequestration of Tc as TcS_2 more favorable under more realistic conditions. For example, the contact between reduced Tc and dissolved oxygen is likely to be limited by diffusion in vadose zone and low-flow groundwater system. Formation of secondary precipitates from iron oxidation and reprecipitation may further protect Tc from oxidation by increasing the thickness of the diffusion barrier. This effect might also explain the relatively stronger resistance to oxidation of aged samples observed in the present study. Dissolved oxygen concentration is likely to be limited due to upstream aerobic respiration by microorganisms, provided sufficient organic matter is present in aquifers. In fact, implementation of ZVI in combination with organic materials into the subsurface to stimulate in situ chemical and biological reduction has become a widely applied strategy in field remediation. With respect to the redox buffer capacity, given the general abundance of iron bearing minerals in the subsurface, the sulfidation process of these mineral phases could result in greater redox buffer capacity. Although the extent of protection exerted by these natural processes is not yet clearly understood, field data tends to show substantially less Tc mobilization than prediction derived from laboratory tests, even for TcO_2.[44]

It should be further noted that even though the high reactivity of iron sulfides for a variety of groups of subsurface contaminants has long been recognized,[45−50] FeS is commonly not considered to be stable in oxic environments. The current study may overestimate the stability of FeS and associated TcS_2 by not considering other biogeochemical processes that can oxidize FeS, such as microbially mediated oxidation (e.g., by Fe-oxidizing bacteria or nitrate-reducing bacteria) or abiotic oxidation by naturally occurring MnO_2.[51] Both of these processes have been shown to play significant roles in controlling the speciation and availability of trace metals in specific types of environments,[23,39,40] but their effects on Tc remobilization remain to be examined. Another important biogeochemical process that merits further investigation is pyritization, not only because pyrite is the ultimate sink for iron and sulfur in sulfidic environments,[52] but also because pyrite is generally considered to be less susceptible to oxidation than mackinawite. Furthermore, effective approaches to inhibit pyrite oxidation have been proposed by many prior studies,[53−55] which might be proven to be useful for further stabilization of reduced Tc sulfide.

dx.doi.org/10.1021/es501607s | Environ. Sci. Technol. 2014, 48, 7409−7417

■ ASSOCIATED CONTENT

Supporting Information

Details on the characterization and properties of original and sulfidated nZVI during oxidation and additional XAS data of Tc in unsulfidated nZVI during oxidation. This material is available free of charge via the Internet at http://pubs.acs.org.

■ AUTHOR INFORMATION

Corresponding Author

*Phone: 503-346-3431; fax: 503-346-3427; e-mail: tratnyek@ohsu.edu.

Present Address

[†]Department of Biology, Clark College, Vancouver, WA, 98663.

Notes

The authors declare no competing financial interest.

■ ACKNOWLEDGMENTS

This material is based on work supported by the Subsurface Biogeochemical Research Program of the U.S. Department of Energy, Award No. DE-SC0001376. This report has not been subject to review by the DOE and therefore does not necessarily reflect agency views and no official endorsements should be inferred. Mössbauer, XPS, μXRD, and TEM/EDS were performed using the Environmental Molecular Sciences Laboratory (EMSL), a national scientific user facility sponsored by the Department of Energy's Office of Biological and Environmental Research and located at Pacific Northwest National Laboratory. XAS was carried out at the Stanford Synchrotron Radiation Lightsource, a Directorate of SLAC National Accelerator Laboratory and an Office of Science User Facility operated for the U.S. Department of Energy Office of Science by Stanford University. The authors would like to thank Sung-Woo Lee for preliminary XAS data collection and discussion, Danielle Jansik and James Szecsody for general discussions.

■ REFERENCES

(1) Jones, T. E.; Khaleel, R.; Myers, D. A.; Shade, J. W.; Wood, M. I. A summary and evaluation of Hanford site tank farm subsurface contamination; Lockheed Martin Hanford: Richland, WA, HNF-2603, 1998.

(2) Beasley, T. M.; Dixon, P. R.; Mann, L. J. ^{99}Tc, ^{236}U, and ^{237}Np in the Snake River Plain aquifer at the Idaho National Engineering and Environmental Laboratory, Idaho Falls, Idaho. *Environ. Sci. Technol.* **1998**, *32*, 3875−3881.

(3) Icenhower, J. P.; Qafoku, N. P.; Zachara, J. M.; Martin, W. J. The biogeochemistry of technetium: A review of the behavior of an artificial element in the natural environment. *Am. J. Sci.* **2010**, *310*, 721−752.

(4) Rard, J. A. Current status of the thermodynamic data for technetium and its compounds and aqueous species. *J. Nucl. Radiochem. Sci.* **2005**, *6*, 197−204.

(5) Fredrickson, J. K.; Zachara, J. M.; Kennedy, D. W.; Kukkadapu, R. K.; McKinley, J. P.; Heald, S. M.; Liu, C.; Plymale, A. E. Reduction of TcO_4^- by sediment-associated biogenic Fe(II). *Geochim. Cosmochim. Acta* **2004**, *68*, 3171−3187.

(6) Lloyd, J. R.; Sole, V. A.; Van Praagh, C. V. G.; Lovley, D. R. Direct and Fe(II)-mediated reduction of technetium by Fe(III)-reducing bacteria. *Appl. Environ. Microbiol.* **2000**, *66*, 3743−3749.

(7) Plymale, A. E.; Fredrickson, J. K.; Zachara, J. M.; Dohnalkova, A. C.; Heald, S. M.; Moore, D. A.; Kennedy, D. W.; Marshall, M. J.; Wang, C.; Resch, C. T.; Nachimuthu, P. Competitive reduction of pertechnetate ($^{99}TcO_4^-$) by dissimilatory metal reducing bacteria and biogenic Fe (II). *Environ. Sci. Technol.* **2011**, *45*, 951−957.

(8) Pearce, C. I.; Liu, J.; Baer, D. R.; Qafoku, O.; Heald, S. M.; Arenholz, E.; Grosz, A. E.; McKinley, J. P.; Resch, C. T.; Bowden, M. E.; Engelhard, M. H.; Rosso, K. M. Characterization of natural titanomagnetites ($Fe_{3-x}Ti_xO_4$) for studying heterogeneous electron transfer to Tc(VII) in the Hanford subsurface. *Geochim. Cosmochim. Acta* **2014**, *128*, 114−127.

(9) Cui, D.; Eriksen, T. E. Reduction of pertechnetate in solution by heterogeneous electron transfer from Fe(II)-containing geological material. *Environ. Sci. Technol.* **1996**, *30*, 2263−2269.

(10) Zachara, J. M.; Heald, S. M.; Jeon, B.; Kukkadapu, R. K.; Liu, C.; McKinley, J. P.; Dohnalkova, A. C.; Moore, D. A. Reduction of pertechnetate [Tc(VII)] by aqueous Fe(II) and the nature of solid phase redox products. *Geochim. Cosmochim. Acta* **2007**, *71*, 2137−2157.

(11) Peretyazhko, T.; Zachara, J. M.; Heald, S. M.; Kukkadapu, R. K.; Liu, C.; Plymale, A. E.; Resch, C. T. Reduction of Tc(VII) by Fe(II) sorbed on Al (hydr)oxides. *Environ. Sci. Technol.* **2008**, *42*, 5499−5506.

(12) Peretyazhko, T.; Zachara, J. M.; Heald, S. M.; Jeon, B.-H.; Kukkadapu, R. K.; Liu, C.; Moore, D.; Resch, C. T. Heterogeneous reduction of Tc(VII) by Fe(II) at the solid−water interface. *Geochim. Cosmochim. Acta* **2009**, *72*, 1521−1539.

(13) Szecsody, J. E.; Jansik, D. P.; McKinley, J. P.; Hess, N. J. Influence of alkaline co-contaminants on technetium mobility in vadose zone sediments, *J. Environ. Radioact.* **2014**, [Online early access], http://dx.doi.org/10.1016/j.jenvrad.2014.1002.1003.

(14) Darab, J. G.; Amonette, A. B.; Burke, D. S. D.; Orr, R. D.; Ponder, S. M.; Schrick, B.; Mallouk, T. E.; Lukens, W. W.; Caulder, D. L.; Shuh, D. K. Removal of pertechnetate from simulated nuclear waste streams using supported zerovalent iron. *Chem. Mater.* **2007**, *19*, 5703−5713.

(15) Um, W.; Chang, H.; Icenhower, J. P.; Lukens, W. W.; Serne, R. J.; Qafoku, N. P.; Westsik, J. J. H.; Buck, E. C.; Smith, S. C. Immobilization of 99-technetium (VII) by Fe(II)-goethite and limited reoxidation. *Environ. Sci. Technol.* **2011**, *45*, 4904−4913.

(16) Maes, A.; Geraedts, K.; Bruggeman, C.; Vancluysen, J.; Rossberg, A.; Hennig, C. Evidence for the interaction of technetium colloids with humic substances by X-ray absorption spectroscopy. *Environ. Sci. Technol.* **2004**, *38*, 2044−2051.

(17) Eagling, J.; Worsfold, P. J.; Blake, W. H.; Keith-Roach, M. J. Mobilization of technetium from reduced sediments under seawater inundation and intrusion scenarios. *Environ. Sci. Technol.* **2012**, *46*, 11798−11803.

(18) McBeth, J. M.; Lear, G.; Lloyd, J. R. Technetium reduction and reoxidation in aquifer sediments. *Geomicrobiol. J.* **2007**, *24*, 189−197.

(19) Burke, I. T.; Boothman, C.; Lloyd, J. R.; Livens, F. R.; Charnock, J. M.; McBeth, J. M.; Mortimer, R. J. G.; Morris, K. Reoxidation behavior of technetium, iron, and sulfur in estuarine sediments. *Environ. Sci. Technol.* **2006**, *40*, 3529−3535.

(20) Chinni, S.; Anderson, C. R.; Ulrich, K.-U.; Giammar, D. E.; Tebo, B. M. Indirect UO_2 oxidation by Mn(II)-oxidizing spores of *Bacillus* sp. strain SG-1 and the effect of U and Mn concentrations. *Environ. Sci. Technol.* **2008**, *42*, 8709−8714.

(21) Liu, C.; Zachara, J. M.; Fredrickson, J. K.; Kennedy, D. W.; Dohnalkova, A. Modeling the inhibition of the bacterial reduction of U(VI) by β-MnO_2(s). *Environ. Sci. Technol.* **2002**, *36*, 1452−1459.

(22) Fredrickson, J. K.; Zachara, J. M.; Kennedy, D. W.; Liu, C.; Duff, M. C.; Hunter, D. B.; Dohnalkova, A. Influence of Mn oxides on the reduction of uranium(VI) by the metal-reducing bacterium *Shewanella putrefaciens*. *Geochim. Cosmochim. Acta* **2002**, *66*, 3247−3262.

(23) Wang, Z.; Lee, S.; Kapoor, P.; Tebo, B. M.; Giammar, D. E. Uraninite oxidation and dissolution induced by manganese oxide: A redox reacton between two insoluble minerals. *Geochim. Cosmochim. Acta* **2013**, *100*, 24−40.

(24) Bargar, J. R.; Williams, K. H.; Campbell, K. M.; Long, P. E.; Stubbs, J. E.; Suvorova, E. I.; Lezama-Pacheco, J. S.; Alessi, D. S.; Stylo, M.; Webb, S. M.; Davis, J. A.; Giammar, D. E.; Blue, L. Y.; Bernier-Latmani, R. Uranium redox transition pathways in acetate-amended sediments. *Proc. Natl. Acad. Sci. U.S.A.* **2013**, *110*, 4506−4511.

(25) Fredrickson, J. K.; Zachara, J. M.; Plymale, A. E.; Heald, S. M.; McKinley, J. P.; Kennedy, D. W.; Liu, C.; Nachimuthu, P. Oxidative dissolution of potential of biogenic and abiogenic TcO_2 in subsurface sediments. *Geochim. Cosmochim. Acta* **2009**, *73*, 2299−2313.
(26) Fan, D.; Anitori, R. P.; Tebo, B. M.; Tratnyek, P. G.; Lezama Pacheco, J. S.; Kukkadapu, R. K.; Engelhard, M. H.; Bowden, M. E.; Kovarik, L.; Arey, B. W. Reductive sequestration of pertechnetate ($^{99}TcO_4^-$) by nano zerovalent iron (nZVI) transformed by abiotic sulfide. *Environ. Sci. Technol.* **2013**, *47*, 5302−5310.
(27) Lee, J.-H.; Zachara, J. M.; Fredrickson, J. K.; Heald, S. M.; McKinley, J. P.; Plymale, A. E.; Resch, C. T.; Moore, D. A. Fe(II)- and sulfide-facilitated reduction of $^{99}Tc(VII)O_4^-$ in microbially reduced hyporheic zone sediments. *Geochim. Cosmochim. Acta* **2013**, *136*, 247−264.
(28) Liu, Y.; Terry, J.; Jurrison, S. Pertechnetate immobilization in aqueous media with hydrogen sulfide under anaerobic and aerobic environments. *Radiochim. Acta* **2007**, *95*, 717−725.
(29) Liu, Y.; Terry, J.; Jurrison, S. Pertechnetate immobilization with amorphous iron sulfide. *Radiochim. Acta* **2008**, *96*, 823−833.
(30) Lukens, W. W.; Bucher, J. J.; Shuh, D. K.; Edelstein, N. M. Evolution of technetium speciation in reducing grout. *Environ. Sci. Technol.* **2005**, *39*, 8064−8070.
(31) Livens, F. R.; Jones, M. J.; Hynes, A. J.; Charnock, J. M.; Mosselmans, J. F. W. X-ray absorption spectroscopy studies of reactions of technetium, uranium and neptunium with mackinawite. *J. Environ. Radioact.* **2004**, *74*, 211−219.
(32) Lee, J.-H.; Fredrickson, J. K.; Kukkadapu, R. K.; Boyanov, M. I.; Kemner, K. M.; Lin, X.; Kennedy, D. W.; Bjornstad, B. N.; Konopka, A. E.; Moore, D. A.; Resch, C. T.; Phillips, J. L. Microbial reductive transformation of phyllosilicate Fe(III) and U(VI) in fluvial subsurface sediments. *Environ. Sci. Technol.* **2012**, *46*, 3721−3730.
(33) Nurmi, J.; Sarathy, V.; Tratnyek, P.; Baer, D.; Amonette, J.; Karkamkar, A. Recovery of iron/iron oxide nanoparticles from solution: comparison of methods and their effects. *J. Nanopart. Res.* **2011**, *13*, 1937−1952.
(34) Bi, Y.; Hyun, S. P.; Kukkadapu, R.; Hayes, K. F. Oxidative dissolution of UO_2 in a simulated groundwater containing synthetic nanocrystalline mackinawite. *Geochim. Cosmochim. Acta* **2012**, *102*, 175−190.
(35) Shi, Z.; Nurmi, J. T.; Tratnyek, P. G. Effects of nano zero-valent iron (nZVI) on oxidation-reduction potential (ORP). *Environ. Sci. Technol.* **2011**, *45*, 1586−1592.
(36) Jeong, H. Y.; Han, Y.; Hayes, K. F. X-ray absorption and X-ray photoelectron spectroscopic study of arsenic mobilization during mackinawite (FeS) oxidation. *Environ. Sci. Technol.* **2010**, *44*, 955−961.
(37) Jeong, H. Y.; Han, Y.; Park, S. W.; Hayes, K. F. Aerobic oxidation of mackinawite (FeS) and its environmental implication for arsenic mobilization. *Geochim. Cosmochim. Acta* **2010**, *74*, 3182−3198.
(38) Holmes, J. Fate of incoporated metals during mackinawite oxidation in sea water. *Appl. Geochem.* **1999**, *14*, 277−281.
(39) Schippers, A.; Jørgensen, B. B. Oxidation of pyrite and iron sulfide by manganese dioxide in marine sediments. *Geochim. Cosmochim. Acta* **2001**, *65*, 915−922.
(40) Schippers, A.; Sand, W. Bacterial leaching of metal sulfides proceeds by two indirect mechanisms via thiosulfate or via polysulfides and sulfur. *Appl. Environ. Microbiol.* **1999**, *65*, 319−321.
(41) Burton, E. D.; Bush, R. T.; Sullivan, L. A. Acid-volatile sulfide oxidation in coastal flood plain drains: iron−sulfur cycling and effects on water quality. *Environ. Sci. Technol.* **2006**, *40*, 1217−1222.
(42) Hampton, M. A.; Plackowski, C.; Nguyen, A. V. Physical and chemical analysis of elemental sulfur formation during galena surface oxidation. *Langmuir* **2011**, *27*, 4190−4201.
(43) Lukens; Bucher, J. J.; Edelstein, N. M.; Shuh, D. K. Products of pertechnetate radiolysis in highly alkaline solution: Structure of $TcO_2 \cdot xH_2O$. *Environ. Sci. Technol.* **2002**, *36*, 1124−1129.
(44) Hu, Q. H.; Rose, T. P.; Zavarin, M.; Smith, D. K.; Moran, J. E.; Zhao, P. H. Assessing field-scale migration of radionuclides at the Nevada Test Site: "mobile" species. *J. Environ. Radioact.* **2008**, *99*, 1617−1630.
(45) Scheinost, A. C.; Charlet, L. Selenite reduction by mackinawite, magnetite, and siderite: XAS characterization of nanosized redox products. *Environ. Sci. Technol.* **2008**, *42*, 1984−1989.
(46) Jeong, H. Y.; Sun, K.; Hayes, K. F. Microscopic and spectroscopic characterization of Hg(II) immobilization by mackinawite (FeS). *Environ. Sci. Technol.* **2010**, *44*, 7476−7483.
(47) Veeramani, H.; Scheinost, A. C.; Monsegue, N.; Qafoku, N. P.; Kukkadapu, R.; Newville, M.; Lanzirotti, A.; Pruden, A.; Murayama, M.; Hochella, M. F. Abiotic reductive immobilization of U(VI) by biogenic mackinawite. *Environ. Sci. Technol.* **2013**, *47*, 2361−2369.
(48) Bulter, E. C.; Hayes, K. F. Factors influencing rates and products in the transformation of trichloroethylene by iron sulfide and iron metal. *Environ. Sci. Technol.* **2001**, *35*, 3884−3891.
(49) Hyun, S. P.; Davis, J. A.; Sun, K.; Hayes, K. F. Uranium(VI) reduction by iron(II) monosulfide mackinawite. *Environ. Sci. Technol.* **2012**, *46*, 3369−3376.
(50) Turcio-Ortega, D.; Fan, D.; Tratnyek, P. G.; Kim, E.-J.; Chang, Y.-S. Reactivity of Fe/FeS nanoparticles: Electrolyte composition effects on corrosion electrochemistry. *Environ. Sci. Technol.* **2012**, *46*, 12484−12492.
(51) Aller, R. C.; Rude, P. D. Complete oxidation of solid phase sulfides by manganese and bacteria in anoxic marine sediments. *Geochim. Cosmochim. Acta* **1988**, *52*, 751−765.
(52) Morse, J. W.; Millero, F. J.; Cornwell, J. C.; Rickard, D. The chemistry of the hydrogen sulfide and iron sulfide systems in natural waters. *Earth-Sci. Rev.* **1987**, *24*, 1−42.
(53) Elsetinow, A. R.; Schoonen, M. A. A.; Strongin, D. R. Aqueous geochemical and surface science investigation of the effect of phosphate on pyrite oxidation. *Environ. Sci. Technol.* **2001**, *35*, 2252−2257.
(54) Zhang, Y. L.; Evangelou, V. P. Formation of ferric hydroxide-silica coatings on pyrite and its oxidation behavior. *Soil Sci.* **1998**, *163*, 53−62.
(55) Kargbo, D. M.; Atallah, G.; Chatterjee, S. Inhibition of pyrite oxidation by a phospholipid in the presence of silicate. *Environ. Sci. Technol.* **2004**, *38*, 3432−3441.

SUPPORTING INFORMATION

Oxidative Remobilization of Technetium Sequestered by Sulfide-transformed Nano Zerovalent Iron

*Dimin Fan, Roberto P. Anitori[1], Bradley M. Tebo, and Paul G. Tratnyek**
Institute of Environmental Health
Oregon Health & Science University
3181 SW Sam Jackson Park Road, Portland, OR 97239
[1]Current address: Department of Biology, Clark College, Vancouver, WA, 98663

Juan S. Lezama Pacheco
School of Earth Sciences, Environmental Earth System Science Department,
Stanford University
Stanford, CA, 94305-4216

Ravi K. Kukkadapu, Libor Kovarik, Mark H. Engelhard, Mark E. Bowden,
Environmental Molecular Sciences Laboratory
Richland, WA, 99354

*Corresponding author:
Email: tratnyek@ohsu.edu, Phone: 503-346-3431, Fax: 503-346-3427

Contents

Composition of Hanford artificial groundwater (HS300)

Table S1. Recipe for Hanford artificial groundwater (HS300[a])

Component	Concentration (mM)
$NaHCO_3$	1.44
$KHCO_3$	0.16
$MgCl_2 \cdot 6H_2O$	0.51
$CaCl_2 \cdot 2H_2O$	0.37
$CaSO_4 \cdot 2H_2O$	0.63
NaH_2PO_4	1.50
NH_4Cl	4.70
HEPES	30.00

[a] Modified from SGW1 medium in Lee et al.[1]

Additional Information on Solid Phase Characterization

Methods

Micro X-ray Diffraction

Powders for diffraction analysis were loaded into 0.5 mm glass capillaries (Charles Supper Co., MA) under nitrogen atmosphere and sealed with wax. Diffraction data were recorded by the 2D image plate of a Rigaku D/Max Rapid II diffractometer. Cr Kα radiation (λ = 2.2910 Å) focused through a 300 μm diameter collimator was used, which avoids the high background produced from fluorescence of Fe-containing samples. The 2-dimensional diffraction data were integrated between 10 and 160° 2θ to give powder traces. Backgrounds were removed using the JADE software (Materials Data Inc. CA) by fitting a smooth spline curve, guided by a trace from an empty capillary.

Mössbauer Spectroscopy

Sample preparation for Mössbauer spectroscopy was identical to the procedures reported in Peretyazhko et al.[2] Mössbauer spectra of the samples were collected using either a WissEl Elektronik (Germany) or Web Research Company (St. Paul, MN) instrument that included a

closed-cycle cryostat SHI-850 obtained from Janis Research (Wilmington, MA), a Sumitomo CKW-21 He compressor unit (Wilmington, MA), and an Ar-Kr proportional counter detector with WissEl setup or a Ritverc (St. Petersburg, Russia) NaI detection system. A ^{57}Co/Rh source (50 mCi to 75 mCi, initial strength) was used as the gamma energy source. With the WissEl setups, the transmitted counts were stored in a multichannel scalar (MCS) as a function of energy (transducer velocity) using a 1024-channel analyzer. The setups data were folded to 512 channels to provide a flat background and a zero-velocity position corresponding to the center shift (CS) of a metal Fe foil at room temperature (RT). Calibration spectra were obtained with a 25 μm thick Fe foil (Amersham, England) placed in the same position as the samples to minimize any geometry errors. The Mössbauer data were modeled with Recoil^{TM} software (University of Ottawa, Canada) using a Voigt-based structural fitting routine.

X-Ray Photoelectron Spectroscopy

The XPS analyses were conducted using a Physical Electronics Quantera Scanning ESCA Microprobe with a focused monochromatic Al Ka X-ray source (1486.7 eV) source and a spherical section analyzer. The mineral powder sample was mounted inside a nitrogen recirculated glove box operated at <0.5 ppm O_2. The samples were pressed onto double sided Scotch tape (#34-8507-5367-3) and supported by 1 cm x 3 cm clean flat Si (100) wafers. The individual Si wafer pieces were mounted onto the standard Physical Electronics 75 mm x 75 mm sample holder using 2-56 stainless steel screws. The sample holder was placed into the XPS vacuum introduction system and pumped to <1 x 10^{-6} Torr using a turbomolecular pumping system prior to introduction into the main ultra-high vacuum system. The main vacuum system pressure is maintained at <5 x 10^{-9} Torr during analysis and pumped using a series of sputter ion pumps and turbo-molecular pumps. For large collections of mineral particles, the X-ray beam was operated at approximately 100 W, focused to 100 μm diameter, and rastered over a 1.3 mm x 0.1 mm rectangle on the sample. The X-ray beam is incident normal to the sample and the photoelectron detector is at 45° off-normal. High energy resolution spectra were collected using a pass-energy of 69.0 eV with a step size of 0.125 eV. For the Ag 3d5/2 line, these conditions produced a FWHM (full width at half maximum) of 0.91 eV. The sample experienced variable degrees of charging. Low energy electrons at ~1 eV, 20 μA and low energy Ar^+ ions were used to minimize this charging. The spectra were aligned to a carbon peak energy of 285.0 eV (adventitious carbon). The compositional results were obtained using the standard sensitivity

factors in the Phi Multipak software package using peak area intensities after a Shirley background substation.

Transmission Electron Microscopy (TEM)

The samples without exposure to Tc were prepared for TEM observations by dispersing a dry powder on a lacey-carbon coated 200 mesh Cu TEM grids under anaerobic conditions. In a subsequent step of loading the sample into the TEM, however, the samples were exposed to aerobic conditions for a period of few minutes. TEM conventional and high-resolution images were performed with spherical aberration corrected FEI Titan 80-300 operated at 300kV. The elemental analysis was performed with EDAX Si (Li) EDS detector and a subsequent analysis was performed with TIA software.

Results

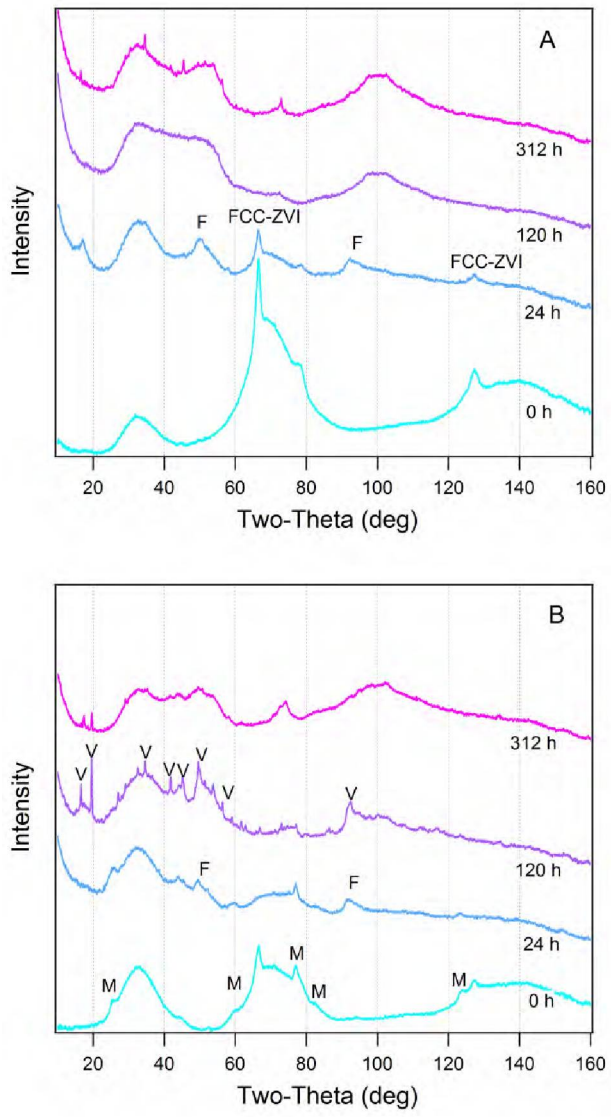

Figure S1. Micro-XRD of nZVI (**A**) and sulfidated nZVI at S/Fe = 0.112 (**B**) after 0, 24, 120, and 312-h oxidation (**F**: ferrihydrite; **V**: vivianite; and **M**: mackinawite).

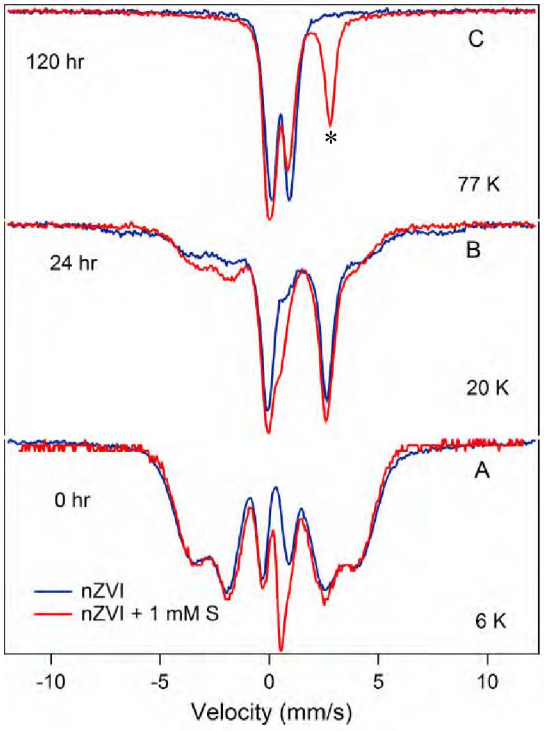

Figure S2. Mössbauer spectra of unsulfidated nZVI (blue) and sulfidated nZVI (red) at (**A**) 0, (**B**) 24, and (**C**) 120-h oxidation. The spectra of two different S/Fe ratios at each time point were superimposed to facilitate direct visual comparison (the data for the 0-h oxidized samples are adopted from our previous Tc reduction study.[3]).

Mossbauer spectroscopy data for nZVI and sulfidated NZVI were compared to show the difference in effect of oxygen on these samples. Comparison of the spectra indicated that nZVI was relatively more oxidized in the non-sulfidated sample (for the same length of exposure), which is evident from: (*i*) lower amounts of nZVI in 24-h oxidized sample at S/Fe = 0, and (*ii*) absence of Fe(II) doublet in 120-h oxidized sample at S/Fe = 0 (high energy peak of the Fe(II) doublet is indicated by *). Also, the differences in 120-h spectra at 77 K (Figure S2C) and 20 K spectrum (Figure 2C) is due to magnetic ordering of ferrihydrite at 20 K. Paramagnetic ferrihydrite transforms to sextet below 77 K.[4]

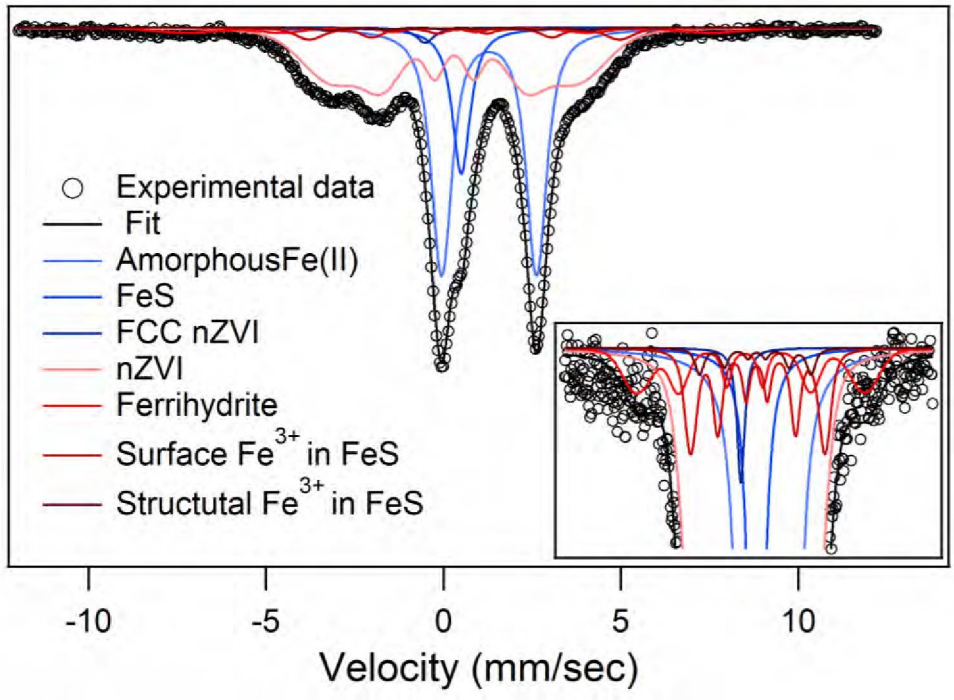

Figure S3. A qualitative modeled fit showing sextet peaks due to structural and surface oxidized Fe^{3+} in mackinawite, as reported in Bi et al.[5]. The fit is not optimum because statistically equivalent fits with different nZVI and oxidized Fe^{3+} are also possible. The fit is mainly shown to indicate oxidized Fe^{3+} in mackinawite sextet positions.

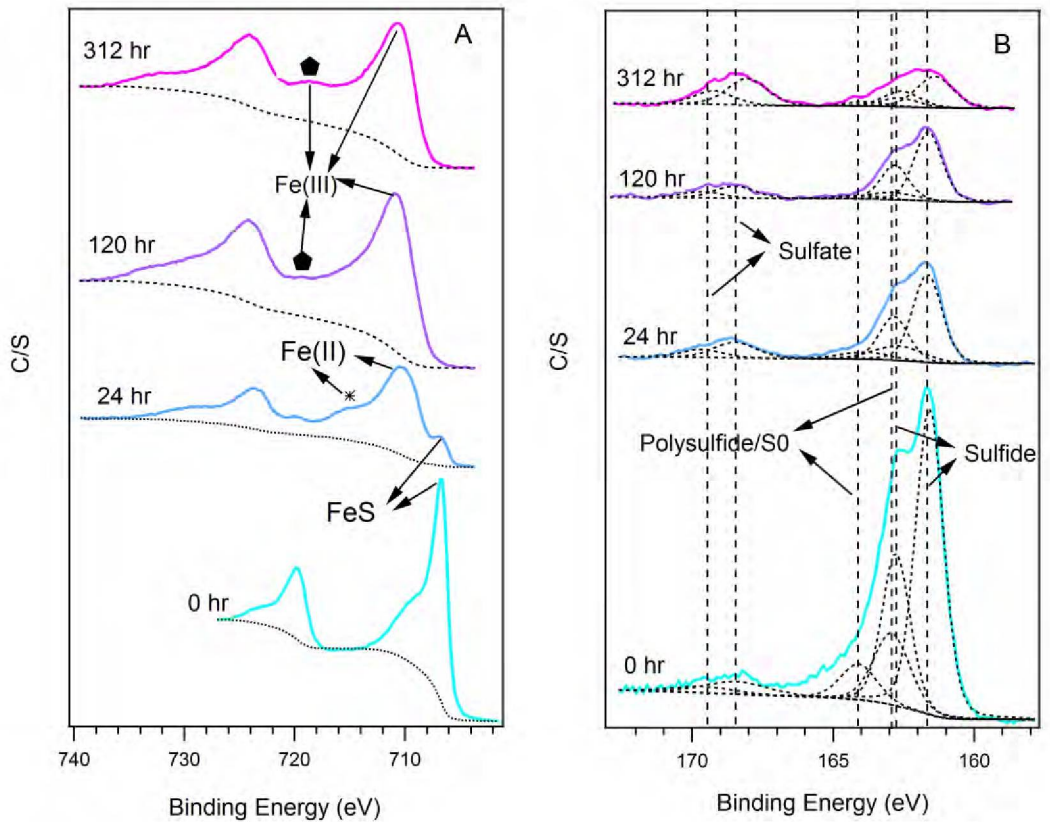

Figure S4. XPS Fe2p (**A**) and S2p (**B**) narrow spectra of sulfidated nZVI (S/Fe = 0.112) after 0, 24, 120, and 312-h oxidation. In Figure S2A, asterisk mark the Fe(II) satellite peak, solid diamonds mark the Fe(III) satellite peaks. Peak assignments are based on literature values obtained from Descostes et al.[6] and Mullet et al.[7] In Figure S2B, spectra were fitted by the modeled individual components of sulfur species, whose binding energies are shown by dashed lines. Small sulfate peaks in 0-h oxidized sample is likely due to surface oxidation even though great care was taken to prevent contact with oxygen.

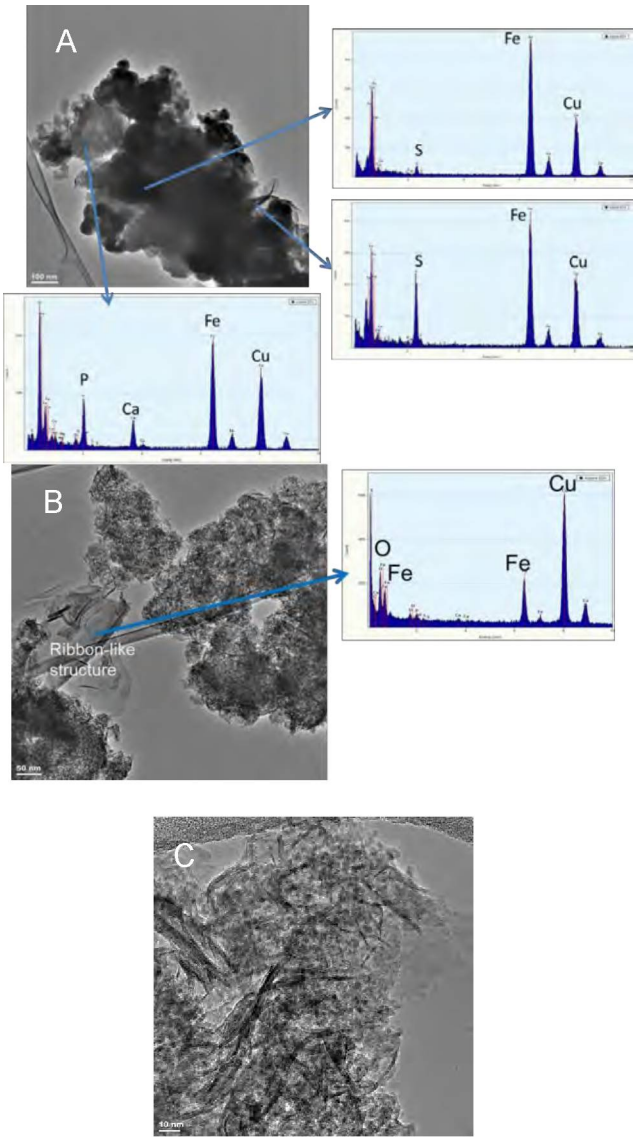

Figure S5. TEM and associated EDX of sulfidated nZVI after (**A**) 24-h oxidation and (**B**) 120-h oxidation. (**C**) High resolution TEM of the ribbon-like structure. In Figure A, EDS spectra were taken in three regions with different morphologies but within the same aggregate.

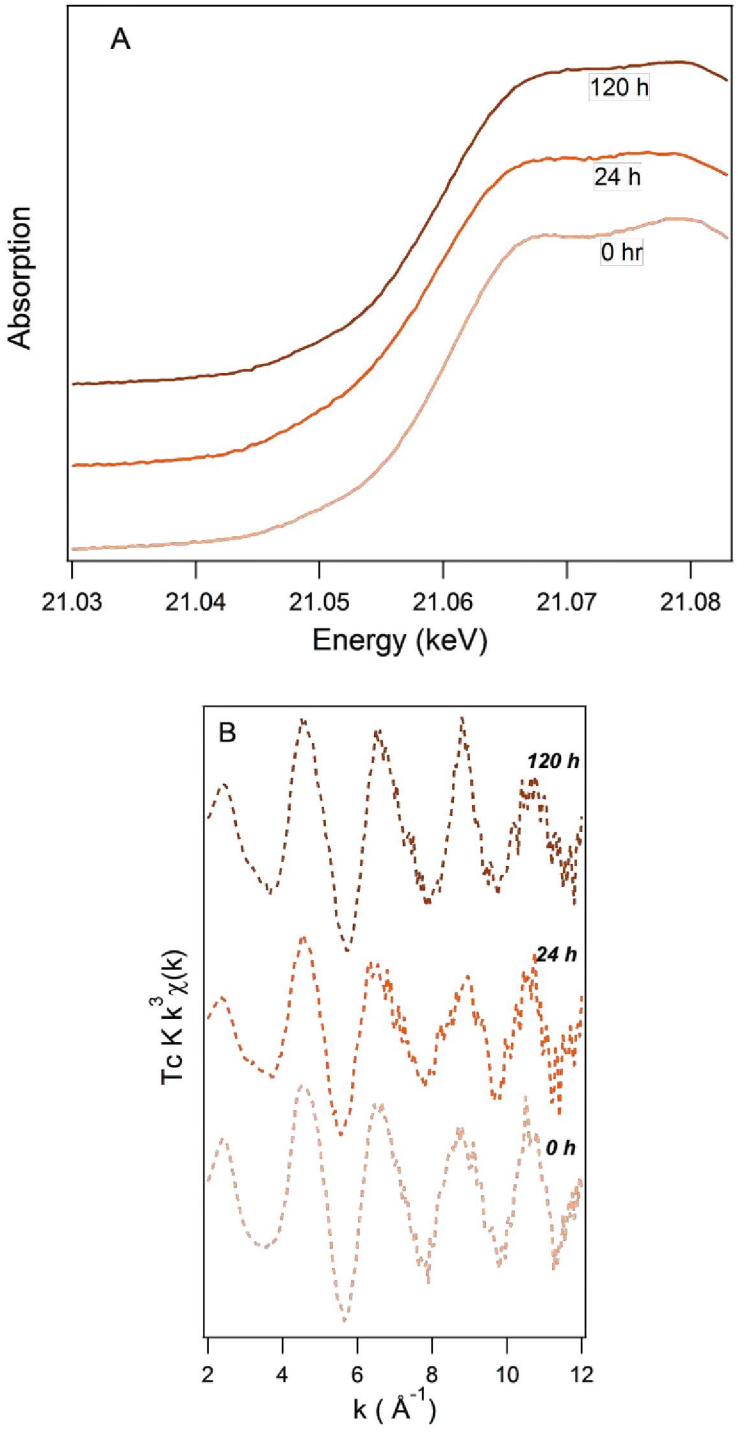

Figure S6. Tc K-edge (**A**) XANES spectra and (**B**) EXAFS spectra of Tc reduced in the absence of sulfide oxidized at 0, 24, and 120 h (Data for the 0-h oxidized sample were adopted from our previous Tc reduction study.[3]).

Table S2. Fitting and calculated Mössbauer parameters for the Mössbauer spectra shown in Figure 2A–2D.

Oxidation time	Temp	Phase[1]	δ_o[2] mm/s	Δ or ε_o[3] mm/s	H[4] Tesla	σ_Δ (mm/s)[5] or σ_H (Tesla)	comp.(%)[6]	χ^2[7]	<CS>[8] mm/s	<Δ> or <ε>[9] mm/s	<H>[10] Tesla	σ_d <Δ> or <H>[11] mm/s	Phase, %[12]
0 h	6 K	nZVI-FCC	-0.5	0*	__[13]	0.1*	100	1.6	-0.5	0.08	__	0.06	1
		FeS	0.5	0.1*	__	7.00E-05	100		0.5	0.1	__	7.00E-05	8
		Amorphous-nZVI	0.28	0*	22.7	4.68	93.9		0.29	-0.02	22.01	5.32	92
					11.15	1.78	6.1						
24 h	20 K	Amorphous Fe(II)	1.29	2.68	__	0.24	100	1.5	1.29	2.68	__	0.24	39
		FeS	0.5	0.12*	__	0.001*	100		0.5	0.12	__	0.001	11
		nZVI-FCC	-0.5	0*	__	0.1*	100		-0.5	0.08	__	0.06	1
		nZVI-amorphous	0.32	0	22	4.78	100		0.32	-0.0003	22.03	4.78	45
		Ferrihydrite	0.05	0.2*	46*	5*	100		0.05	0.2	46	5	4
120 h	20 K	Vivianite	1.27	2.76	__	0	100	4.1	1.27	2.76	__	0	20
		Fe(III)-(oxyhdr)oxide	0.53	0.12*	__	0.25	100		0.53	0.22	__	0.17	7
		Ferrihydrite	0.47	-0.03	47.05	2.15	31.53		0.47	-0.03	35.4	13.35	73
					41.9	3.8	22						
					24.2	12.4	46.4						
312 h	12 K	Ferrihydrite	0.47	-0.014	47.21	2.01	43.15	1.4	0.47	-0.014	41	11.15	98
					43	3.3	37						
					22.4	16.2	19.7						
		Vivianite	1.38	2.79	__	0.1*	100		0.47	-0.014	__	0.1	2

[1]Spectral component; [2]center shift; [3]quadrupole splitting or quadruple shift parameter ; [4]hyperfine magnetic field; [5]std deviation of the component; [6]the weight of the Gaussian component; [7]reduced chi square; [8]average center shift; [9]average quadruple or average quadruple shift parameter; [10]average magnetic hyperfine field; [11]standard deviation; [12]spectral percent; [13]not applicable

Modeling was carried out using Voight-based fitting method of Rancourt and Ping [8] with RecoilTM Software; * These parameters are frozen during modeling; Lorentzian half widths at half maximum (HWHM) of all elemental Lorentzians in all elemetal doublet and sextets were ~0.2 mm/sec (0 h) and ~0.25 mm/sec (> 24 h samples); No coupling was allowed between CS, QS or e and average H; the A+/A- areas of doublet are fixed at 1; A1/A3 and A2/A3 areas are fixed at 2 and 3.

References

(1) Lee, J.-H.; Fredrickson, J. K.; Kukkadapu, R. K.; Boyanov, M. I.; Kemner, K. M.; Lin, X.; Kennedy, D. W.; Bjornstad, B. N.; Konopka, A. E.; Moore, D. A.; Resch, C. T.; Phillips, J. L. Microbial reductive transformation of phyllosilicate Fe(III) and U(VI) in fluvial subsurface sediments, *Environ. Sci. Technol.* **2012**, *46*, 3721-3730.

(2) Peretyazhko, T. S.; Zachara, J. M.; Kukkadapu, R. K.; Heald, S. M.; Kutnyakov, I. V.; Resch, C. T.; Arey, B. W.; Wang, C. M.; Kovarik, L.; Phillips, J. L.; Moore, D. A. Pertechnetate (TcO_4^-) reduction by reactive ferrous iron forms in naturally anoxic, redox transition zone sediments from the Hanford Site, USA, *Geochim. Cosmochim. Acta* **2012**, *92*, 48-66.

(3) Fan, D.; Anitori, R. P.; Tebo, B. M.; Tratnyek, P. G.; Lezama Pacheco, J. S.; Kukkadapu, R. K.; Engelhard, M. H.; Bowden, M. E.; Kovarik, L.; Arey, B. W. Reductive sequestration of pertechnetate ($^{99}TcO_4^-$) by nano zerovalent iron (nZVI) transformed by abiotic sulfide, *Environ. Sci. Technol.* **2013**, *47*, 5302-5310.

(4) Murad, E.; Cashion, J. Iron Oxides. In: *Mössbauer Spectroscopy of Environmental Materials and Their Industrial Utilization*; Springer, **2004**; pp. 159-188.

(5) Bi, Y.; Hyun, S. P.; Kukkadapu, R.; Hayes, K. F. Oxidative dissolution of UO_2 in a simulated groundwater containing synthetic nanocrystalline mackinawite, *Geochim. Cosmochim. Acta* **2012**, *102*, 175-190.

(6) Descostes, M.; Mercier, F.; Thromat, N.; Beaucaire, C.; Gautier-Soyer, M. Use of XPS in the determination of chemical environment and oxidation state of iron and sulfur samples: constitution of a data basis in binding energies for Fe and S reference compounds and applications to the evidence of surface species of an oxidized pyrite in a carbonate medium, *Appl. Surf. Sci.* **2000**, *165*, 288-302.

(7) Mullet, M.; Boursiquot, S.; Abdelmoula, M.; Genin, J.; Ehrhardt, J. Surface chemistry and structural properties of mackinawite prepared by reaction of sulfide ions with metallic iron, *Geochim. Cosmochim. Acta* **2002**, *66*, 829-836.

(8) Rancourt, D. G.; Ping, J. Y. Voigt-based methods for arbitrary-shape static hyperfine parameter distributions in Mössbauer spectroscopy, *Nucl. Instrum. Meth. B* **1991**, *58*, 85-97.